



Norwegian University of  
Science and Technology

# Design of Mooring Systems in Extreme Seastates with focus on Viscous Drift Force Modelling

**Ruoqi Wang**

Marine Technology

Submission date: June 2016

Supervisor: Kjell Larsen, IMT

Norwegian University of Science and Technology  
Department of Marine Technology



## Preface

The work for this master's thesis concludes the degree of Master of Science in Marine Technology at the Norwegian University of Science and Technology (NTNU). The thesis is weighted 30 ECTS and conducted during the spring of 2016.

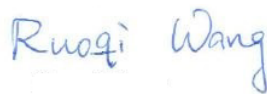
First of all, I would like to express my sincere gratefulness to Professor II Kjell Larsen for providing me guidance and motivation through my thesis work. Our weekly meeting benefits me a lot since Kjell followed my work all the time and gave advice and instant feedback. I appreciate a lot for him being so patient and supportive.

In addition I would like to thank Vegard Øgård Aksnes at MARINTEK for providing important guidance on SIMA software and specific advices according to my questions. Special thanks is also given to PhD candidate Xiaopeng Wu for troubleshooting with SIMO and RIFLEX application in mooring system.

Then I want to express my appreciation to all the professor who had taught me in the past two years. I have learnt so much and got much improvement.

Last but not least, I would also like to thank my parents and my friends. Their love, patience and support make me have the chance to study abroad and enjoy my everyday in NTNU.

Trondheim, 2016-06-10



Ruoqi Wang





## MASTER THESIS SPRING 2016

for

**Stud. tech. Ruoqi Wang**

### **Design of Mooring Systems in Extreme Seastates with focus on Viscous Drift Force Modelling**

*Analyse av forankringssystemer i ekstreme sjøtilstander – fokus på modeller for viskøse driftkrefter*

#### Background

The purpose of the mooring system is to keep a floating vessel safely at a required position. It normally consists of 8-16 mooring lines of heavy chain, steel wire ropes and/or synthetic polyester ropes connected to a seabed anchor.

During the past years, the requirements to the mooring and station keeping systems of mobile and permanent units have become more complex;

- The industry is moving into new frontiers (ultra-deep water down to 3000m depth and into arctic areas).
- There are more operations adjacent to other installations (flotel operations and tender support vessel operations).
- The new mobile units are becoming larger and many units are at the end of their lifetime.

In addition, mooring failure rate is unacceptably high. Some incidents have been multiple line failures, leading to vessel drifting. The investigations show a variety of direct causes covering both inaccurate design, bad quality on mooring line components and lack of personnel competence related to operation of the system. A particular design issue is that today's analysis methods usually neglects the excitation related to viscous drift forces. This is considered a major shortcoming for the mooring design of small semisubmersible platforms. In spite of the advances in the numerical procedures for mooring analysis, there have been a too large number of incidents with mooring line failures over the recent years. These incidents point to the possibility that mooring lines are overloaded during storms. In fact, several mooring line failures have been reported for North Sea floating structures along the recent years during severe conditions in storms and typhoons worldwide. This has uncovered a need to improve methods, procedures and standard industry practice in design prediction of nonlinear wave loadings in high and steep seas. In particular, the methods for prediction of viscous drift forces and wave-current interaction effects on the slow drift wave excitation.

The response quantities to be studied comprise extreme motions (offset) of the floating vessel and extreme tensions in the most loaded mooring lines. Acceptable design is controlled by check of the ultimate limit state (ULS) and accidental limit state (ALS) design criteria. Focus of this thesis shall be on the load effect related to the viscous drift forces.

Analysis methods for estimating ultimate mooring line tension and vessel offset can be

divided into frequency domain (FD) methods and time domain (TD) methods. Using FD methods, the low frequency (LF) load effects and the wave frequency (WF) load effects are analysed separately and then combined into characteristic values used in recipes for ULS and ALS design. The dynamic system describing the behavior of the vessel must be linearized and the maxima of vessel motions and line tensions are usually assumed to be statistically distributed according to the Rayleigh distribution. Sometimes empirical corrections for non-Rayleigh distributions are, however, performed. When using TD methods, all non-linearities in the dynamic system (stiffness and damping) and in the excitation can be taken into account. The results of TD simulations are time series of selected responses that must be carefully analysed by relevant statistical methods in order to establish an accurate estimate of the characteristic load effect.

### Scope of Work

- 1) Describe the ULS and ALS acceptance criteria (safety factors and recipes) relevant for the Norwegian Continental Shelf (NCS).
- 2) Review relevant literature and describe the different aspects and differences of FD and TD analysis methods for analysis of extreme vessel offset and extreme mooring line tension based on the short term storm approach. In particular an assessment and study of different models for viscous load effects and the resulting impact of viscous drift forces on vessel response shall be made. This shall include a review of the different models available for modelling viscous drift forces. The models shall be described and an assessment shall be made on their availability in present software packages.
- 3) Establish numerical simulation models for TD analysis in SIMA. Select the water depth, mooring system and metocean design basis studied during the project work. Establish characteristic vessel offset and mooring line tensions according to recipes in rules and regulations. Make a thorough comparison of the FD and TD results. The comparison shall cover both mean, LF and WF responses as well as the total response. The contribution of the viscous effects to the resulting response shall be discussed. As a part of this, a comparison shall be made with an existing empirical model for correction of wave drift forces (to be discussed and agreed together with the supervisor).
- 4) Conclusions and recommendations for further work.

### General information

The work scope may prove to be larger than initially anticipated. Subject to approval from the supervisor, topics may be reduced in extent.

In the thesis the candidate shall present his personal contribution to the resolution of problems within the scope of the thesis work

Theories and conclusions should be based on mathematical derivations and/or logic reasoning identifying the various steps in the deduction.

The candidate should utilise the existing possibilities for obtaining relevant literature.

### Thesis format

The thesis should be organised in a rational manner to give a clear exposition of results, assessments, and conclusions. The text should be brief and to the point, with a clear language. Telegraphic language should be avoided.

The thesis shall contain the following elements: A text defining the scope, preface, list of contents, summary, main body of thesis, conclusions with recommendations for further work, list of symbols and acronyms, references and (optional) appendices. All figures, tables and equations shall be numerated.

The supervisor may require that the candidate, in an early stage of the work, presents a written plan for the completion of the work.

The original contribution of the candidate and material taken from other sources shall be clearly defined. Work from other sources shall be properly referenced using an acknowledged referencing system.

The report shall be submitted in two copies:

- Signed by the candidate
- The text defining the scope included
- In bound volume(s)
- Drawings and/or computer prints which cannot be bound should be organised in a separate folder.

### Ownership

NTNU has according to the present rules the ownership of the thesis. Any use of the thesis has to be approved by NTNU (or external partner when this applies). The department has the right to use the thesis as if the work was carried out by a NTNU employee, if nothing else has been agreed in advance.

### Thesis supervisor:

Prof. II Kjell Larsen (Statoil/NTNU)

**Deadline: June 10, 2016**

Trondheim, May , 2016

Kjell Larsen (date and signature):

June 10<sup>th</sup>, Kjell Larsen

Ruoqi Wang (date and signature):

June 10<sup>th</sup>, Ruoqi Wang



## Abstract

Recent years floating structure are widely used for different marine operations. So increases the usage of mooring system rapidly to perform its position-keeping function. However, high failure rate of mooring system catches people's attention. The overloaded mooring lines in operation uncovers the hidden danger in insufficient prediction of low-frequency excitation and damping force. Based on previous theoretical analysis and model tests, the failure is mainly due to the ignorance of viscous effect on the structure. Therefore this thesis mainly focuses on viscous drift force modelling on a semi-submersible under extreme weather condition.

Important theory were developed first. Three viscous models were established with their expressions derived. Then the Frequency Domain method and Time Domain method were explained and compared. They had different ways to deal with a given signal with their own advantages and shortcomings. Different software were applied accordingly. For calculating the tension in mooring line, quasi-static method and dynamic method were explained and compared.

Floatel Superior was modeled with 12 mooring lines evenly spread in shallow water with 150m depth. The mooring lines consisted of chain and fibre. The structure was researched under 100-year return period weather condition. Since it had been researched in Frequency Domain by MIMOSA in Autumn 2015, in order to keep the model with same characteristic and vessel file as before, the SIMO input file was verified with the MIMOSA file before doing further analysis.

Force coefficients, transfer functions, restoring force, decay test and structural response under one specific case were compared one by one. Only the linear damping value in SIMO file was modified. All results showed that SIMO file was consistent with MIMOSA file, only with a relative lower damping value.

In order to take viscous effect into account, two different methods were applied: slender element method and correction formula method. They had different strategy to account for viscous force. Based on the increase in tension and motion, it was concluded that viscous effect was really important in structure response analysis. Ignoring viscous effect will certainly induce an underestimation of LF excitation force and damping force, then further provide a conserva-

tive estimation in mooring line tension and structure motion.

Both methods were effective, while slender elements brought a more accurate and reliable result and correction formula was doubted. Extra damping modification were applied to improve the correction formula method. It worked but not so realistic in real practice.

A sensitivity test was performed to know how the variation in drag coefficient affect the response. The 'tuning' equation was applied to tune the drag coefficient on column and pontoon. Two parallel comparison group were created. The smaller coefficient would induce a smaller drag force on structure.

In order to figure out the relative importance of different loads, the model was researched under single environment load separately. According to the response result, wave was dominating among all three loads, and it had interaction with current when they existed at the same time. Wind gave largest effect in static analysis, due to its large velocity and large exposure area of structure.

The most-loaded line was selected and modeled in RIFLEX. The 3-hour motion series from SIMO was imported as input and the corresponding tension result was used to compare with the SIMO result. The motion series was verified to be consistent through the export and import among software. From the plot, tension result from RIFLEX and SIMO had almost overlapped with each other, which means they were consistent. Only in Wave Frequency band, the RIFLEX result had larger standard deviation value, and had a larger crest and trough in the figure. Due to RIFLEX used the Finite Element Method and dynamic method to calculate the tension, it had a higher tension result. Therefore it gave an amplification effect to the SIMO result. The Dynamic Amplification Factor was calculated as well.

# Contents

Preface . . . . .	i
Abstract . . . . .	vii
List of Figures . . . . .	xiii
List of Tables . . . . .	xv
Acronyms . . . . .	xvii
<b>1 Introduction</b>	<b>1</b>
1.1 Background . . . . .	1
1.2 Historical review . . . . .	2
1.3 Objectives . . . . .	4
1.4 Outlines . . . . .	4
<b>2 Theoretical development</b>	<b>7</b>
2.1 Viscous effects . . . . .	7
2.1.1 Viscous drift force due to free surface . . . . .	8
2.1.2 Viscous drift force due to wave-current interaction . . . . .	10
2.1.3 Viscous drift force due to cross-flow on pontoon . . . . .	11
2.2 Mooring system analysis methods . . . . .	13
2.2.1 Equation of motion . . . . .	13
2.2.2 Frequency domain analysis method . . . . .	18
2.2.3 Time domain analysis method . . . . .	21
2.2.4 Comparison between TD and FD analysis . . . . .	24
2.3 Calculation methods of mooring line tension . . . . .	26
2.3.1 Quasi-staic method (QS) . . . . .	26

2.3.2	Dynamic method (DM)	26
2.3.3	Difference between QS and DM	27
<b>3</b>	<b>Rules and regulation for mooring systems</b>	<b>29</b>
3.1	Category of Design Limit State	29
3.1.1	Ultimate limit state (ULS)	29
3.1.2	Accidental Limit State (ALS)	30
3.1.3	Fatigue Limit State (FLS)	31
3.2	Characteristic capacity for ULS and ALS	31
3.3	Safety factor of main body	32
3.4	Partial factor	34
3.4.1	Partial factor for ULS	35
3.4.2	Partial factor for ALS	36
<b>4</b>	<b>Software programs</b>	<b>37</b>
4.1	MIMOSA	37
4.2	SIMO	37
4.3	RIFLEX	38
<b>5</b>	<b>Establishing and verification of SIMO model</b>	<b>39</b>
5.1	Vessel description	39
5.2	Environmental condition description	42
5.3	Project review	44
5.4	Verification of SIMO model	45
5.4.1	Comparison of vessel file	45
5.4.2	Comparison of restoring force	46
5.4.3	Decay test	47
5.4.4	Comparison of results for a specific case	49
<b>6</b>	<b>Assessment and comparison of models for viscous loads</b>	<b>57</b>
6.1	Slender elements method	58
6.1.1	Create slender elements	58

6.1.2	Drag coefficients from theory . . . . .	59
6.1.3	Sensitivity test of drag coefficients . . . . .	61
6.2	Correction formula method . . . . .	62
6.3	Comparison between two methods . . . . .	64
6.4	Case summary . . . . .	65
6.5	Result analysis . . . . .	66
6.5.1	Comparison in motion . . . . .	67
6.5.2	Comparison in tension . . . . .	69
6.6	Modify damping term in Case 5 . . . . .	71
6.6.1	Comparison in motion . . . . .	72
6.6.2	Comparison in tension . . . . .	74
6.6.3	Evaluation of damping increase . . . . .	75
<b>7</b>	<b>Relative importance of different environmental load effects</b>	<b>77</b>
7.1	Separation of environmental excitation . . . . .	77
7.2	Result analysis . . . . .	79
7.2.1	Comparison in motion . . . . .	79
7.2.2	Comparison in tension . . . . .	81
<b>8</b>	<b>Effect of line dynamics-comparison of results between SIMO and RIFLEX</b>	<b>83</b>
8.1	Difference between SIMO and RIFLEX . . . . .	83
8.2	Process . . . . .	85
8.3	Results analysis . . . . .	88
8.4	DAF calculation . . . . .	92
<b>9</b>	<b>Conclusion</b>	<b>95</b>
<b>10</b>	<b>Recommendation for further work</b>	<b>97</b>
	<b>Bibliography</b>	<b>99</b>
<b>A</b>	<b>Comparison between two input files</b>	<b>102</b>
A.1	Quadratic wind coefficient . . . . .	102

A.2 Quadratic current coefficient . . . . .	103
A.3 Second order wave drift force . . . . .	103
A.4 First order motion transfer function . . . . .	105
<b>B All lines tension comparison in viscous cases</b>	<b>108</b>
<b>C All lines tension comparison with different damping value</b>	<b>111</b>
<b>D All lines tension comparison under different environment condition</b>	<b>114</b>

# List of Figures

2.1	Relative importance of mass, viscous, diffraction forces on marine structures . . . .	7
2.2	Cylinder in waves . . . . .	10
2.3	Sketch for calculation of the viscous drift force contribution from pontoon of a semi-submersible . . . . .	12
2.4	Wind force composition . . . . .	14
2.5	Sketch of forces on a two-dimensional mooring line . . . . .	15
2.6	Geometry stiffness sketch . . . . .	16
2.7	Elastic stiffness sketch . . . . .	17
2.8	De-coupled and coupled analysis . . . . .	22
2.9	Sketch of quasi-static method . . . . .	26
2.10	Sketch of dynamic method . . . . .	27
2.11	Motion explanation in sketch . . . . .	27
3.1	Safety factor for (a) Mobile mooring system (b) Permanent mooring system . . . .	33
3.2	Safety factor for standby condition flotel(Larsen K., 2014) . . . . .	34
5.1	Floatel Superior overview . . . . .	40
5.2	Mooring system layout in MIMOSA (a) top view (b) side view . . . . .	41
5.3	Mooring system layout in SIMO (a) top view (b) side view . . . . .	42
5.4	100-year extreme contour lines in the $H_s - T_p$ plane . . . . .	43
5.5	Restoring force curve from MIMOSA and SIMO . . . . .	46
5.6	Decay test before adjusting the damping level . . . . .	47
5.7	Linear damping value of SIMO input file [Ns/m] . . . . .	48

5.8	Decay test after adjusting the damping level . . . . .	48
5.9	Maximum tension in mooring lines (0°) . . . . .	49
5.10	Offset under (a) combined LF and WF effects (b) LF and WF components respectively	50
5.11	Post-processor chart to find max value in one simulation . . . . .	50
5.12	Inner-workflow in SIMO to find maxima . . . . .	51
5.13	Fitted Gumbel distribution of maximum tension in Line 1 . . . . .	51
5.14	Result comparison in (a) max tension (b) mean tension (unit:[kN]) . . . . .	53
6.1	(a)Dimension (b)Placement of columns and pontoons in global coordinate system	58
6.2	Drag coefficients for rectangular cross-section . . . . .	59
6.3	Wave drift coefficient in surge under 0° . . . . .	63
8.1	3D view of the most-loaded line in RIFLEX . . . . .	83
8.2	Example of a typical line segment composition in RIFLEX . . . . .	84
8.3	Motion series in (a) x direction (b) z direction . . . . .	86
8.4	Zoomed motion series in (a) x direction (b) z direction . . . . .	87
8.5	Tension series (a) original (b) zoomed . . . . .	89
8.6	Tension series (a) in Low Frequency band (b) in Low Frequency band after zoom .	90
8.7	Tension series (a) in Low Frequency band (b) in Low Frequency band after zoom .	91
8.8	Tension components in (a) SIMO (b) RIFLEX . . . . .	92
A.1	Quadratic Wind Coefficient in Surge . . . . .	102
A.2	Quadratic Current Coefficient in Surge . . . . .	103
A.3	Wave Drift Force in Surge under 0 deg . . . . .	104
A.4	Wave Drift Force in Sway under 90 deg . . . . .	104
A.5	1 <sup>st</sup> Order Motion Transfer Function in (a) Surge;0 deg (2) Sway; 90 deg . . . . .	105
A.6	1 <sup>st</sup> Order Motion Transfer Function in Heave; 0 deg . . . . .	106
A.7	1 <sup>st</sup> Order Motion Transfer Function in (a) Roll; 90 deg (b) Pitch; 0 deg (c) Yaw; 45 deg	107

# List of Tables

2.1	Excitation regimes	19
2.2	Properties of Frequency Domain and Time Domain	25
3.1	Partial safety factors for ULS	35
3.2	Partial safety factors for ALS	36
5.1	Principle dimension of Floatel Superior	40
5.2	Mooring line characteristic	41
5.3	Wind input value	43
5.4	Wave input value	43
5.5	Current input value	44
5.6	Maximum tension in mooring lines from SIMO (0°) (unit:[kN])	52
5.7	Motion from SIMO input file (unit:[m])	52
5.8	Motion comparison (unit:[m])	53
6.1	Coordinates of slender elements	58
6.2	Base drag coefficient for slender elements	60
6.3	Quadratic drag coefficient for slender element	60
6.4	Tuned drag coefficient on columns and pontoons	62
6.5	Input drag coefficient in Case 3	65
6.6	Input drag coefficient in Case 4	66
6.7	Cases summary for viscous effect	66
6.8	Motion in all cases (unit:[m])	67
6.9	Tension of line 6 and 7 in all cases (unit:[kN])	70

6.10 Extra damping comparison group . . . . .	72
6.11 Motion results after modification in damping (unit:[m]) . . . . .	72
6.12 Tension of Line 6 and 7 after modification in damping (unit:[kN]) . . . . .	74
6.13 Damping level comparison . . . . .	75
7.1 Cases summary for single environment excitation . . . . .	79
7.2 Motion for single environments (unit:[m]) . . . . .	80
7.3 Tension for single environments (unit:[kN]) . . . . .	81
8.1 Segments setting in RIFLEX . . . . .	88
8.2 Tension components in both software . . . . .	93
B.1 Max tension result of all lines in viscous cases(unit:[kN]) . . . . .	108
B.2 Mean tension result of all lines in viscous cases(unit:[kN]) . . . . .	109
B.3 Standard deviation result of all lines in viscous cases(unit:[kN]) . . . . .	109
C.1 Max tension result of all lines with different damping value(unit:[kN]) . . . . .	111
C.2 Mean tension result of all lines with different damping value(unit:[kN]) . . . . .	112
C.3 Standard deviation result of all lines with different damping value(unit:[kN]) . . . . .	112
D.1 Max tension result of all lines under different environment condition(unit:[kN]) . . . . .	114
D.2 Mean tension result of all lines under different environment condition(unit:[kN]) . . . . .	115
D.3 Standard deviation result of all lines under different environment condition(unit:[kN]) . . . . .	116

## Acronyms

<b>TLP</b>	Tension leg platform
<b>FD</b>	Frequency domain
<b>TD</b>	Time domain
<b>LF</b>	Low frequency
<b>WF</b>	Wave frequency
<b>d.o.f</b>	Degree of freedom
<b>FEM</b>	Finite Element Method
<b>ULS</b>	Ultimate limit state
<b>ALS</b>	Accidental limit state
<b>FLS</b>	Fatigue limit state
<b>NCS</b>	Norwegian Continental Shelf
<b>SF</b>	Safety factor
<b>QS</b>	Quasi-static method
<b>DM</b>	Dynamic method
<b>RAO</b>	Response Amplitude Operator
<b>MWL</b>	Mean water line
<b>SIMO</b>	Simulation of Marine Operations
<b>DAF</b>	Dynamic Amplification Factor



# Chapter 1

## Introduction

### 1.1 Background

Offshore floating structures have their usage increased rapidly because of their recognition of good performances concerning small motion and stability, and may be a viable economic alternative to conventional bottom standing structures. At the same time, in order to keep the floating structure at desired position, mooring systems are always applied. The requirements for mooring systems have become more strict and complex as well. The reasons are as follows.

1. The amount of marine operation activity keeps increasing. Especially most of them are performed adjacent to other installations, under those cases the impact on other unit and the safety distance between them should be considered.
2. The industry is moving into new frontiers, i.e. in ultra-deep water down to 3000m depth and into arctic areas. Then the material type, mooring line length and diameter should be assessed carefully.
3. Many units are at the end of their lifetime, thus the fatigue and fracture detection and maintenance of structure should be considered. More severe, new operation units are needed whose dimension becomes much larger.

In addition, the unacceptable high failure rate of mooring system in real practice also catches our attention. Several incidents have been reported for floating structure in North Sea along

recent years, that the mooring lines are overloaded during extreme weathers (Kvitrud (2014)). It means that the preliminary estimation of external load is not accurate and has great discrepancy from the real one. Also more model testing of semi-submersible floating production units has shown that presently available analysis methods are insufficient to predict both the excitation forces and the damping forces (Stansberg et al. (2015)). All the facts uncover a need to improve the analysis methods.

Offshore structures often operate under severe environmental conditions and the motions and mooring tension are dominated by an extremely complex environmental loading particularly combined by waves, currents and winds. The insufficient prediction of excitation and damping force are due to the ignorance of viscous drift force and wave-current interaction effects on slow drift wave excitation. It is always the main reason for the inaccurate estimation in analysis, also the main shortcoming of the analysis.

## 1.2 Historical review

The wave drift force on a floating structure has been the subject of many investigation in the past few years. The drift forces on ships or barges are computed by the conservation of momentum principle (Newman (1967)). For large offshore structures, a three-dimensional source-sink method and the second-order Bernoulli's equation are applied to obtain the second-order wave drift force (Pinkster (1974)). These methods are generally satisfactory for certain type of structures, when the viscous force is less dominant. However, for other types of structures, e.g. semi-submersibles, tension leg platforms .etc, whose columns and pontoons have small ratio of cross-section dimension, viscous effect on the wave drift force can be equally or more important. Thus it is important to know when the viscous effect is dominant and should be included in the overall analysis.

In this section, a review is given concerning the past developments in both theories and experiments related with viscous drift forces on vertical cylinders and floating structures, like semi-submersibles and TLPs.

Pijfers et al. (1977) investigated a method to calculate the viscous drift forces on semi-submersible structures due to wave-current interaction. The semi-submersible structure can be either free

floating or fixed. Drag coefficient is used as a weighted average value under the effect of both Reynold number and Keulegan-Carpenter number. The influence of current velocity on the drift forces was shown by subtracting the force due to current from the total force due to steady flow. Also a method was given to calculate the slowly varying drift force in irregular waves in time domain.

[Ferretti and Berta \(1980\)](#) applied the Morison equation to calculate the mean drift force on a vertical cylinder due to potential effects and provided numerical results. Drag coefficient used were obtained from potential theory. Those results were compared with those by [Newman \(1967\)](#) for both fixed and floating conditions. It was showed that wave height on the splash zone caused the viscous mean drift force. Finally the wave-current interaction effects were explained at mean water level, and the interaction effect showed much stronger influence than the linear superimposing effect.

[Lundgren et al. \(1982\)](#) discussed the contributions for the potential and viscous mean drift forces on a fixed cylinder in a particular sea state condition. Wave-current interaction effects were also discussed. The derivation is only valid when current velocity is less then 10% of the maximum wave velocity. This approach would lead to erroneous result when considering wave-current interaction.

[Burns \(1983\)](#) researched on the TLP structure and discussed the three different modes of structural horizontal motion when subjected to wind, wave and current. He came up with an idea to generate a “viscous drift” transfer function incorporating these effects using Morrison equation. The proposed transfer function is valid when the current velocity is higher than the maximum water particle velocity.

[Kobayashi et al. \(1987\)](#) showed that the viscous drift force is a significant component besides wave drift force. He calculated the viscous drift force for regular wave conditions considering the fluctuation of the wet surface area of a TLP. Comparing the wave drift force from theoretical calculation result and from experiment result, a big difference existed and should not be ignored. However, after adding the viscous contribution, the result improved.

[Standing et al. \(1991\)](#) contributed an expression for the mean drag force of a single column of a semi-submersible. Wave-current interaction and free surface elevation were accounted for. The theoretical mean surge force had a big improvement after adding the viscous mean drift

force to the potential mean drift force. He suggested the variation of drag coefficients cause the discrepancy between predicted and measured low frequency motion.

It is concluded from the review that most articles and researchers share a common a view that viscous drift force plays an important role in the analysis and it can not be ignored for most cases related with semi-submersibles or TLPs.

### 1.3 Objectives

Based on the industry background and historical review, this thesis mainly focuses on the following parts:

1. Describe the ULS and ALS acceptance criteria relevant for Norwegian Continental Shelf (NCS);
2. Review relevant literature regarding viscous effect and compare the Frequency Domain (FD) analysis method and Time Domain (TD) analysis method theoretically;
3. Illustrate and compare different models in viscous effect and derive related expressions;
4. Establish numerical simulation models for TD analysis in SIMA, and study the response quantities which include extreme motions of the floating vessel and extreme tensions in the most loaded mooring lines with and without viscous effect; discuss the contribution of viscous effect;
5. Run sensitivity test of drag coefficient and check the corresponding change in structure response; check the structure response under single environment force and analyze the contribution/interaction of forces.

### 1.4 Outlines

In Chapter 1, the research background and historical review related with viscous effect are summarized; and accordingly set the main objective of this paper: research the response of Floatel

Superior under 100-years return period with and without viscous effect in time domain; compare the response quantities so as to figure out the importance of viscous effect.

In Chapter 2, a systematic theory development is presented. It is mainly divided into three parts. The first part illustrates three available models for modeling viscous drift force, which are due to free surface, wave-current interaction and cross-flow on pontoon respectively. Then the second part explains the mooring system analysis methods on the basis of the equation of motion. Frequency domain analysis method and time domain analysis method are developed and compared, including relative expressions derived. The last part is about the calculation methods of mooring line tension. Both quasi-static method and dynamic method are explained with sketch and compared in aspect of motion components.

In Chapter 3, details are presented about the Norwegian rules and regulations related with the mooring system in operation. Three different limit states mainly in use are illustrated with important parameters. Then the ULS and ALS acceptance criteria equation is presented based on breaking strength and safety factor.

In Chapter 4, three software for mooring system analysis are introduced. MIMOSA is mainly applied in frequency domain, while SIMO and RIFLEX are used in time domain. SIMO uses quasi-static method to calculate the mooring line tension while the other two use dynamic method.

In Chapter 5, the vessel description is provided first with the layout in MIMOSA and SIMO. The preliminary result in frequency domain in master project in Autumn 2015 is introduced roughly. Then the SIMO input file is verified by comparing with the MIMOSA input file. The verification is done in aspects of vessel file, restoring force and decay test. The restoring force shows great matching and consistent result; while the 1<sup>st</sup> order motion transfer function in vessel file and decay test show too low damping condition in SIMO file. Then the linear damping value in surge and sway is modified according to MIMOSA file. The new linear damping value is around 30% of critical damping and it becomes reasonable.

Then one special seastate with  $H_s=16\text{m}$ ,  $T_p=18.2\text{s}$  is picked out, the tension of the most-loaded mooring lines and the maximum motion are compared between MIMOSA and SIMO. A discrepancy exists, but in a tolerable range. Based on the comparison, it is concluded that the SIMO input file is consistent with the MIMOSA file and is reasonable and valid to use.

In Chapter 6, in order to take the viscous effect into account, two methods are applied. First is slender elements method, with six slender elements created along columns and pontoons. For columns, the viscous models due to free surface and wave-current interaction apply; while for pontoons, only the cross-flow on pontoon applies. The drag coefficients are chosen and calculated based on the regulation DNV-RP-C205. Later the drag coefficient is modified for a sensitivity test.

The second method is correction formula method, whose strategy is to correct the wave drift coefficient by using an empirical formula. Viscous-induced wave drift force is taken into account and added to the potential-flow induced drift force. Then all the results are compared.

Based on the result, both methods are valid to account for viscous effect since an obvious increase in both motion and tension is observed. However, the correction formula method shows dramatic effect of great doubt, which may due to the ignorance of viscous effect on damping term. Then the damping level of this case is modified to match with other cases.

In Chapter 7, relative importance of single environmental load effect is checked by separating the external force. Then the contribution of each force and their interaction is analyzed.

In Chapter 8, RIFLEX is used as an extra verification of simulation result. It analyzes the most-loaded line under the same environment condition. The motion series from SIMO is used as input for RIFLEX, and the corresponding tension result of the most loaded line is compared. Dynamic amplification factor is calculated to show the difference between two sources of result.

Chapter 9 gives the main conclusion of this thesis work and Chapter 10 provides some recommendation for further work.

# Chapter 2

## Theoretical development

### 2.1 Viscous effects

As illustrated in Chapter 1, neglecting of viscous drift forces becomes a big shortcoming in structural analysis, since it may underestimate the excitation and damping, especially in LF band, on marine structures. According to Faltinsen (1993), both viscous effects and potential flow effects may be important in determine the wave-induced motions and loads on marine structures, while the potential flow includes wave diffraction and radiation around structure. In order to judge when viscous effects or different types of potential flow effects are important, it is useful to refer to Figure 2.1.

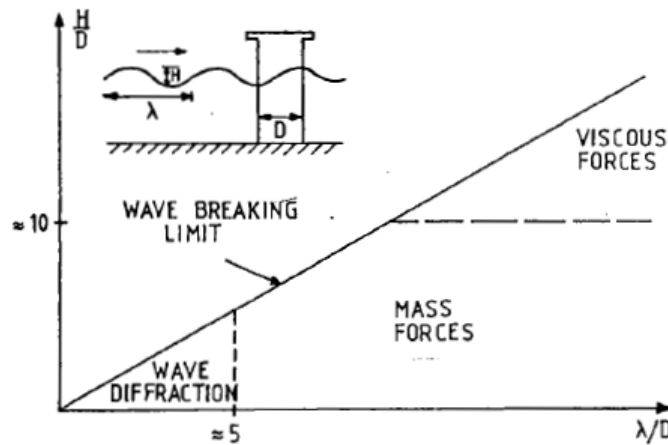


Figure 2.1: Relative importance of mass, viscous, diffraction forces on marine structures

The parameters in the figure are:  $H$ : wave height;  $D$ : diameter of column;  $\lambda$ : wave length.

The purpose of this section is to show the development of expressions for the various drift forces on a semi-submersible due to viscous effects, both on columns and pontoons. Here simple cylinder model is considered: a vertical cylinder across the mean water line (MWL) modelling the column, and a horizontal submerged cylinder modelling the pontoon.

### 2.1.1 Viscous drift force due to free surface

The forces on a small vertical cylinder due to wave is represented by the Morrison equation. For a unit length of the submerged portion of cylinder, the drag force is given by [Morison et al. \(1950\)](#):

$$f_D = \frac{1}{2} \rho D C_D |u| u \quad (2.1)$$

where  $u$ : wave particle velocity;

$C_D$ : drag coefficient;

$\rho$ : mass density of water;

$D$ : cylinder diameter.

After replacing  $u$  by  $u = u_0 \cos \omega t$ , the Equation 2.1 becomes:

$$f_D = \frac{1}{2} \rho D C_D u_0^2 |\cos \omega t| \cos \omega t \quad (2.2)$$

where  $u_0$ : maximum water particle velocity.

$\omega$ : wave frequency;

$t$ : time.

Here the expressions apply to fixed cylinder. If the cylinder is allowed to oscillate harmonically with a displacement amplitude of  $x_0$  at a phase angle of  $\alpha$  with respect to the wave, then Equation 2.1 becomes:

$$f_D = \frac{1}{2} \rho D C_D |u - \dot{x}| (u - \dot{x}) \quad (2.3)$$

where  $\dot{x} = \omega x_0 \cos(\omega t - \alpha)$ .

Then the force per unit length can be written as:

$$f_D = \frac{1}{2} \rho D C_D V^2 |\cos(\omega t + \phi)| (\omega t + \phi) \quad (2.4)$$

where the quantities  $V$  and  $\phi$  are defined as:

$$V = [u_0^2 + (\omega x_0)^2 - 2\omega u_0 x_0 \cos \alpha]^{1/2} \quad (2.5)$$

$$\phi = \arctan\left(\frac{\omega x_0 \sin \alpha}{u_0 - \omega x_0 \cos \alpha}\right) \quad (2.6)$$

Comparing Equations 2.2 and 2.4, it is concluded that for a moving structure in waves,  $u_0$  should be replaced by  $V$ , and  $\omega t$  by  $\omega t + \phi$ . That is the only difference between fixed cylinder and oscillating cylinder.

This form of drag force in Equations 2.2 and 2.4 at a submerged location has a zero mean over one wave cycle, but it is not case at the free surface zone. Due to the changing in free surface, the force will produce a mean drift force at MWL. In order to obtain the expression of the free surface force on a vertical cylinder, Morison equation is used. Current is not considered here since current is generally considered present up to the MWL. Then the derivations of the mean drift force are provided as follows, and all derivations are done only for a fixed cylinder.

According to Chakrabarti (1984), the linear theory is assumed to be applicable to surface zone with the maximum velocity  $u_0$  is given as:

$$u_0 = \frac{gkH \cosh ky}{2\omega \cosh kd} \quad (2.7)$$

where  $H$ : wave height;

$k$ : wave number;

$d$ : water depth;

$y$ : elevation from bottom.

Then the total force is obtained from integral along the wave elevation:

$$F = \int_0^\eta f_D dy \quad (2.8)$$

Based on the integral, the drag force due to free surface effect has a average value over one wave cycle after normalized by  $\rho g D C_D / k^2$  as:

$$\frac{\bar{F}}{\rho g D C_D / k^2} = \frac{(kH)^3}{12\pi} \left[ \frac{1}{\sinh 2kd} + C_1 (kH) \coth 2kd \right] \quad (2.9)$$

where  $C_1$  is a function of  $kH$  between 0 to 1.0 (Chakrabarti (1984)).

From Equation 2.9, it is observed that the mean drift force from free surface effect is a function of cubic of the wave height.

### 2.1.2 Viscous drift force due to wave-current interaction

Wave-current interaction happens both in splash zone and submerged zone, which covers the transition area from MWL up to instantaneous sea level, and area from MWL down to the bottom of the cylinder. The current velocity is considered as constant over MWL, and varies according to the exponential term  $e^{kz}$  with the increase of water depth (Figure 2.2). When current is present along with waves, a non-zero mean drift force is generated from the drag force.

The expression is derived at MWL with the maximum wave particle velocity. However, in order to calculate the total mean drift force on the complete submerged zone, the submerged zone is divided into many small segments. The water particle velocity at center of each segment is used as mean velocity to calculate the wave drift force. Then the wave-current interaction is considered accurately.

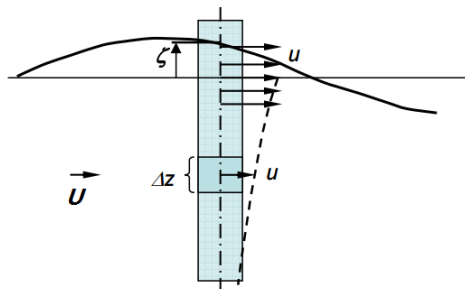


Figure 2.2: Cylinder in waves

Here horizontal wave orbital speed  $u$  is assumed constant across splash zone. For submerged strips the speed decays and the speed at the centre is used.  $U$  is the current velocity.

With the speed of current  $U$ , the drag force is given by:

$$f_D = \frac{1}{2} \rho D C_D |u + U| (u + U) \quad (2.10)$$

For  $|U| \geq u_0$ ,

$$f_D = \pm \frac{1}{2} \rho D C_D \left[ U^2 + \frac{1}{2} u_0^2 (1 + \cos 2\omega t) + 2U u_0 \cos \omega t \right] \quad (2.11)$$

where the negative sign applies to the case of negative current.

For  $|U| < u_0$ ,

$$f_D = \pm \frac{1}{2} \rho D C_D \left[ U^2 + \frac{1}{2} u_0^2 (1 + \cos 2\omega t) + 2U u_0 \cos \omega t \right] \times \text{sgn}(u + U) \quad (2.12)$$

in which  $\text{sgn}$  is a sign function and takes on values of  $\pm 1$ .

When normalized by  $\frac{1}{2} \rho D C_D u_0^2$ , these quantities for unit submerged length of a vertical cylinder are given as follows. In order to make the expressions simpler and clearer, a new quantity  $\psi$  is introduced:

$$\psi = \cos^{-1} \left( -\frac{U}{u_0} \right), 0 \leq \psi \leq \pi \quad (2.13)$$

Then for  $|U| \geq u_0$ ,

$$\frac{\bar{f}_D}{\frac{1}{2} \rho D C_D u_0^2} = \pm \left[ \frac{1}{2} + \left( \frac{U^2}{u_0^2} \right) \right] \quad (2.14)$$

For  $|U| < u_0$ ,

$$\frac{\bar{f}_D}{\frac{1}{2} \rho D C_D u_0^2} = \frac{1}{\pi} \left\{ \left( \frac{U}{u_0} \right)^2 (2\psi - \pi) + 4 \frac{U}{u_0} \sin \psi + \left( \psi - \frac{\pi}{2} + \frac{1}{2} \sin 2\psi \right) \right\} \quad (2.15)$$

where  $\bar{f}_D$  denotes the average mean drift force value over a wave cycle.

### 2.1.3 Viscous drift force due to cross-flow on pontoon

As [Faltinsen \(1993\)](#) explained, when wave drift forces become small, viscous effects may contribute to drift forces. A horizontal submerged cylinder that has heave and surge motion is considered. With a simple cross-flow around, the forces can be decomposed into components along the global coordinate system. By averaging the forces over one wave period, a non-zero

mean wave loads that are proportional to the cube of the wave amplitude is obtained. For a semi-submersible, this effect always applies to pontoon.

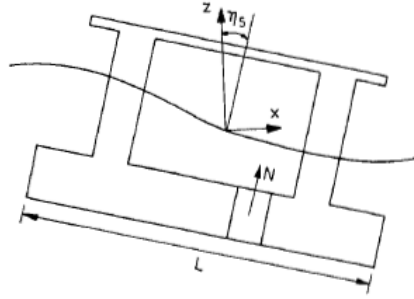


Figure 2.3: Sketch for calculation of the viscous drift force contribution from pontoon of a semi-submersible

Here is the equation for incident wave potential:

$$\phi = \frac{g\check{\zeta}_a}{\omega} e^{kz} \cos(\omega t - kx) \quad (2.16)$$

This means the vertical incident fluid velocity can be written as

$$w = \frac{\partial \phi}{\partial z} = \omega \check{\zeta}_a e^{kz} \cos(\omega t - kx) \quad (2.17)$$

The drag force normal to pontoon in the N-direction can be written as

$$F_N = -2 \int_{-L/2}^{L/2} \frac{\rho}{2} C_D b V_R |V_R| dx \quad (2.18)$$

Here  $V_R$  is the relative velocity in the N-direction between a strip of the platform and the incident wave field. it can be written approximately as

$$V_R \approx \frac{d\eta_3}{dt} - x \frac{d\eta_5}{dt} - w \quad (2.19)$$

This result in a viscous drift force in surge direction:

$$F_x = F_N \eta_5 \quad (2.20)$$

This also applies to the structure when it turns to port-side and has an opposite N direction.

## 2.2 Mooring system analysis methods

### 2.2.1 Equation of motion

The mooring system analysis methods are based on the motion equation as Equation 2.21.

$$(M + A(\omega)) \cdot \ddot{r} + C(\omega) \cdot \dot{r} + D_l \cdot \dot{r} + D_q \cdot \dot{r} |\dot{r}| + K(r) \cdot r = Q(t, r, \dot{r}) \quad (2.21)$$

where  $M$ : mass matrix

$A(\omega)$ : frequency-dependent added mass matrix

$r$ : positive vector

$C(\omega)$ : frequency-dependent potential damping matrix

$D_l$ : linear damping matrix

$D_q$ : quadratic damping matrix

$K(r)$ : stiffness matrix (non-linear)

$Q(t, r, \dot{r})$ : excitation force vector

Since surge, the translation in x direction, is more important compared to other degree of freedoms, the equation will be simplified into only focusing on one degree of freedom as Equation 2.22, and further analysis will be based on this.

$$(M + A(\omega)) \cdot \ddot{x} + C(\omega) \cdot \dot{x} + D_l \cdot \dot{x} + D_q \cdot \dot{x} |\dot{x}| + K(x) \cdot x = Q(t, x, \dot{x}) \quad (2.22)$$

#### 1. Excitation Force and Moment

The excitation forces and moments  $Q(t, x, \dot{x})$  are added to the right side of the equations of motions. The external forces on the structure are typically environmental loads, which includes wind force  $q_{wi}$ , current force  $q_{cu}$  and wave force  $q_{wa}$ , and may be composed Equation 2.23:

$$Q(t, x, \dot{x}) = q_{wi} + q_{cu} + q_{wa} \quad (2.23)$$

If the system is thruster assisted, it will have additional thruster force.

- *Part A*: Wind forces

Wind force  $q_{wi}$  under low frequency are characterized by a combination(Figure 2.4):

- mean value due to mean wind speed
- LF forces due to wind gust

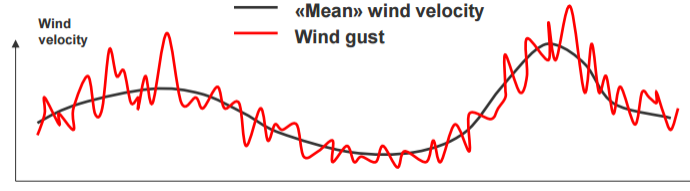


Figure 2.4: Wind force composition

Wind forces is expressed as:

$$Q_{wi} = C_{wi} \cdot U(t)^2 = C_{wi} [(\bar{U} + u(t)) - x_{LF}]^2 \quad (2.24)$$

where  $(\bar{U} + u(t)) - x_{LF}$  represents the relative velocity between wind and LF motion. Here we assume  $\bar{U} \gg x_{LF}$  and  $\bar{U} \gg u(t)$ , then Equation 2.24 is simplified as:

$$Q_{wi} = C_{wi} [\bar{U}^2 + 2\bar{U}u(t) - 2\bar{U}x_{LF}] \quad (2.25)$$

where the wind coefficient is  $C_{wi} = \frac{1}{2}\rho_{air} \cdot C_D \cdot A$ . The force components from left to right are constant force, LF excitation force and LF damping force.

- *Part B: Current force*

Similarly to wind force, current force  $q_{cu}$  are also characterized by two parts:

- mean value due to mean current velocity
- current turbulence is neglected

Current forces is expressed as:

$$Q_{cu} = C_{cu} (\bar{V} - x_{LF}) |\bar{V} - x_{LF}| = C_{cu} (\bar{V} - x_{LF})^2 \quad (2.26)$$

where  $\bar{V} - x_{LF}$  represents the relative velocity of current and LF motion. Here we assume  $\bar{V} \gg x_{LF}$ , then Equation 2.26 is simplified as:

$$Q_{cu} = C_{cu} (\bar{V}^2 - 2\bar{V}x_{LF}) \quad (2.27)$$

where the current coefficient is  $C_{cu} = \frac{1}{2}\rho_{water} \cdot C_D \cdot A$ . The force component from left to right are constant force and damping effect.

- *Part C: Wave force*

Compared to wind force and current force, wave force is more complicated, since it has three components as follows:

- 1<sup>st</sup> order forces (wave drift) proportional with wave amplitude, described by force transfer functions
- mean value due to 2<sup>nd</sup> order wave loads
- LF forces excited by 2<sup>nd</sup> order wave loads

In FD, wave force will be divided into WF and LF band; while in TD it is treated as a complete signal in analysis. More explanations are in the following sections.

## 2. Stiffness

Stiffness  $K(x)$  provides the restoring force of the system and controls the mean offset and LF motion. It is provided by both geometric and elastic properties and both of them are based on the catenary equation. Figure 2.5 shows the catenary model.

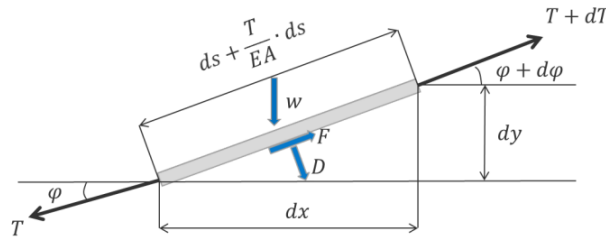


Figure 2.5: Sketch of forces on a two-dimensional mooring line

The following equations can be obtained under the static equilibrium of a segment of length  $ds$ :

Tangential direction:

$$dT = \left[ \omega \sin \psi - F \left( 1 + \frac{T}{EA} \right) \right] \cdot ds \quad (2.28)$$

Normal direction:

$$T \cdot d\psi = \left[ \omega \cos \psi + D \left( 1 + \frac{T}{EA} \right) \right] \cdot ds \quad (2.29)$$

Horizontal offset:

$$x = \frac{1}{\omega} \int_{\psi_0}^{\psi} \frac{T_0}{\cos \alpha} \cdot \cos \psi_0 d\alpha \quad (2.30)$$

- Geometric stiffness  $K_G$

It is mainly provided by:

- line weight or separate clump weights
- line buoyancy or separate buoys

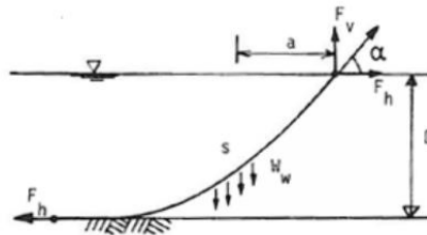


Figure 2.6: Geometry stiffness sketch

When talking about line weight, the weight of chain segment is dominate, while the influence from fiber part is too small to mention. Thus the catenary equation is used without elasticity ( $\frac{T}{EA} \ll 1$ ).

The equilibrium equation for this model is expressed as:

$$F_h \cdot D = W_w \cdot a \quad (2.31)$$

- Elastic stiffness  $K_E$

$K_E$  is provided by line axial elongation (stretch) and fiber segment is the mainly supplier of the elastic stiffness. At this time, the elasticity has to be considered ( $EA$ ).

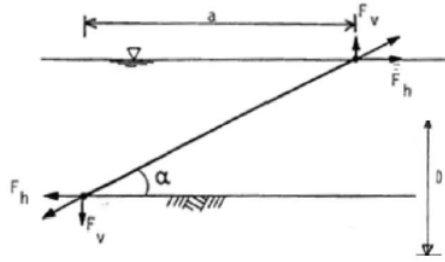


Figure 2.7: Elastic stiffness sketch

The equilibrium equation for this model is expressed as:

$$F_h \cdot D = F_v \cdot a \quad (2.32)$$

- Total stiffness  $K_T$

The total stiffness  $K_T$  can be obtained by Equation 2.33.

$$\frac{1}{K_T} = \frac{1}{K_G} + \frac{1}{K_E} \quad (2.33)$$

### 3. Damping

The LF damping forces  $D_l \cdot \dot{x} + D_q \cdot \dot{x} |\dot{x}|$  are important in order to limit resonant LF motions in surge, sway and yaw. The damping forces reduce the LF motion. The main resource of damping are as follows (Larsen K., 2014):

- Viscous loads on the floater hull (provided by skin friction and flow separation)
- Wave drift damping (since the wave drift forces change with floater velocity)
- Drag forces on mooring lines and risers
- Damping due to wind (wind loads also change with floater velocity)
- Propellers and thrusters

In FD analysis method, the damping term, which consists both quadratic damping and linear damping, should be linearized.

### 2.2.2 Frequency domain analysis method

FD analysis refers to the analysis of mathematical functions or signals with respect to frequency, rather than time. It is always linear because of the linear superposition principle. All sources of non-linearity should be linearized by either a direct linearization approach or an iterative linearization approach (Low and Langley (2006)).

The methodology of FD analysis is based on separation of WF motion ( $T=5-30s$ ), and LF motion ( $T=30-500s$ ). But these two parts are not totally isolated, they have effect on each other. On one hand, there are damping effects from WF that will have an effect on the LF motions, which should be included as input transfer functions; on the other hand, in shallow water with a non-linear stiffness, the LF motion will have impact on the WF line tension estimates due to the variation of the geometric stiffness of the mooring line.

#### 1. Separation of excitation

The excitation components is explained in the last section, however, the wave force needs more detailed derivation in frequency domain since it has more complex components in LF and WF band.

In *WF* band, the Response Amplitude Operators  $H_{WF\eta}(w)$  are used as input transfer functions connecting wave spectrum  $S_{\eta}(\omega)$  and WF motion spectrum  $S_{WF(\omega)}$  as Equation 2.34.

$$S_{x_{WF(\omega)}} = |(H_{WF\eta}(w))|^2 \cdot S_{\eta}(\omega) \quad (2.34)$$

In *LF* band, the non-linear components in motion equation (Equation 2.22) should be linearized according to linear superposition principle as Equation 2.35.

$$(M + A) \cdot \ddot{x}_{LF} + D_{eq} \cdot \dot{x}_{LF} + K_{eq} \cdot x_{LF} = Q \quad (2.35)$$

where  $D_{eq}$  and  $K_{eq}$  are the equivalent terms after linearization. Further analysis is based on this equation.

The mean drift force is expressed by the wave drift force coefficient with the wave spec-

trum:

$$q_{wa}^- = C_{wa} \cdot \eta^2 \quad (2.36)$$

where the amplitude  $\eta$  can be illustrated by the wave spectrum as  $\eta^2 = 2S_\eta(\omega) d\omega$ , and the mean drift force is obtained by integrating the Equation 2.36 along the spectrum as:

$$q_{wa}^- = 2 \int_0^\infty C_{wa}(\omega) S_\eta(\omega) d\omega \quad (2.37)$$

And the LF wave drift force with frequency  $\mu$  is expressed as:

$$S_{wa} = 8 \int_0^\infty C_{wa}\left(\omega + \frac{\mu}{2}\right) \cdot C_{wa}\left(\omega + \frac{\mu}{2}\right) \cdot S_\eta(\omega) \cdot S_\eta(\omega + \mu) d\omega \quad (2.38)$$

To make it more clear and logic, the excitation regimes are concluded in Table 2.1.

Table 2.1: Excitation regimes

Excitation	Mean(static)	Wave frequency	Low frequency
Wave	mean 2 <sup>nd</sup> order	1 <sup>st</sup> order force	LF 2 <sup>nd</sup> order force
Wind	mean wind speed		wind gust
Current	mean current speed		

## 2. Separation of motion

Accordingly, the total motion consists of three parts, the mean offset of system  $\bar{X}$ , the WF motion  $X_{WF}$ , and the LF motion  $X_{LF}$ . After separating the excitation, the corresponding motion can be obtained correspondingly.

- *Part A: Mean motion*

The mean motion is obtained by setting the damping and mass components in the motion equation as zero. Thus Equation 2.22 is simplified into  $K(x) \cdot \bar{X} = \bar{Q}$ , where  $\bar{Q}$  means mean excitation force, which consisting of mean wind force, mean current force and mean wave drift force.

$$\bar{Q} = C_{wi} \bar{U}^2 + C_{cu} \bar{V}^2 + 2 \int_0^\infty C_{wa}(\omega) S_\eta(\omega) d\omega \quad (2.39)$$

- *Part B: WF motion*

In WF band, the 1<sup>st</sup> order wave force provides all the external excitation. In order to get the motion in WF band, the Equation 2.34 is used. Based on the transfer functions between wave elevation amplitude and WF motion amplitude

$$H_{x_{WF}\eta}(\omega) = \frac{x_{WF,a}(\omega)}{\eta_a(\omega)} \quad (2.40)$$

The corresponding standard deviation of response is computed using Equation 2.41.

$$\sigma_{x_{WF}} = \sqrt{\int_0^{\infty} S_{x_{WF}}(\omega) d\omega} \quad (2.41)$$

In order to calculate the significant and largest motion it is assumed that the response is a narrow-banded Gaussian process, so that the peaks are Rayleigh distributed. The significant value is the mean value of the one-third highest peaks of motion from Rayleigh distribution and it is almost twice the value of the standard deviation. On this basis, the significant and largest motion are defined as:

$$X_{WF}^{sig} = 2\sigma_{x_{WF}} \quad (2.42)$$

$$X_{WF}^{max} = \sigma_{x_{WF}} \sqrt{2 \ln N_{WF}} \quad (2.43)$$

where  $N_{WF}$  is the number of WF structure oscillation in the duration of the environmental state. It is normally 3 hours.

- *Part C: LF motion*

The LF response is obtained by using the linear motion equation (Equation 2.35).  $Q$  here consists of two parts, wind gust and 2<sup>nd</sup> order wave drift force. Using the frequency-response method, the motion spectrum is obtained from the force spectrum.

$$S_{x_{LF}}(\omega) = |H(\omega)|^2 \cdot S_{q_{LF}}(\omega) \quad (2.44)$$

Here the force spectrum is a combination of wave drift spectrum  $S_{q_{WaveDrift}}(\omega)$  and wind gust spectrum  $S_{q_{Wind}}(\omega)$ . And transfer function is expressed with the lin-

earized equivalent terms as:

$$|H(\omega)|^2 = \frac{1}{K_{eq} - [M + A(0) \cdot \omega^2]^2 + D_{eq}^2 \cdot \omega^2} \quad (2.45)$$

Then the corresponding standard deviation is also obtained:

$$\sigma_{xLF} = \sqrt{\int_0^\infty S_{xLF}(\omega) d\omega} \quad (2.46)$$

Similarly with WF, for LF motion:

$$X_{LF}^{sig} = 2\sigma_{xLF} \quad (2.47)$$

$$X_{LF}^{max} = \sigma_{xLF} \sqrt{2 \ln N_{LF}} \quad (2.48)$$

where  $N_{LF}$  is the number of LF structure oscillation in the duration of the environmental state. It is normally 3 hours.

- *Part D: Combination of motions*

After obtaining all the motion components, FD analysis have to combine all the components in a proper way to get the final result. The total motion in surge is expresses as:

$$X_{max} = \bar{X} + max \begin{cases} X_{LF}^{max} + X_{WF}^{sig} \\ X_{WF}^{max} + X_{LF}^{sig} \end{cases} \quad (2.49)$$

### 2.2.3 Time domain analysis method

TD analysis is the analysis of mathematical functions, physical signals or time series of environmental data, with respect to time. It is able to model the nonlinear effects. The signal or function's value is known for all real numbers, for the case of continuous time, or at various separate instants in the case of discrete time.

The equations of motions is solved in the time domain by dividing the desired time period into a number of time steps and perform equilibrium iterations at each time step. The solution is obtained by using the start conditions from the previous time step and assuming a motion

pattern. The solution will then in turn become the start conditions for the next time step.

### 1. Two Approaches for Analysis

In time domain, there are two approaches to do analysis to a mooring system.

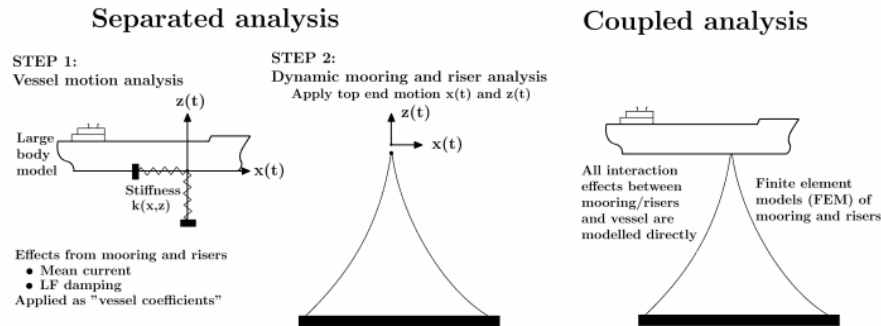


Figure 2.8: De-coupled and coupled analysis  
(Ornberg and Larsen (1998))

- De-coupled approach

Use two different models: one for vessel and one for the mooring system. First step, simulate the top end motions (in x-z plane) by the vessel model with simplified even neglected influence from mooring lines. Step 2, simulate the mooring tensions by the mooring system model, and take the top end motions of vessel from Step 1 as input for the second model.

The main shortcomings of a de-coupled approach are: (a) mean loads on mooring lines due to current is normally not accounted for, particularly in deep water; (b) The important damping effect from the mooring system on the LF motion can only be included in a simplified way.

- Coupled approach

Vessel and mooring system are simulated simultaneously in a complete model: the vessel is simulated as a large body hydrodynamic model, while the mooring system is simulated as a finite element slender model.

The main reason for performing a coupled analysis is to avoid the limitations of the de-coupled approach and take the important coupling effects into account. Conse-

quently, the estimates of the vessel motions and the dynamic responses in the mooring lines will be more accurate. The main disadvantage is that the coupled analysis is time-consuming and require a large data storage.(Ornberg et al. (1997))

## 2. Frequency-dependent Coefficient

The main focus in time domain analysis, also its unique part, is to solve the frequency-dependent term added mass coefficient  $A(\omega)$  and damping coefficient  $C(\omega)$  on a time series. (Reinholdtsen and Falkenberg (2001))

Assume the Equation 2.22 can be transformed into the following equation:

$$(M + A(\omega)) \cdot \ddot{x} + C(\omega) \cdot \dot{x} + K(x) \cdot x = Q - D_l \cdot \dot{x} - D_q \cdot \dot{x}|\dot{x}| = f'(t) \quad (2.50)$$

With regard to frequency-dependent coefficient only, the equation of dynamic equilibrium can be written:

$$A(\omega) \cdot \ddot{x} + C(\omega) \cdot \dot{x} = f(t) = f'(t) - K(x) \cdot x - m\ddot{x} \quad (2.51)$$

provided that the right hand side force varies sinusoidally at one single frequency,  $\omega$ . In frequency domain, Equation 2.51 is written:

$$[-\omega^2 A(\omega) + i\omega C(\omega)] X(\omega) = F(\omega) \quad (2.52)$$

Using the following relations:

$$A(\omega) = A_\infty + a(\omega) \quad C(\omega) = C_\infty + c(\omega) \equiv 0 \quad (2.53)$$

where  $A_\infty = A(\omega = \infty)$  and  $C_\infty = C(\omega = \infty)$

Then Equation 2.52 is written as:

$$-\omega^2 A_\infty X(\omega) + i\omega a(\omega) + c(\omega) i\omega X(\omega) = F(\omega) \quad (2.54)$$

Using the inverse Fourier transform,

$$A_{\infty}\ddot{x}(t) + \int_{-\infty}^{+\infty} h(t-\tau)\dot{x}(\tau)d\tau = f(t) \quad (2.55)$$

Physically, when  $t < 0$  or  $\tau > t$ , values of  $h(t-\tau) = 0$ .

Substitute  $f(t)$  from Equation 2.55 and  $f'(t)$  from Equation 2.50. Then the equation of motion becomes:

$$(M + A_{\infty}) \cdot \ddot{x} + D_l \cdot \dot{x} + D_q \cdot f(\dot{x}) + K \cdot x + \int_0^t h(t-\tau)\dot{x}(\tau)d\tau = Q(t, x, \dot{x}) \quad (2.56)$$

The retardation function  $h(\tau)$  can be computed by the frequency-dependent added-mass term and damping term:

$$h(\tau) = \frac{1}{\pi} \int_0^{\infty} [c(\omega) \cos(\omega\tau) - \omega a(\omega) \sin(\omega\tau)] d\omega \quad (2.57)$$

From causality,  $h(\tau) = 0$ :

1. For  $\tau < 0$ , the two parts in the integral must be opposite;
2. For  $\tau > 0$ , the two parts in the integral must be identical mathematically. Thus for  $\tau > 0$ ,

$$h(\tau) = \frac{2}{\pi} \int_0^{\infty} c(\omega) \cos(\omega\tau) d\omega = -\frac{2}{\pi} \int_0^{\infty} \omega a(\omega) \sin(\omega\tau) d\omega \quad (2.58)$$

This means that the frequency-dependent mass and damping components can be found from the retardation function:

$$a(\omega) = -\frac{1}{\omega} \int_0^{\infty} h(\tau) \sin(\omega\tau) d\tau \quad c(\omega) = -\int_0^{\infty} h(\tau) \cos(\omega\tau) d\tau \quad (2.59)$$

#### 2.2.4 Comparison between TD and FD analysis

After the detailed explanation of TD analysis and FD analysis, main differences between them can be summarized here:

1. FD analysis uses spectrum to analyze the signal during the process; while TD analysis

depends on numerical integration of the whole period signal.

2. FD analysis mainly gives analysis about how much of the signal lies within specific frequency band; while TD analysis analyzes how a signal change over time.
3. FD analysis separates the low frequency and wave frequency components, and obtains the corresponding tension and motion respectively, then combines them together to get the final result.

However, TD analysis always does the whole analysis at one go, and gets the final results directly. If the result in different frequency band is needed, frequency filter is used. After setting the cut-off frequency, the high-pass filter is used to save the high frequency components, which corresponds to the wave frequency result. And the low-frequency filter is used to save the low frequency component, which is the low frequency result.

4. During the analysis process, FD method will pick out all the non-linear components and linearizes them due to linear superposition principle. TD method just takes all the non-linear components into account directly.
5. In order to get the maximum of the result, FD analysis always assumes Rayleigh distribution; while TD assumes Weibull distribution to get the maxima. If a series of samples is given, the distribution of the maximum should be obtained is modeled by Gumbel distribution.

Both methods discussed have their advantages and disadvantages. These have to be considered before performing an analysis. Requirements on accuracy, computational effort, and degree of non-linearity in the system will often determine the choice of method. The most important properties of these methods are listed in Table 2.2.

Table 2.2: Properties of Frequency Domain and Time Domain

	Frequency Domain	Time Domain
Advantages	Low computational cost No statistical uncertainty	Non-linearity included Transient response
Disadvantages	Require linearisation Only steady response	Statistical uncertainty, require more simulations High computational cost

## 2.3 Calculation methods of mooring line tension

Since mooring line tension is one of the important parameter to assess the structural response, it is necessary to know how it comes to a result. The following section will talk about the two calculation methods of it and the difference between. For illustration, only horizontal motion is used.

### 2.3.1 Quasi-staic method (QS)

In this approach, only the top end position gives the mooring line tension,  $T = T(x)$ . Force actions are taken into account by statically offsetting the structure by environment-induced motion. Dynamic actions on the mooring lines associated with mass, damping and fluid acceleration are neglected.

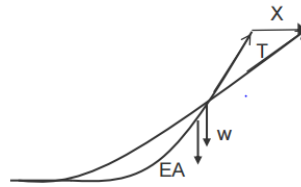


Figure 2.9: Sketch of quasi-static method

where  $X$ : the top end position

$T$ : mooring line tension

$w$ : submerged mooring line weight

$EA$ : linear axial stiffness

### 2.3.2 Dynamic method (DM)

In dynamic method, the top end motion gives the mooring line tension  $T = T(x, \dot{x}, \ddot{x})$ , which includes position  $x$ , velocity  $\dot{x}$ , acceleration  $\ddot{x}$  with drag force and inertia force accounted. The time-varying effects are calculated with 6 d.o.f motions. Dynamic models are used to predict mooring line response on the fairlead motions.

where  $X$ ,  $T$ ,  $w$ , and  $EA$  are as same as those in QS method;

$K_d$ : drag resistance

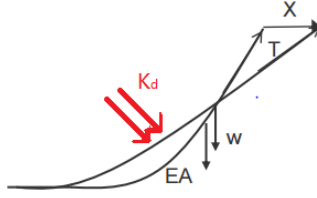


Figure 2.10: Sketch of dynamic method

### 2.3.3 Difference between QS and DM

Here is a sketch of motion and force components explaining the difference of Quasi-static and Dynamic Method (Figure 2.11).

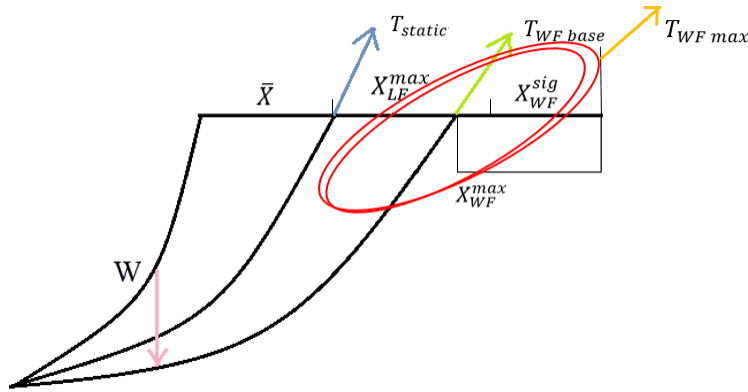


Figure 2.11: Motion explanation in sketch

In quasi-static method, the total motion is divided into three parts in frequency domain as Equation 2.49: mean motion  $\bar{X}$  corresponds to static force, max motion under LF effect  $X_{LF}^{max}$ , significant motion under WF effect  $X_{WF}^{sig}$ . And the corresponding max tension is calculated at the mooring line terminal at max offset.

However, the dynamic method has different calculation process. The analysis starts from the max total motion and subtracts the  $X_{WF}^{max}$  from it as Equation 2.60. Then the WF dynamic force, which is the combination of  $T_{WF}^{base}$  and  $T_{WF}^{max}$ , is obtained at the new offset X.

$$X = X_{max} - X_{WF}^{max} \quad (2.60)$$

The  $T_{static}$  and  $T_{WF}^{base}$  can be calculated based on catenary equation. But the  $T_{WF}^{max}$  has to be calculated by Finite Element Method, which divides the mooring line into many sub-elements

and the force for each element is calculated and combined. That's also the reason why dynamic method is always more accurate than quasi-static method.

# Chapter 3

## Rules and regulation for mooring systems

Before designing an offshore structure, also including applied mooring system, it is necessary to think about which rules and regulations are necessary to be taken into account. Those rules and regulations can be both generally with broad applicability; and locally, which related with the location of the structure.

For a mooring system, the main body are the mooring lines. Mooring lines shall resist all known loads with a sufficient margin, in the representation of maximum tension and offset from origin position. Different design limit states have to be checked for this purpose.

### 3.1 Category of Design Limit State

Norwegian Continental Shelf (NCS) is mostly used in Norway as mooring system design code. It is design against overload according to three limit states in order to ensure no failure of the mooring lines.

#### 3.1.1 Ultimate limit state (ULS)

Ultimate limit state refers to design against overload for an *intact* mooring system under extreme environmental loads (Veritas (2008) DNV-OS-E301). The extreme environmental loads is typically taken to be the value corresponding to an annual exceedance probability of  $10^{-2}$ , which also called the 100-year return period seastate (Snell et al. (2008)). By ULS control it shall be ensured that all foreseen loads can be resisted with an adequate margin.

For characteristic line tension, two components are considered:

- $T_{C-mean}$ : the characteristic mean line tension, also the mean tension, due to pretension and mean environmental loads. The mean environmental loads are caused by static wind, current and mean wave drift forces.
- $T_{C-dyn}$ : the characteristic dynamic line tension induced by LF and WF motions.

For motion, the following response statistics are determined in each environmental state considered:

- $X_{mean}$ : mean horizontal distance of the upper terminal point of the mooring line from the anchor.
- $\sigma_{xLF}$ : standard deviation of horizontal, LF motion of the upper terminal point in the mean mooring line direction.
- $\sigma_{xWF}$ :
  - In Quasi-static method: standard deviation of horizontal, WF motion of the upper terminal point in the mean mooring line direction.
  - In Dynamic method: standard deviation of the WF component of line tension, which is computed for a specific location  $X$  as Equation 2.60.

If all lines are identical, then the statistics are only needed for the line having the maximum tension. If the lines are different, then the statistics are needed for each line.

### 3.1.2 Accidental Limit State (ALS)

Accidental damage limit state refers design against overload for a *damaged* mooring system under extreme environmental loads. The extreme environmental loads is typically taken to be the value corresponding to an annual exceedance probability of  $10^{-4}$ , which also called the 10000-year return period seastate. By ALS control it shall be ensured that a given accidental scenario does not lead to a complete loss of the integrity of the structure.

In order to do the ALS control, one mooring line is always assumed to have failed and removed from the analysis.

- If all mooring lines are identical, one mooring line should be picked out in order to identify its impact on maximum tension on an adjacent line.
- If the mooring lines are not identical, it is necessary to consider different cases with different breaking lines, so as to check the maximum resulting tension in each line.

### 3.1.3 Fatigue Limit State (FLS)

Fatigue limit state is also an important design control regarding safety. It is design against fatigue failure taking all possible seastates into account, and ensures that the structure is designed with proper margin against fatigue failures. The characteristic fatigue damage refers to the summation of the accumulated damage in a mooring line component as a series of repetitive loading.

$$d_c = \sum_{i=1}^N d_i \quad (3.1)$$

Also a S-N curve can be used to represent the fatigue process.

## 3.2 Characteristic capacity for ULS and ALS

A mooring line is usually assembled from different material components of a few types. It is known that the strength of a long line is expected to be less than the average strength of the components that make up the line. This effect is taken into account when considering the characteristic capacity.

The following parameters are required for checking the system:

- $T_C$ : Characteristic tension in line
- $SF$ : Safety Factor, representing the margin of strength of the lines
- $S_{MBS}$ : Minimum breaking strength of the line

And characteristic capacity equation is obtained:

$$T_C \cdot SF \leq S_{MBS} \quad (3.2)$$

In a mooring system, this equation should be satisfied for every mooring line in order to be a qualified system. (Haver et al. (2001))

### 3.3 Safety factor of main body

From the previous section, Equation 3.2 is obtained to check capacity of mooring line. If changing the form of the equation, expression of safety factor is obtained as Equation 3.3:

$$SF = \frac{S_{MBS}}{T_C} \quad (3.3)$$

Since  $S_{MBS}$  for a certain type of mooring line always has a constant value and is tabulated, while  $T_C$  can be obtained through software analysis, a calculated  $SF$  can be obtained. It can be used as a reference to check whether the mooring line has enough strength margin under specific occasion by comparing the calculated  $SF$  with the standard  $SF$  given from regulation.

According to connecting unit type, operation objective and working duration, mooring system can be divided into mobile mooring system, permanent mooring system and weather restricted mooring system; while the first two types are more widely used in the offshore industry. Correspondingly, the safety factor also have two categories as  $SF$  for permanent mooring system and  $SF$  for mobile mooring system as Figure 3.1.

	Consequence class		
	Class 3	Class 2	Class 1
<b>Analysis</b>	Dynamic	Dynamic	Dynamic
Intact condition	2,20	2,00	1,50
One failure	1,50	1,35	1,20
One failure, transient	1,10	1,10	1,05
Two failures	1,50	1,35	N/A
Two failures, transient	1,10	1,10	N/A

(a)

	Consequence class		
	Class 3	Class 2	Class 1
<b>Analysis</b>	Dynamic	Dynamic	Dynamic
Intact condition	1,90	1,80	1,50
One line failure	1,30	1,20	1,10
One line failure, transient	1,10	1,10	1,05

(b)

Figure 3.1: Safety factor for (a) Mobile mooring system (b) Permanent mooring system

Based on the two tables in the figure, it is observed that the safety factors are divided into three consequence classes depending on operation conditions and units type. The description of consequence classes are as follows:

- *Class 1:* Apply to drilling unit when it is disconnected to the well;
- *Class 2:* Apply to production unit in shut-down condition with a flotel nearby in stand-off state; or drilling unit with connection to well, but not in operation;
- *Class 3:* Apply to production unit with a flotel nearby; or a drilling production which is operating.

The classes are ranked according to the severity of the consequence, with severity increasing from Class 1 to Class 3. From the description of classes, it is observed that the production unit with flotel will never be in Class 1, which implies that its operation condition is always more complex, and its consequence is usually severe.

However, since the model Flotel Superior is researched under 100-year return period weather condition and max operation condition, which is also regarded as the standby condition; the

above tables for safety factor are not suitable for this case. The standard  $SF$  used here should refer to Figure 3.2. (Lecture note of TMR4225 Marine Operation)

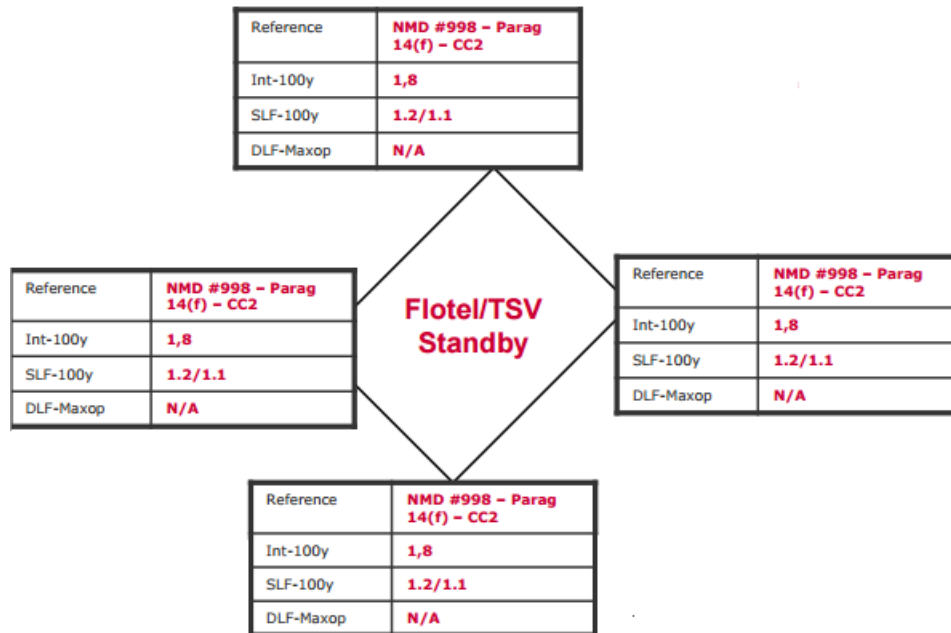


Figure 3.2: Safety factor for standby condition flotel(Larsen K., 2014)

### 3.4 Partial factor

After the main body is designed to have strength margin over the breaking strength, other components in the mooring line such as connecting links and terminations should also be designed to have strength exceeding the characteristic strength  $S_C$  of the main body of the mooring line, with high level of confidence. Thus partial safety factor is introduced.

Two consequence classes are introduced in the ULS and ALS, defined as:

- Class 1, where mooring system failure is unlikely to lead to unacceptable consequences such as loss of life, collision with an adjacent platform, uncontrolled outflow of oil or gas, capsizing or sinking.
- Class 2, where mooring system failure may well lead to unacceptable consequences of these types.

The partial safety factors given in Section 3.4.1 and 3.4.2 are applicable to chain, steel wire ropes and synthetic fibre ropes.

### 3.4.1 Partial factor for ULS

The design equation for the ULS is given by:

$$S_C - T_{C-mean}\gamma_{mean} - T_{C-dyn}\gamma_{dyn} \geq 0 \quad (3.4)$$

where  $T_{C-mean}$  and  $T_{C-dyn}$  are defined above;

$S_C$  is the characteristic strength of mooring line;

$\gamma_{mean}$  and  $\gamma_{dyn}$  are partial factor on mean tension and dynamic tension respectively.

Partial safety factor need in Equation 3.4 are given in Table 3.1.

Table 3.1: Partial safety factors for ULS

Consequence class	Type of analysis of WF tension	Partial safe factor on $T_{C-mean}$ $\gamma_{mean}$	Partial safe factor on $T_{C-dyn}$ $\gamma_{dyn}$
1	Dynamic	1.10	1.50
2	Dynamic	1.40	2.10
1	Quasi-static		1.70
2	Quasi-static		2.50

**Remark:**

- If  $T_{C-mean} > \frac{2}{3}T_{C-dyn}$ , when applying a dynamic analysis in consequence class 1, then a common value of 1.3 shall be applied as the partial factor instead of the separate static and dynamic safety factors given in Table 3.1. This is intended to ensure adequate safety in cases dominated by the mean tension component.
- For several types of single point mooring systems, the system is designed without redundancy. Therefore ALS is not applicable. These systems may be accepted provided that the safety factors given in Table 3.1 are increased by a factor of 1.2 and further that the loss of the mooring system is not resulting in a major pollution or major damage to the unit.

### 3.4.2 Partial factor for ALS

The design equation for the ALS is identical to the ULS, but the partial safety factors are given in Table 3.2.

Table 3.2: Partial safety factors for ALS

Consequence class	Type of analysis of WF tension	Partial safe factor on $T_{C-mean}$ $\gamma_{mean}$	Partial safe factor on $T_{C-dyn}$ $\gamma_{dyn}$
1	Dynamic	1.00	1.10
2	Dynamic	1.00	1.25
1	Quasi-static		1.10
2	Quasi-static		1.35

The combination of an accidental line failure with characteristic loads based on a 100-year return period is relatively conservative. Hence, the partial safety factors in Table 3.2 are relatively small.

# Chapter 4

## Software programs

### 4.1 MIMOSA

MIMOSA mooring software is mainly used for Frequency Domain analysis, and it offers to calculate the vessel's motion and mooring line tension by separating different frequency bands. What's more, several options are available for analysis of the properties of the mooring system and individual mooring lines. (Lie et al. (2003))

MIMOSA mooring software is interfaced with WADAM to ease the input of frequency dependent transfer functions and wave drift coefficients.

### 4.2 SIMO

According to the user manual, SIMO (Simulation of Marine Operations) is a time domain simulation program for study of motions and station-keeping of multi-body systems. It is interactive and modular, i.e. the results from one module becomes the input for the next module. The vessels are described with a set of coefficients that are frequency-dependent. The hydrodynamic coefficients like added-mass and radiation damping, the 1<sup>st</sup> order wave force and 2<sup>nd</sup> order mean drift forces are usually obtained from a diffraction solver like WAMIT or WADAM. Wind and current forces are computed by a set of direction-dependent coefficients, which includes both quadratic and linear forces (Reinholdtsen and Falkenberg (2001)).

Since the purpose of SIMO is to give good description of the floater motion, the slender ele-

ment structures can only be included with a crude finite element (FE) model. the mooring lines are assumed to form catenaries, and are modelled by the catenary equations. The results are presented as time series, statistics and spectral analysis of all forces and motions of the bodies in the analysed system.

### 4.3 RIFLEX

Originally, according to the user manual ([Fylling et al. \(1998\)](#)), RIFLEX is a computer program developed as a tool for analyzing flexible marine riser systems. However the program can also be used for analyzing other types of slender marine structures (e.g. mooring lines and umbilical). It is developed by MARINTEK and based on the non-linear finite element time domain formulation. The program features an extremely efficiency for irregular wave analysis; and high flexibility in modelling, enabling analysis for a wide range of structures.

The mooring lines are represented by a detailed FE model. Each slender element has two supernodes, one at the coordinate of anchor and the other one on the surface vessel. Each line may be built up by several segments with different length and properties. It ensures a convenient configuration of the mooring lines.

The surface vessel usually is modelled as a supply vessel, and floater motion must be given as an input to the analysis. Then the dynamic analysis can provide the corresponding response in tension.

# Chapter 5

## Establishing and verification of SIMO model

In the autumn semester of 2015, I have done the master project with the topic “Analysis and design of mooring system in harsh environment”. During that project, the Floatel Superior was the main research target. Its maximum offset in surge and max tension in mooring line were analyzed in frequency domain by using MIMOSA under different seastates.

In this thesis, this structure will be continually studied and focuses more on the viscous force modelling by using SIMO.

### 5.1 Vessel description

The model Floatel Superior is an accommodation and construction support vessel, also a stabilized semi-submersible vessel. The buoyancy is provided by two pontoons and four rectangular shaped stability columns. The water depth is 150m, which is typical shallow water. The structure is shown in Figure 5.1.



Figure 5.1: Floatel Superior overview

The principle dimension of it are as follows:

Table 5.1: Principle dimension of Floatel Superior

Principle Dimension	
Length Overall (Approx.)	96.0m
Breadth Overall	91.0m
Length of Pontoon	64.5m
Gangway height above water at operational draft	25.0m
Transit draft	8.425m
Survival draft	13.0m
Operational draft	18.0m
Transit displacement (Approx.)	21,385t
Survival displacement (Approx.)	25,472t
Operational displacement (Approx.)	29,030t
Transit draft air gap from MWL	19.08m
Survival draft air gap from MWL	14.50m
Operation draft air gap from MWL	9.50m

It is designed with 12 mooring lines evenly distributed, which combines chain and fibre. The basic characteristic of the mooring lines are summarized in Table 5.2.

Table 5.2: Mooring line characteristic

Segment	Material	Diameter[m]	Length[m]	Elastic modulus[kN/m <sup>2</sup> ]	Breaking strength[kN]	$C_{Dn}$	$C_{Dl}$
1	Chain	0.084	1200	60040000	8500	2.6	1.4
2	Fibre	0.185	1200	6430000	8500	1.8	0.18
3	Chain	0.084	250	60040000	8500	2.6	1.4

In MIMOSA, the segment number is counted from anchor to fairlead, which means segment 1 is near the anchor while segment 3 has the top end. Figure 5.2 shows the mooring system layout in MIMOSA.

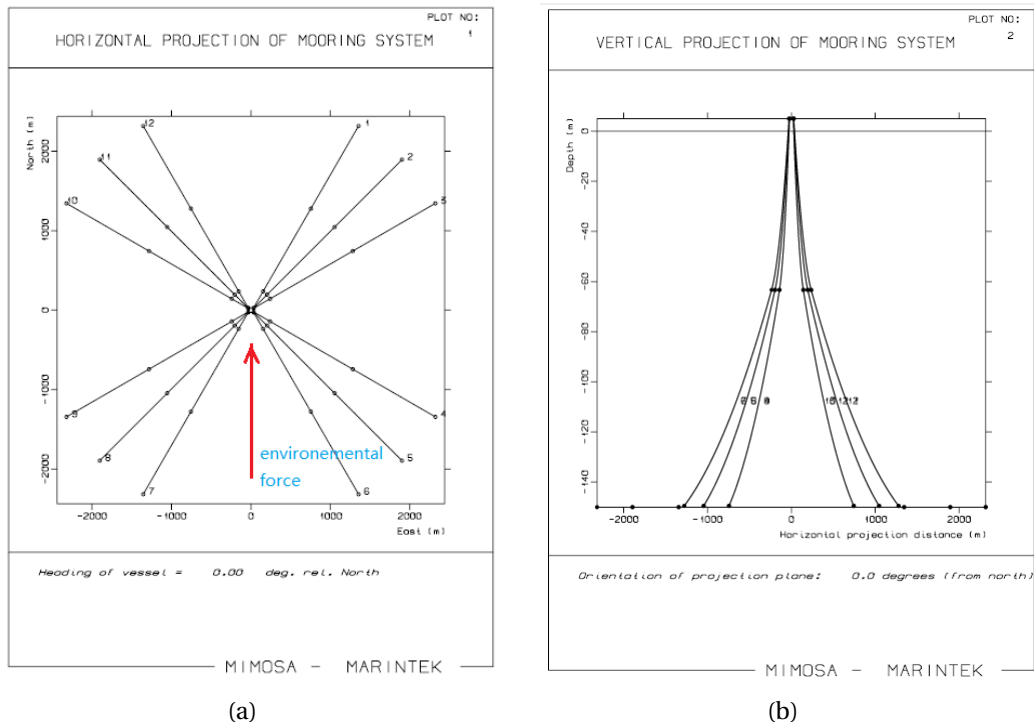
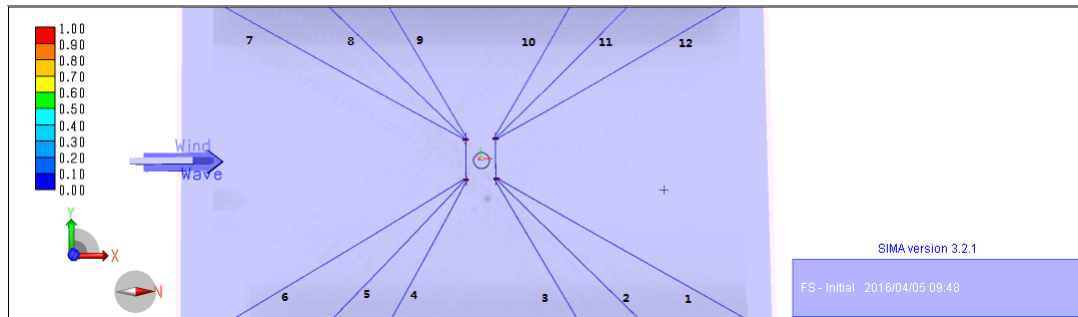
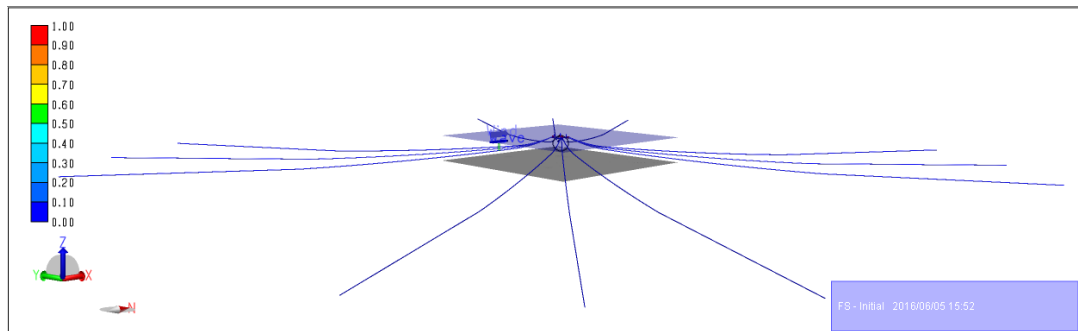


Figure 5.2: Mooring system layout in MIMOSA (a) top view (b) side view

In SIMO, the coordinate system is different from MIMOSA. The system setting is as follows.



(a)



(b)

Figure 5.3: Mooring system layout in SIMO (a) top view (b) side view

The structure is set as Bodytype 1 in SIMO, which represents large volume structure, with total motion simulated in time domain with 6 degrees of freedom.

## 5.2 Environmental condition description

Here 100-year return period environmental condition is selected as the extreme weather condition. It includes the 100-year wind case, 100-year wave case and 10-year current case.

- Wind

According to [Veritas \(2008\)](#), a 1-hour mean wind speed at 10m above the sea level, with a return period of 100 years is normally be used. The wind load is treated as a steady component in combination with a time varying gust component. The time varying wind is here described by a NPD wind spectrum.

Table 5.3: Wind input value

	Return Period	Wind Height	Wind Speed
Wind	100 years	10m above MWL	36m/s

- Wave

Seastates with return periods of 100 years shall normally be used as well. Combinations of significant wave height and peak period along the 100-year contour, defined by the Hei-drun Metocean Design Basis (Figure 5.4), shall be applied. The peak point of the contour is selected as the input for the comparison case in Section 5.4.4.

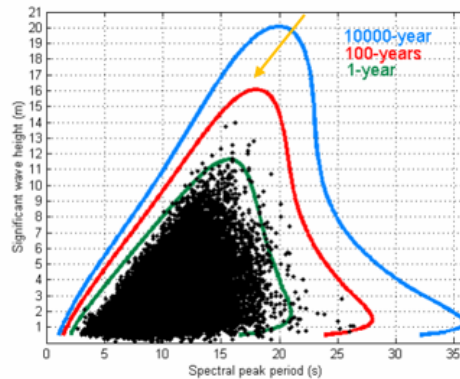
Figure 5.4: 100-year extreme contour lines in the  $H_s - T_p$  plane

Table 5.4: Wave input value

	Return Period	$H_s$	$T_p$
Wave	100 years	16m	18.2s

A JONSWAP double peaked wave spectrum is used for modelling the seastate. The waves are given with an average propagation direction without any spreading function.

- Current

A surface current speed with a 10-year return period should normally be used, based on the marginal distribution of current speeds at the location. Different from wave and wind such are stochastic process, current is always assumed to be stationary, with its speed and direction constant with time. However it can vary with water depth. Thus a current

profile is specified by setting the current speed and direction constant with increase of water depth.

Table 5.5: Current input value

	Return Period	Water Depth	Current Direction	Current Speed
Current	10 years	0m	0°	0.94m/s
		-25m	0°	0.94m/s
		-50m	0°	0.94m/s

All the environmental loads are assumed to be acting in the same direction, 0°, which is along the positive x-axis.

### 5.3 Project review

In the master project, Floatel Superior was researched under three different seastates with different combinations of  $H_s$  and  $T_p$ : (a)  $H_s=16\text{m}$ ,  $T_p=18.2\text{s}$ ; (b)  $H_s=15.5\text{m}$ ,  $T_p=15.5\text{s}$ ; (c)  $H_s=15.5\text{m}$ ,  $T_p=19.8\text{s}$ . Two different force incoming directions (0° and 45°) were performed in MIMOSA.

Under ULS, the intact system was analyzed and the maximum offset in surge and maximum tension in mooring lines were obtained as the required response reference. Line 7, the first line encountering the incoming force (see Figure 5.2), always showed the highest tension among all the lines. It also had the lowest  $SF$ , which was used to compare with standard  $SF$  in Figure 3.2. If it was smaller than the standard one, it was assumed to be risky and have great possibility to break in real practise. But if it had great margin over the standard  $SF$ , it was assumed to be safe and could be modified to be more efficient, i.e. reduce the diameter or length of mooring lines.

Later, different lines were designed to break in order to check the whole structure stability under ALS. Three seastates were used as well. Line with the second largest tension (line 8) and the closest line to line 7 in layout (line 6) were designed as failure one by one. Correspondingly, when there was one line failure, line 7 showed an obvious increase in tension value, while the whole structure shifted a larger offset from original point.

The seastate with severest consequence under ULS and ALS were picked out respectively and their motion components were analyzed. Later in Section 5.4.4, one special case is picked and compared with the result of SIMO file.

Then the sensitive test was carried. Different parameters, i.e. elastic modulus of fibre, pre-tension of all lines, damping coefficient and normal drag coefficient, were modified to see the change in structural response. The elastic modulus gave the largest impact on the response due to the great length of fibre segment. It reduced the offset from original point but increased the mooring line tension. Thus modification on elastic modulus required a careful balance between these two impacts.

## 5.4 Verification of SIMO model

Though the model under research are the same, the SIMO input file and the MIMOSA input file are from different sources. Also the global coordinate system setting in these two software are different from each other. Thus all the coordinates of structure and force direction should be revised. What's more, the MIMOSA input file is of 3 d.o.fs, while the SIMO input file is 6 d.o.fs; several parameters are obtained by hand calculation. Thus it needs to verify that the SIMO input file has consistency with the MIMOSA input file and is valid to use for further analysis.

### 5.4.1 Comparison of vessel file

The vessel file here includes different coefficients and transfer functions. All parameters are compared between two input files. The detailed comparison and analysis are in [Appendix A](#).

Based on all the comparison, some conclusions are obtained:

1. The SIMO input file is consistent with MIMOSA input file in all checked parameters. Even some of the plots show little discrepancy in phase or amplitude, the same trend is guaranteed. Therefore it is reasonable to use SIMO input file in the future analysis;
2. In the aspect of 1<sup>st</sup> order motion transfer function, the SIMO input file has consistency in all translation d.o.fs, but shows a lower damping level in rotation d.o.fs, which may cause some difference in the future comparison about dynamic analysis. More analysis regarding this effect will be discussed later.

### 5.4.2 Comparison of restoring force

Plot of restoring force can reflect the hydrostatic stiffness of the vessel. A static analysis is performed given an expected offset in surge in order to obtain the restoring force. The offset is limited within 30m, which is about 20% of the water depth. It should not be too large, since the flotel always works and connects to other units, the safety distance should be kept. Then the plot of restoring force versus offset can be obtained as Figure 5.5.



Figure 5.5: Restoring force curve from MIMOSA and SIMO

#### *Observation:*

The blue line represents the restoring force obtained in MIMOSA. When the offset is zero, the restoring force for the whole system is also zero; when the offset reaches the maximum, the restoring force increases to 9500 kN. And the restoring force curve is really linear. Thus no more linearization is needed.

After setting the non-environment condition and running the static analysis, the restoring force curve in SIMO is obtained as the red line. It is observed that when the offset is zero, the restoring force for the whole system is almost zero; when the offset reaches the maximum, the restoring force increases to 9200 kN approximately. And the restoring force curve is also really linear.

#### *Comparison:*

It is concluded that they match with each other well, since they have nearly same slope, which means the two files have similar hydrostatic stiffness. There is little discrepancy between

two lines when reaching the maximum offset. It is due to the lower damping level of the SIMO input file, however, it doesn't affect much. Thus in aspect of restoring force, the SIMO file is consistent with MIMOSA file.

### 5.4.3 Decay test

A motion decay test, often called a free oscillation test, is carried out by giving the system an initial displacement and then leaving the system free to oscillate. It discovers the damping level of the structure. Here the initial displacement is set as 20m, and the structure is released without any external environmental effects. Only the effect of linear damping drives the structure have the trend to do the pendulum action and stop at the original point gradually. The decay graph is obtained as Figure 5.6.

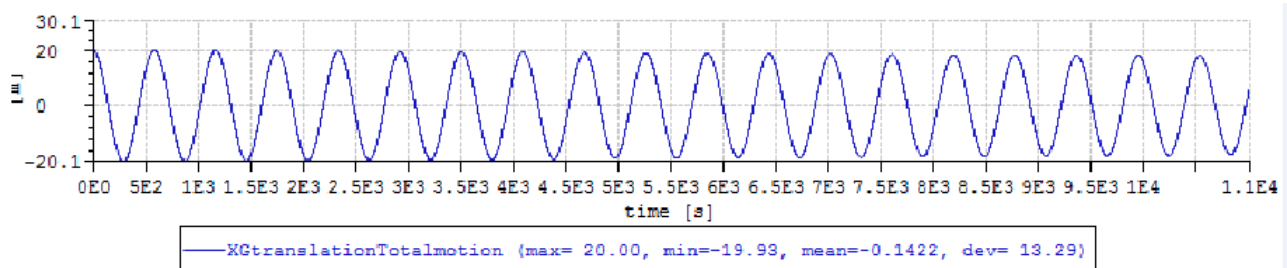


Figure 5.6: Decay test before adjusting the damping level

But the preliminary result is not so satisfying, since Figure 5.6 shows little decay among such a long period of time. Thus it is assumed that the damping level of the SIMO input file is too low. This is also the conclusion from the comparison of vessel file between two inputs (referred to Section 5.4.1). Then the linear damping value from the input file is checked.

Figure 5.7 shows the original data of linear damping. The damping value in surge and sway seem to be a factor 1000 too low compared to other degree of freedom.

	Surge	Sway	Heave	Roll	Pitch	Yaw
Surge	2078.8	0.0	0.0	0.0	0.0	0.0
Sway	0.0	1610.3	0.0	0.0	0.0	0.0
Heave	0.0	0.0	1.9053e+06	0.0	0.0	0.0
Roll	0.0	0.0	0.0	1.1609e+09	0.0	0.0
Pitch	0.0	0.0	0.0	0.0	1.1712e+09	0.0
Yaw	0.0	0.0	0.0	0.0	0.0	0.0

Figure 5.7: Linear damping value of SIMO input file [Ns/m]

Then the damping level is adjusted according to the MIMOSA file. The damping value in surge and sway are increased to  $1.5 \times 10^6$  Ns/m, then a more satisfying result is obtained as Figure 5.8. In order to show an accurate decay period, the picture is zoomed to a proper scale. It is observed that the motion decays to zero quite quickly, within 100 seconds.

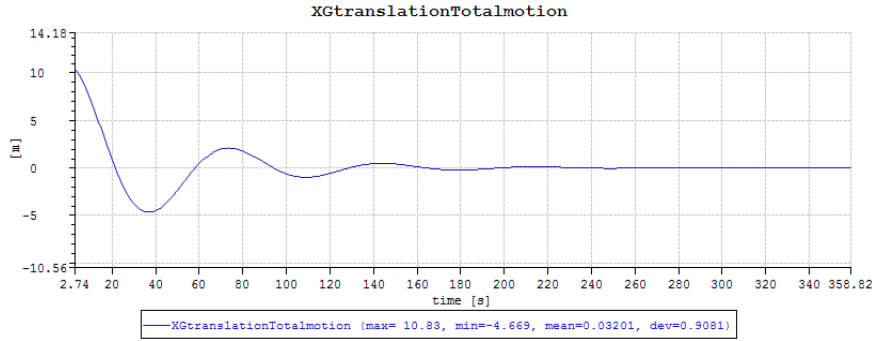


Figure 5.8: Decay test after adjusting the damping level

In order to check whether the modified damping value is reasonable, the damping level in surge is checked.

$$\lambda = \frac{\text{LinearDamping}}{\text{CriticalDamping}} \quad (5.1)$$

Theoretically, the linear damping should be around 30% of the critical damping, which means the value of  $\lambda$  is around 0.3. This empirical requirement is always used to check whether the linear damping value is reasonable.

Since the restoring plot is obtained in the last section, accordingly the hydrostatic stiffness  $K$  is obtained as the slope of the plot. Thus  $K = 3.07 \times 10^5$  N/m. From the input file, the mass

components is obtained as  $M = 2.5603 \times 10^7$  kg. Then the critical is calculated as follows:

$$D_{cri} = 2\sqrt{(M + A)K} = 5.61 \times 10^6 \text{Ns/m} \quad (5.2)$$

Then  $\lambda$  is obtained as 0.267, which is quite close to 0.3. Then it is concluded the modification in linear damping value is reasonable. The modified linear damping value is used afterwards in the analysis.

#### 5.4.4 Comparison of results for a specific case

Here a special case under ULS is picked out and the results from both files are compared. The environmental condition is set as Section 5.2.

*In MIMOSA:*

The max tension in all mooring lines are calculated by dynamic analysis and listed in Figure 5.9. Among them, line 7 is regarded as the most-loaded line with the lowest  $SF$  1.78. By comparing it with the standard  $SF$  1.70 from Figure 3.2, it is clear that line 7 still has some margin over the break limit. It means that line 7 has higher risk than others lines in real practise, but still in a controllable and safe status under extreme weather condition. The static force and the standard deviation are obtained as well and of importance in the later comparison.

\* MAXIMUM LINE TENSIONS. LF AND WF MOTION \*

---

Line No.	Top tension (kN)							Safety Segm.	
	Static	StD LF	Max LF	WF Base	StD WF	Max WF	Max Tot	factor	No.
1	684.3	102.1	322.6	953.5	205.2	842.3	1795.8	4.73	3
2	715.9	100.1	335.2	958.6	173.9	713.1	1671.7	5.08	3
3	773.7	86.0	305.9	966.5	137.1	567.8	1534.4	5.54	3
4	1358.6	209.0	1077.6	2176.3	153.9	611.8	2788.1	3.05	3
5	1547.7	329.7	1798.4	2954.9	220.1	864.0	3818.9	2.23	3
6	1703.9	431.4	2418.5	3634.0	272.0	1072.7	4706.6	1.81	3
7	1730.2	438.2	2446.2	3687.0	272.8	1075.9	4762.9	1.78	3
8	1568.5	337.6	1829.7	3005.6	221.1	867.5	3873.1	2.19	3
9	1373.6	216.0	1109.2	2220.5	154.5	613.5	2834.0	3.00	3
10	780.9	85.2	302.1	972.2	137.0	566.4	1538.6	5.52	3
11	718.4	99.8	331.1	959.1	173.4	710.7	1669.8	5.09	3
12	683.7	100.4	316.2	948.5	204.4	839.4	1787.9	4.75	3

Figure 5.9: Maximum tension in mooring lines (0°)

On the other hand, the motion of the structure is divided into three parts as Equation 2.49. The mean offset is obtained as the equilibrium position of the structure, which is 12.52m. Then the vessel is moved to the equilibrium position and further calculate the vessel motion under the combination effect of LF and WF. Its maximum offset in surge is around 36.75m from equilibrium position. It is combined with the LF max offset and the WF significant offset, referred to Figure 5.10.

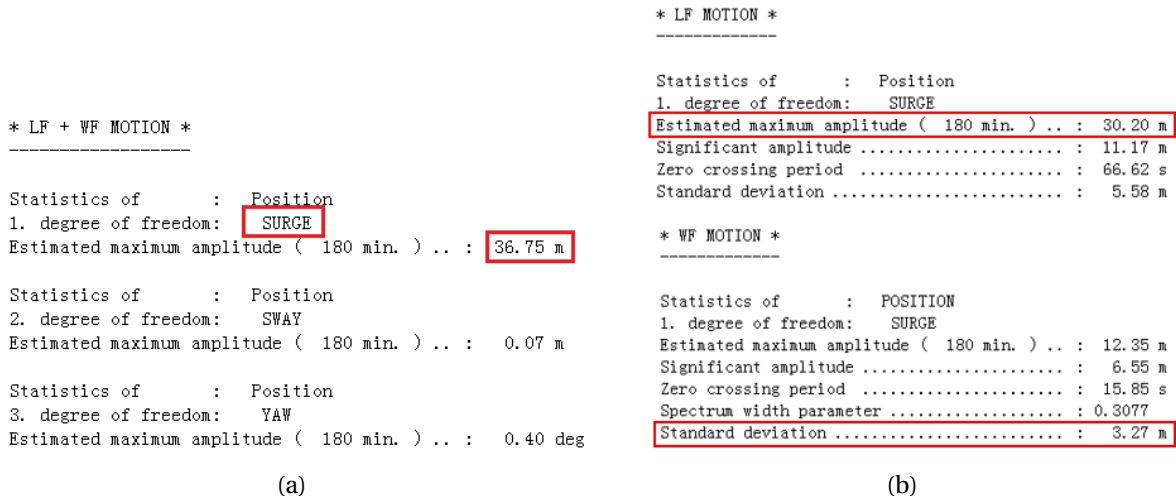


Figure 5.10: Offset under (a) combined LF and WF effects (b) LF and WF components respectively

Three motion components consist the max offset of model in MIMOSA, which is 49.27m.

*In SIMO:*

A 3-hour simulation is performed in time domain. With the same environment condition, the structural response is obtained following the post-processor chart as Figure 5.11.

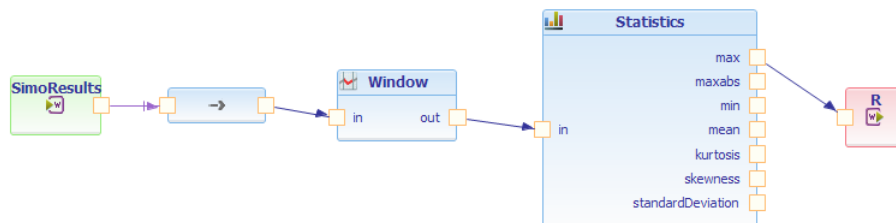


Figure 5.11: Post-processor chart to find max value in one simulation

The 'window' filter is used to limit the signal from 1200s to 12000s, since the very beginning of the signal is unstable and meaningless to mention. From the 'statics', many options are avail-

able. Usually the max value, mean value and standard deviation are necessary for analysis. Both tension and motion are available after analysis.

Then the wave seed is set as a variable, which controls the phase of the wave input. Each seed represents one 3-hour simulation, and the maximum tension in one simulation is obtained through the inner-workflow in SIMO, as Figure 5.12.

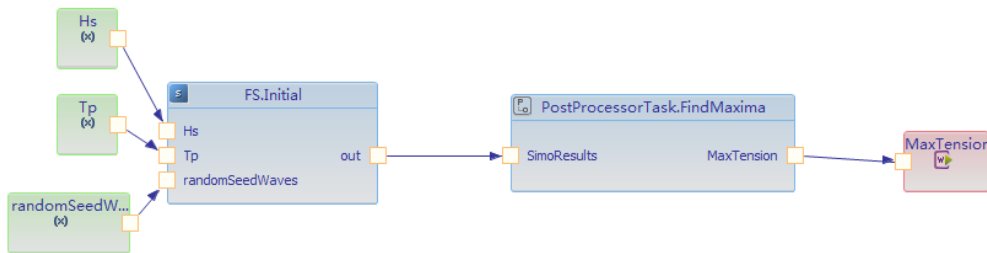


Figure 5.12: Inner-workflow in SIMO to find maxima

20 simulations are carried by variation in wave seeds and the series of result data are fitted to Gumbel Distribution as a straight line as Figure 5.13. Gumbel distribution is used to model the distribution of the maximum of a number of samples. A 90% probability maximum tension in 3-hour simulation is obtained as the tension result in a specific line.

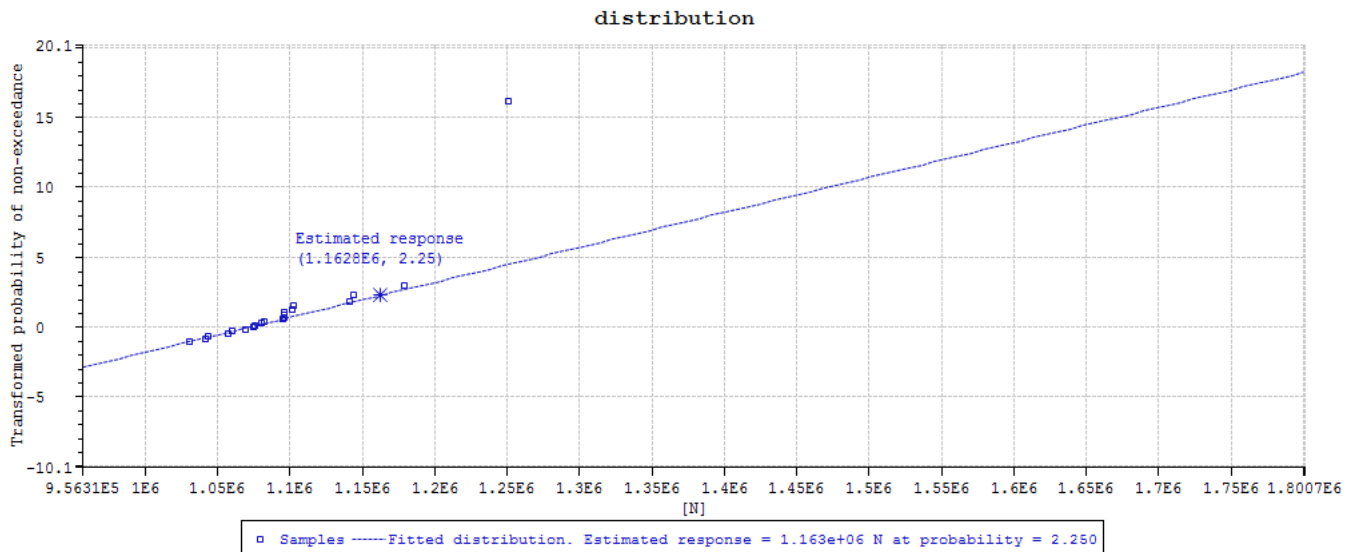


Figure 5.13: Fitted Gumbel distribution of maximum tension in Line 1

Similarly, all the tension in lines are obtained. Furthermore, static force—represented as mean tension, and standard deviation are also obtained. Since SIMO doesn't separate the LF and

WF effect, so there is only one combination result of standard deviation. Then this parameter will be just observed roughly instead of numerically. The detailed results are summarized as Table 5.6.

Table 5.6: Maximum tension in mooring lines from SIMO (0°) (unit:[kN])

Line No.	Max Tension	Mean Tension	Standard Deviation
1	1162.8	711.16	79.478
2	1131.9	746.18	73.704
3	1094.3	800.81	63.847
4	2441.4	1358.8	171.85
5	3194.7	1544.7	267.98
6	3791	1698.2	346.31
7	3787.6	1708.8	348.06
8	3200.4	1551.7	269.49
9	2454.6	1362.4	173
10	1095.5	803.02	64.056
11	1136.7	746.58	73.807
12	1171.8	710.13	79.448

Then the offset is obtained as well following the same workflow. Here only the motion in surge is of great importance. Since SIMO doesn't separate the frequency band, so in order to obtain the LF max offset and the WF significant offset, frequency filter is used. A low-frequency pass filter is used to get the LF max offset. It allows the signal whose frequency is lower than cut-off frequency to pass through. According to the LF period range  $T > 30s$ , the cut-off frequency is set as  $0.03333[1/s]$ . Also a high-frequency pass filter is applied to get the WF significant offset. It allows the signal whose frequency is higher than the cut-off frequency to pass through. According to the WF period range  $T = 5 - 30s$ , the cut-off frequency is also set as  $0.03333[1/s]$ . Then the motion result is obtained with different components contribution.

Table 5.7: Motion from SIMO input file (unit:[m])

Translation	Max	Mean	$LF_{max}$	$WF_{sig}$
x(surge)	38.27	12.27	29.99	3.3

### Summary:

To make the comparison more clear, the tension result from two files are presented in the same plot. The horizontal axis represents the line number while the vertical axis represents the

tension.

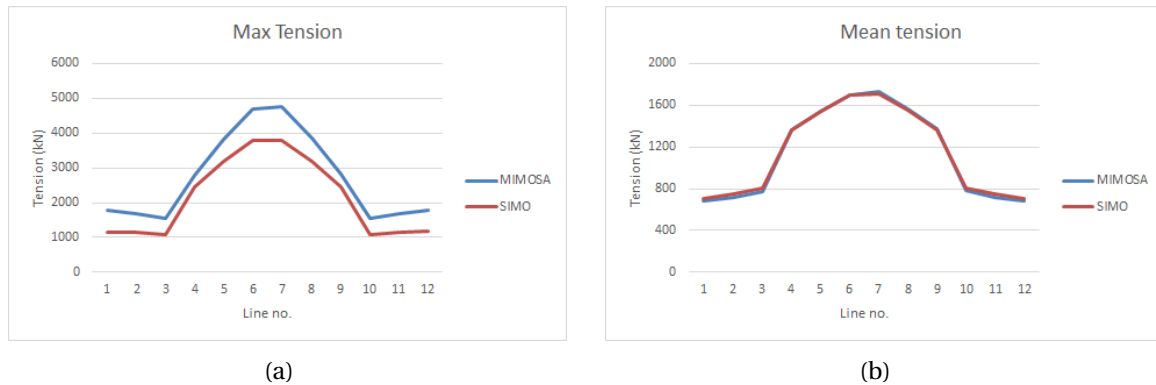


Figure 5.14: Result comparison in (a) max tension (b) mean tension (unit:[kN])

And the motion comparison is showed in Table 5.8:

Table 5.8: Motion comparison (unit:[m])

Translation in surge	Max	Mean	$LF_{max}$	$WF_{sig}$
MIMOSA	49.27	12.52	30.2	3.27
SIMO	38.27	12.27	29.99	3.3

*Observation:*

After comparison, there are some observations of great interest.

1. Based on Figure 5.14, the tension plot is symmetry for both files. It is due to the layout of the mooring lines. The lines which locate symmetrical about the force propagation direction always have similar tension value. It applies to both files.
2. There is certain discrepancy between the results from two software. Based on Figure 5.14(a), max tension values in MIMOSA—the blue line, are usually higher than the results from SIMO, represented by the red line. The difference between two largest tension value is almost 1000kN. The similarity is that, lines near environmental propagation (line 4-9) have larger tension value while the other side lines are in a more slack condition with lower tension.

However, it doesn't apply to mean tension. Mean tension results are really close, and the two lines almost overlap with each other. This applies to all mooring lines.

3. In SIMO, line 6 shows the highest maximum tension about 3791kN, and line 7 has a really close value following. In MIMOSA, it is line 7 which has the highest tension. Both line 6 and 7 are the first lines encountering directly with environment forces and they are in a symmetry layout. Thus no matter which one has the highest tension, it is quite reasonable.
4. In SIMO, all the results are obtained based on 20 simulations with the variation in wave seeds. The mean tension values and standard deviation values don't show much difference in 20 simulations. Then the 90% maximum value of them after fitted to Gumbel distribution, are quite close to the whole series of data. Therefore it is concluded that the wave seeds, which controls the wave phase, doesn't have much impact on mean tension and standard deviation.
5. In SIMO result, when trying to add three components of motion together, the sum is close to the max offset. Thus it matches with the motion Equation 2.49. It is a nice way to check the validity of the results. It doesn't require the sum has exactly same result with the max offset. Because each components is based on 20 simulations and obtained after filtering the frequency band, thus they can't appear at the same time. The sum is similar to the total one is good enough.
6. Based on Table 5.8, the motion components, i.e. mean offset,  $LF_{max}$  offset and  $WF_{sig}$  offset, from both files have quite similar value, but the max offset is quite different from each other. The max offset from SIMO is smaller than MIMOSA, because the SIMO result is based on 20 simulation and takes the 90% maximum value as the motion components. Frequency filter is also used. The 'max' result can't appear at the same time. What's more, MIMOSA achieves the result by separating the frequency band and doing the dynamic analysis; while SIMO just uses frequency filter and ignore the dynamic effect. Thus the result from MIMOSA is more accurate and larger.

*Explanation:*

The main reasons for the differences are analyzed as follows:

1. Analysis methods are different

MIMOSA uses Frequency Domain analysis method, which means that the force and motion are divided into low frequency band and wave frequency band, then the final result is combined from the two parts. And also all the non-linear components are linearized before doing the calculation. SIMO uses Time Domain analysis method, which does the analysis in one-go, ignoring the effect of different frequencies. All the non-linear components are taken into account directly.

The detailed difference between these two analysis methods refers to Section [2.2.4](#).

## 2. Calculation methods are different

MIMOSA calculates tension and motion by Dynamic Method with the top end motion giving the mooring line tension  $T = T(x, \dot{x}, \ddot{x})$ . It takes the drag force and inertia force into account. Discretion is also applied to the mooring lines according to Finite Element Method. However, SIMO uses Quasi-static method to do calculation, that only the top end position gives the mooring line tension,  $T = T(x)$ .

Thus the MIMOSA result is more accurate than SIMO result due to the discretion and it should be larger than SIMO result since it includes the drag dynamic effect. The detailed difference between these two calculation methods refers to Section [2.3](#).

## 3. MIMOSA file has a higher force coefficient

Based on Section [5.4.1](#) and Appendix [A](#), it is observed that MIMOSA input file has a higher value in several coefficients and transfer functions compared to the SIMO input file. It has certain effect on the tension and offset.



# Chapter 6

## Assessment and comparison of models for viscous loads

Based on the illustration of three different types of viscous effect model in Chapter 2, two methods are applied in order to add viscous effect on Floatal Superior.

### 1. Slender element method

Slender element method is to create slender elements along columns and pontoons, select proper drag coefficients from regulation and calculate the external effect on the slender elements. Then the excitation on slender elements is added to the whole structure to get the total external excitation. However, the excitation on the slender elements also includes the current force, which means the same effect is counted twice. Thus the corresponding quadratic current coefficients from the input file should be set as zero when using the slender elements in the analysis.

### 2. Correction formula method

Correction formula method is to use an empirical formula to modify the wave drift coefficient. The original wave drift coefficients in the input file is only based on the potential flow, and the extra viscous-induced wave drift force on structure should be added by using the formula. No extra elements are needed, only use the formula and calculate a new series input data of wave drift coefficients.

## 6.1 Slender elements method

### 6.1.1 Create slender elements

In order to account for viscous effect on Floatel Superior, several slender elements are created along columns and pontoons. The length of the slender elements are exactly same with the original column or pontoon. When determining the coordinates of slender elements, the survival air gap and draft are used (referred to Table 5.1). The detailed dimension of columns and pontoons, and their placement number are set as Figure 6.1.

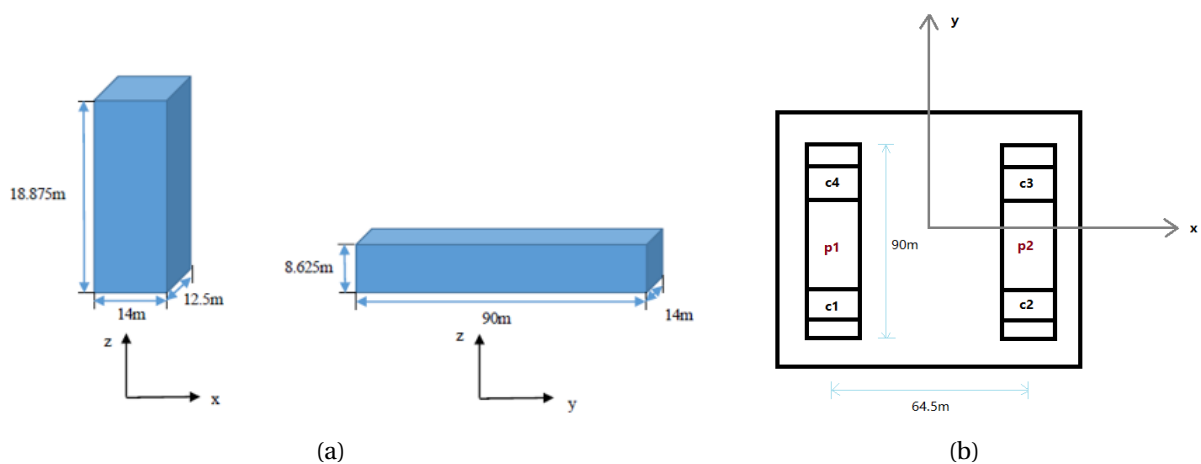


Figure 6.1: (a)Dimension (b)Placement of columns and pontoons in global coordinate system

Then the coordinates of slender elements are obtained in Table 6.1. And the local coordinate system is built accordingly as the new x-axis is set from point 1 to point 2. (Reinholdtsen and Falkenberg (2001))

Table 6.1: Coordinates of slender elements

Slender Element	Point 1 [m]			Point 2 [m]		
	x	y	z	x	y	z
Column 1	-25.25	-25.5	14.5	-25.25	-25.5	-4.375
Column 2	25.25	-25.5	14.5	25.25	-25.5	-4.375
Column 3	25.25	25.5	14.5	25.25	25.5	-4.375
Column 4	-25.25	25.5	14.5	-25.25	25.5	-4.375
Pontoon 1	-25.25	45	-8.6875	-25.25	-45	-8.6875
Pontoon 2	25.25	45	-8.6875	25.25	-45	-8.6875

### 6.1.2 Drag coefficients from theory

After determining the coordinates of slender elements in previous section, the quadratic drag coefficient of them need to be figured out. When using Morison's equation to calculate the hydrodynamic loads on a structure, one should take care of the variation of drag coefficients. It is expressed as a function of Reynolds number, Keulegan-Carpenter number and the roughness.

$$C_D = C_D(R_e, KC, \Delta) \quad (6.1)$$

Here the regulation DNV-RP-C205 "Environmental Conditions and Environmental Loads" is used as reference (Veritas (2010)). In this regulation, drag force per unit length of slender element is expressed as:

$$f = \frac{1}{2} \rho C_{DS} D u^2 \quad (6.2)$$

where  $C_{DS}$  represents drag coefficient in steady flow;  $D$  is the characteristic width[m].

Since the cross-sections of columns and pontoons are rectangular with rounded corners, 'Type 4' is selected from the regulation as the base case.

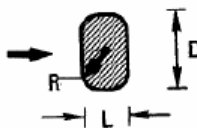
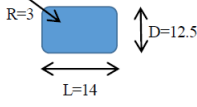
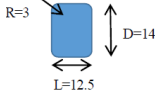
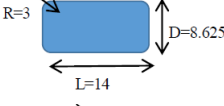
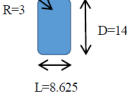
4. Rectangle with rounded corners		L/D	R/D	$C_D$	L/D	R/D	$C_D$
	0.5	0	2.5	2.0	0	1.6	
		0.021	2.2		0.042	1.4	
		0.083	1.9		0.167	0.7	
		0.250	1.6		0.50	0.4	
	1.0	0	2.2	6.0	0	0.89	
		0.021	2.0		0.5	0.29	
		0.167	1.2				
		0.333	1.0				
$R_e \sim 10^5$							

Figure 6.2: Drag coefficients for rectangular cross-section

The drag coefficients are selected in two directions on the cross-sections of columns and pontoons. These two directions corresponds to the y and z in local coordinate system. The proposed drag coefficients are summarized in Table 6.2.

Table 6.2: Base drag coefficient for slender elements

Element	Cross-section	L/D	R/D	$C_{DS}$
Column		$\approx 1$	0.24 $\rightarrow$ 0.167	$C_{dy} = 1.2$
		$\approx 1$	0.21 $\rightarrow$ 0.167	$C_{dz} = 1.2$
Pontoon		$\approx 2$	0.347 $\rightarrow$ 0.50	$C_{dy} = 0.4$
		$\approx 0.5$	0.214 $\rightarrow$ 0.25	$C_{dz} = 1.6$

However, value in Table 6.2 can not be used directly in SIMO. Because the quadratic drag coefficient in SIMO is defined as:

$$C_D = \frac{1}{2} \rho C_{DS} D \tag{6.3}$$

with unit  $[Ns^2/m^3]$ .

Then the input values of quadratic drag coefficient are calculated accordingly as Table 6.3:

Table 6.3: Quadratic drag coefficient for slender element

	$C_{2x}$	$C_{2y}$	$C_{2z}$
Column	0	7687.5	8610
Pontoon	0	1768.1	11480

*Explanation:*

1.  $C_{2x}$  is set as zero since only the cross-flow is of great importance and gives the drag force and lift force to the column or pontoon, which corresponds to the force from  $C_{2y}$  and  $C_{2z}$ . And  $C_{2x}$ , corresponding to local axis x, but in global coordinates, corresponds to the heave direction. Vibration and velocity in heave is too small compared to other directions. Thus the effect from  $C_{2x}$  can be regarded as zero.
2. The selected coefficient only applies to steady flow according to the regulation. In our

case, the oscillating flow should be considered. For oscillating flow, the drag coefficient is considered as the coefficient in steady flow multiply with a factor as Equation 6.4.

$$C_{DO} = C_{DS} \times factor \quad (6.4)$$

Now, the preliminary comparison will be done in order to see the effect of taking viscous force into account. So the  $C_{DS}$  is used as a base case.

After settling the drag coefficients, the original current coefficient in surge are set as zero in order to avoid the double-calculation of current force. Since only surge motion matters in this paper, only current coefficients in surge are set as zero. All directions are chosen, instead of only force propagating direction  $0^\circ$ , since even current comes in other directions, it will also have a partial component in  $0^\circ$ . In this way all current effects are eliminated totally

### 6.1.3 Sensitivity test of drag coefficients

In this section, a sensitivity test about drag coefficients is done. The value of drag coefficient is tuned, and the structural response is analyzed correspondingly. The change in motion and tension reflects the influence of drag coefficients on viscous effect.

$$C_{Cu}^{File} = 4C_D^{Column} + 2C_D^{Pontoon} \quad (6.5)$$

Equation 6.5 is used for tuning the drag coefficient. Based on the equation, it is easy to see that the viscous effect are contributed from both columns and pontoons. Then the strategy for the sensitivity test is to assume all viscous effect are coming from only one source, i.e only from column or only from pontoon. Since only the cross-flow is important for the viscous effect, then only the drag coefficient in y direction ( $C_{2y}$  in local system) is considered.

The quadratic current coefficient under  $0^\circ$  force direction in surge is set as the value of  $C_{Cu}^{File}$ , due to it has the most important direction of force and degree of freedom. So  $C_{Cu}^{File} = 3.129 \times 10^5 N s^2 / m^3$ . Then when assuming all viscous effect comes from pontoons, the coefficients of column is set as zero and a tuned  $C_D^{Pontoon}$  is obtained; similarly, when assuming all viscous effect comes from columns, the coefficients of pontoon is set as zero and a tuned  $C_D^{Column}$  is

obtained. Table 6.4 represents the result of tuned drag coefficients.

Table 6.4: Tuned drag coefficient on columns and pontoons

Tuned Case	$C_D^{Column}$	$C_D^{Pontoon}$
a	4144.37	0
b	0	1738.33

Compared the tuned drag coefficient from Table 6.4 with the proposed drag coefficient from Table 6.3, it is obvious to see the  $C_D^{Column}$  decreases almost 50% while  $C_D^{Pontoon}$  has a quite similar value. By using the tuned coefficient, it is expected to see the impacts of variation in drag coefficients.

## 6.2 Correction formula method

Stansberg et al. (2015) provided a research in The Joint Industry Project (EXWAVE) and confirmed the need to improve or at least apply adjustments on theoretical models applied in the industry for slowly varying forces based on the 1<sup>st</sup> order potential theory, for applications in high seastate and with current.

Until generally accepted improved methods and procedures have been established, some immediate precautions should be taken by industry. A simple empirical correction formula for wave drift force coefficients of semis is proposed. It applies to high waves and in current, which is in the direction of wave propagation and with a current component  $U$  parallel to the waves. It is a sum of two terms as Equation 6.6: the first term from potential flow effects and the second term from viscous effects.

$$f_D = F_D(\omega, U, H_s) / A^2 = [f_{d,pot} * (1 + C_p * U) + B(G * U + H_s)] \quad (6.6)$$

- From potential flow:

$f_{d,pot} = 2^{\text{nd}}$  mean wave drift coefficients from 1<sup>st</sup> potential theory

$A =$  wave amplitude

$C_p =$  potential flow wave-current interaction coefficient, chosen to be 0.25

- From viscous effect:

$$B = B' * d_{sum}; \text{ where } B' = k * p, d_{sum} = \sum d_i$$

$$k = \text{wave number} = \frac{\omega^2}{g}$$

$$p = \exp[-1.25 (kD_0)^2], [\text{kN}/\text{m}^3]$$

$D_0$  = diameter of main columns

$G = 10$  (with dimension time, [s]), this parameter comprises the viscous wave-current interaction part, found empirically

The basic idea of the viscous drift formulation in  $B = B' * d_{sum} = k * p * \sum d_i$  is adopted from the Morison equation drag force approach (Veritas (2010), DNV-RP-C205). The extra parameter  $p$  limits the upper frequency range in which viscous effects are included, determined from the normalized upper wave number  $kD_0$ , and based upon the assumption that viscous drift force do not contribute significantly in short waves.

Since the environmental force propagating in  $0^\circ$ , and the motion in surge is more important than other d.o.fs, the wave drift coefficients in surge under  $0^\circ$  force is modified according to the formula. Here is the comparison.

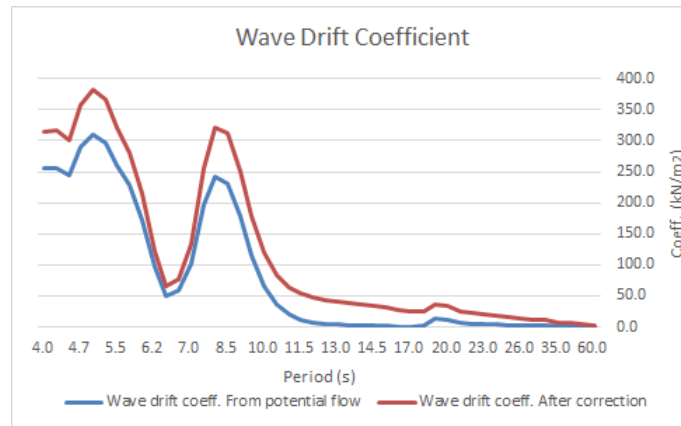


Figure 6.3: Wave drift coefficient in surge under  $0^\circ$

The blue line represents the original wave drift coefficient which is only based on potential flow. The red line represents the corrected wave drift coefficient with viscous effect. It is clear that the new curve shows a higher coefficient value and comes to zero at a later period (also can say at small frequency band). The discrepancy between the two lines is due to the extra viscous

effect on the structure. It is believed that new coefficient will give more accurate response result than the previous one.

### 6.3 Comparison between two methods

Both methods try to take viscous effect into analysis. Their aims are the same, but with different approaches.

Section 6.1 uses slender element method by introducing new slender elements along pontoons and columns. The extra wave drift force due to viscous effect is added to the structure. This method has impact both on excitation and damping term.

Current force on a strip is expressed as Equation 2.26. But for slender elements, the velocity form in the equation is modified.

$$Q_{cu} = C_{cu} [(\bar{V} + u) - x_{tot}] |(\bar{V} + u) - x_{tot}| \quad (6.7)$$

$$Q_{cu} = C_{cu} [(\bar{V} + u) - (x_{LF} + x_{WF})] |(\bar{V} + u) - (x_{LF} + x_{WF})| \quad (6.8)$$

The original relative velocity  $\bar{V} - x_{LF}$ , is replaced by  $(\bar{V} + u) - x_{tot} = (\bar{V} + u) - (x_{LF} + x_{WF})$ . Here  $(\bar{V} + u)$  is the total velocity of both current and wave, which results from external excitation;  $(x_{LF} + x_{WF})$  is the structural oscillating velocity.

As this equation can be separated, it is observed that it not only includes a term to increase the external excitation, i.e.  $C_{cu} (\bar{V} + u)^2$ , but also has a term to increase the damping, i.e.  $C_{cu} (x_{LF} + x_{WF})^2$ , which can be moved to the left side of the motion equation.

When the damping term increases, the response of structure will be suppressed. But when the external excitation increase, the structure will have larger response. Thus slender element method is working under the balance of damping and excitation.

However, correction formula method focuses on modifying the wave drift coefficient directly to account for the viscous drift force, which only has an positive impact on the excitation. Thus it is expected to have a more obvious change in response compared to slender element method.

More comparison in response under these two different methods will be illustrated in following section.

## 6.4 Case summary

This section mainly gives the description of all design cases and establish the comparison group.

- *Case 1*

Case 1 can be also called as the original case. "Original" means that it is the standard base case. It only uses the SIMO input file directly without any method related with viscous effect (the file after modifying the linear damping value, referred to Section 5.4.3).

- *Case 2*

From Case 2, all the cases try to take viscous effect into account by different methods. Case 2 is regarded as the main viscous model, since the slender elements method is assumed quite reasonable and accurate. It introduces the slender elements as Section 6.1.1 and find the proposed drag coefficient as Section 6.1.2. In order to avoid double-calculation of the current effect on structure, the current coefficient in surge under all directions are set as zero.

- *Case 3*

Case 3 is a further development of Case 2, since it not only takes viscous effect into account, but also tries to test the sensitivity of viscous effect by adjusting drag coefficient.

Case 3 introduces slender elements and proposed drag coefficient as Case 2. And it assumes all the viscous effect are from columns by setting current coefficient of pontoon as zero, then a tuned value of  $C_{Cu}^{Column}$  is obtained. The input drag coefficient is as Table 6.5, also corresponds to Table 6.4 tuned case a.

Table 6.5: Input drag coefficient in Case 3

	$C_{Cu}^{Column}$	$C_{Cu}^{Pontoon}$
Case 3	4144.37	0

- *Case 4*

Case 4 is another further development of Case 2, paralleling with Case 3. It introduces slender elements and proposed drag coefficient as Case 2. And it assumes all the viscous

effect are from pontoons by setting current coefficient of column as zero, then a tuned value of  $C_{Cu}^{Pontoon}$  is obtained. The input drag coefficient is as Table 6.6, also corresponds to Table 6.4 tuned case b.

Table 6.6: Input drag coefficient in Case 4

	$C_{Cu}^{Column}$	$C_{Cu}^{Pontoon}$
Case 4	0	1738.33

- *Case 5*

Case 5 represents the correction formula method, corresponding to Section 6.2. It mainly use an empirical equation to correct the wave drift coefficient in surge. The original wave drift coefficient results from potential flow only, while the new one includes the effect from viscous flow. Since the correction equation is empirical, the accuracy of this method is not certain or clear. This case will be used to compare with other cases to assess the level of accuracy.

To make it more straight-forward, all the cases and the main characters are summarized as Table 6.7.

Table 6.7: Cases summary for viscous effect

Case no.	Slender elements	Quadratic current coefficient $C_{21} = 0$	Tuned $C_d$	Correction formula
1				
2	×	×		
3	×	×	×, tuned $C_C$	
4	×	×	×, tuned $C_P$	
5				×

## 6.5 Result analysis

After defining all the cases, the same SIMO analysis in time domain (as Section 5.4.4) is applied and the corresponding structural response is obtained.

### 6.5.1 Comparison in motion

All motion components in surge is summarized as Table 6.8. The  $LF_{max}$  offset and  $WF_{sig}$  offset are obtained by using frequency filter as the same process in Section 5.4.4.

Table 6.8: Motion in all cases (unit:[m])

Case	Max	Mean	$LF_{max}$	$WF_{sig}$
1	38.27	12.27	29.99	3.3
2	42.38	13.9	34.73	3.26
3	39.33	10.94	31.79	3.33
4	38.57	12.09	30.65	3.29
5	53.45	15.65	42.91	3.35

*Observation:*

1. Based on data of the 5<sup>th</sup> column, it is observed that  $WF_{sig}$  offset don't have much difference in value among all the cases. The difference in maximum offset is due to the variation in mean offset and  $LF_{max}$  offset.
2. Compare Case 1 with Case 2: the increase in offset reflects the extra viscous-induced effect on columns and pontoons.
3. Compare Case 1 with Case 5: there is really dramatic increase in motion components, especially in  $LF_{max}$  offset and mean offset. The correction in wave drift coefficients has great impact on the structural response.
4. Compare Case 2 with Case 5: both two cases are used to include viscous effect in the analysis. From the result, both cases have certain good effect in introducing viscous effect on structural response, while the correction formula has much more obvious influence. Since Case 5 uses the empirical formula, the accuracy of the result is not certain to us.
5. Case 3 and 4 are established for sensitivity test of drag coefficient. Both cases assume that viscous effect only originates from one type of elements and adjust the drag coefficient correspondingly. Then it is obtained that a relative smaller motion response compared to Case 2.

*Analysis:*

1. From observation 1,  $WF_{sig}$  offset doesn't change much because offset in WF band is controlled by transfer function from potential flow. All the modification, i.e. introduce slender elements or use correction formula, only have effect on LF and mean excitation.
2. From observation 2, it is concluded that slender elements method can indeed include the viscous effect in the analysis. Since model Floatel Superior is a really big structure, it always has inertia dominated response. But in high seastate, viscous effect may have large impact. According to Section 6.3, the slender element method has impact both on excitation and damping: larger excitation makes larger motion while larger damping suppresses the motion.

From the motion result, the structure still has larger translation in surge compared to the original one. Then it is assumed that the impact on excitation is more dominated than the impact on damping. As the main viscous model, it is believed that result from Case 2 is quite reasonable.

3. From observation 3, Case 5 shows a much larger motion value than Case 1, especially in  $LF_{max}$  offset and mean offset. It can be explained by the expression for the mean drift force and LF wave drift force illustrated in Chapter 2.

$$q_{wa}^- = 2 \int_0^{\infty} C_{wa}(\omega) S_{\eta}(\omega) d\omega$$

$$S_{wa} = 8 \int_0^{\infty} C_{wa}\left(\omega + \frac{\mu}{2}\right) \cdot C_{wa}\left(\omega + \frac{\mu}{2}\right) \cdot S_{\eta}(\omega) \cdot S_{\eta}(\omega + \mu) d\omega$$

After using the correction formula, the wave drift coefficient  $C_{wa}$  increases a lot. Thus  $q_{wa}$  and  $S_{wa}$  have an increase at different extent. That's why Case 5 has extremely obvious increase in these two term.

4. From observation 4, it is concluded that correction formula method has great impact on the structure by including viscous-induced wave drift force. It matches with the expectation in Section 6.3.

However, the accuracy of this formula is uncertain. Since it has too much difference from Case 2, which is due to the effect of damping term, it is assumed that it may exaggerate the viscous effect by ignoring the viscous-induced damping term and not so accurate to use.

5. From observation 5, it is reasonable to have smaller motion in Case 3 and 4 than Case 2. Because Case 2 accounts for viscous effect both from column and pontoons; while Case 3 accounts that only from columns and Case 4 accounts that only from pontoons. Also, according to Table 6.4, all the tuned coefficient are smaller than the original calculated ones. Thus it is expected to have smaller result.

If comparing the Case 3 and Case 4, which represents the difference in viscous sources, Case 3 has a bit larger motion than Case 4, which means the viscous effect from column is stronger than that from pontoon. According to Section 2.1, it is easy to determine that, viscous in Case 3 is mainly based on the first two models about free surface and wave-current interaction, while Case 4 is based on the third model related with cross-flow on pontoon.

It is concluded that, viscous effect due to free surface and wave-interaction is more dominating in practise than that due to cross-flow on pontoon.

### 6.5.2 Comparison in tension

Based on the comparison case in Section 5.4.4, it is observed that line 6 and 7, which are in symmetrical layout as Figure 5.3, are the first group of lines encounter the propagating environmental force, and also the most-loaded line. Thus in this section, only line 6 and 7 will be picked out and compare their tension in different cases. Detailed tension information for all lines can be found in Appendix B.

Here is the summary table of tension of line 6 and 7 in all cases.

Table 6.9: Tension of line 6 and 7 in all cases (unit:[kN])

Case	Line 6			Line 7		
	Max	Mean	Standard Deivation	Max	Mean	Standard Deivation
1	3791	1698.2	346.31	3787.6	1708.8	348.06
2	4139.1	1813.6	382.97	4149.2	1824.1	384.65
3	3876.6	1613.8	360.81	3884	1623.4	360.81
4	3812.4	1686.7	347.03	3815.7	1696.7	349.01
5	5115.6	1947.1	493.72	5109.7	1958.4	494.81

*Observation:*

1. For all tension components, line 6 and 7 share quite close value in all cases.
2. Compare Case 1 with Case 2: the increase in tension components reflects that both lines are in a more stretching status. It has consistency with the increase in offset.
3. Compare Case 1 with Case 5: there is really dramatic increase in tension value. The net increase amount in tension is assumed as the viscous-induced wave drift force. However, the accuracy level of this method is still a doubt .
4. Compare Case 2 with Case 5: both two cases are used to include viscous effect in the analysis. From the result, both cases have certain good effect in introducing viscous effect on structural response, while the correction formula has much more obvious influence.
5. Case 3 and 4 are established for sensitivity test of drag coefficient. The tension results have same trend with the motion result. Both cases have a relative smaller tension value than Case 2.

*Analysis:*

1. For observation 1, line 6 and 7 are symmetrical about the force propagating direction in the system layout, with same exposure area and angle to the propagating environment forces. Thus they are expected to have similar tension response.
2. The tension value of mooring system always varies corresponding to the fairlead displacement. If the fairlead has a positive displacement, and make the lines become more

stretching, then the tension will increase; on the contrary, if the fairlead have a negative displacement and make the line stay in a more slack status, the tension in line will decrease.

In all the cases, since the structure moves in positive surge direction, so do the fairlead displacements of line 6 and 7, their tension also increase in consistency with offset.

3. The difference between Case 2 and Case 5 is explained in Section 6.3, which mainly about the damping term. The damping term also has great impact on the tension result. That's why Case 5 has a extremely higher value than Case 1 and Case 2.

## 6.6 Modify damping term in Case 5

Case 2 and Case 5 use different methods to take viscous effect into account and obtain the response in motion and tension respectively. Based on the result analysis in the last section, it is found that both cases shows a higher value in tension and motion, which represents that the viscous-induced structural response is included in the analysis. However, Case 5 shows a dramatic increase in both results, whose accuracy is doubted.

The main difference between these two methods are the damping term. Since slender elements method is a "play" about the balance between excitation and damping, it is supposed have a more realistic result. On the contrary, Case 5 only cares about the viscous effect on excitation and ignore effect on dynamic terms.

The purpose of this section mainly focus on improving the correction formula method and raising the accuracy of the analysis. It is glad to know how much extra damping is still needed to have a better result. Here Case 2 is assumed to be reliable, and the damping term in Case 5 will be modified, in order to match its result with Case 2.

Four new cases are created by adjusting the linear damping value with other input keep the same. It is increased little by little, from 50% to 300% of the original value. The extra damping cases and their character are summarized in Table 6.10.

Table 6.10: Extra damping comparison group

Case	Original linear damping [Ns/m]	Increase	New linear damping [Ns/m]
Slender element(Case 2)		/	/
Correction formula(Case 5)		0	$1.5 \times 10^6$
Modify Case 5 with extra damping	<i>i</i>	$1.5 \times 10^6$	$2.25 \times 10^6$
	<i>ii</i>	50%	$3 \times 10^6$
	<i>iii</i>	100%	$4.5 \times 10^6$
	<i>iv</i>	200%	$6 \times 10^6$
		300%	

### 6.6.1 Comparison in motion

After adjusting the linear damping value as Table 6.10, all response under different cases are obtained followed the sme process as before. All results are based on 20 simulations. Here the motion results are listed in Table 6.11, including Case 2 and Case 5 as comparison groups.

Table 6.11: Motion results after modification in damping (unit:[m])

Cases	Motion				
	Max	Mean	$LF_{max}$	$WF_{sig}$	
Slender element(Case 2)	42.38	13.9	34.73	3.26	
Correction formula(Case 5)	53.45	15.65	42.91	3.35	
	<i>i</i>	51.53	15.63	40.75	3.29
Modify Case 5 with extra damping	<i>ii</i>	49.86	15.6	39	3.23
	<i>iii</i>	47.04	15.55	36.22	3.09
	<i>iv</i>	44.63	15.49	34.12	2.94

*Observation:*

1. Comparing Case 5 and those modification cases from *i* to *iv*, the damping term shows a depressive effect on the motion response. When the linear damping value increases, the max offset decreases, which is mainly due to the decrease in  $LF_{max}$ . But the mean offset doesn't have much change.  $WF_{sig}$  shows a trend to decrease, but with very small and slow progress.
2. The depressive effect is not so obvious if the damping term only increases a little. Until the damping term increase by 300%, it finally has a closer result to the Case 2 . At that time, the  $LF_{max}$  has the closest value with Case 2.

*Analysis:*

1. The mean motion is obtained by setting the damping and mass components in the motion equation as zero. Thus the motion equation is simplified into  $K(x) \cdot \bar{X} = \bar{Q}$ . Damping term only has influence on mean wave drift force, while mean wind and current excitation have the stable which is expressed as the following Equation.

$$\bar{Q}_{wa}^- = 2 \int_0^\infty C_{wa}(\omega) S_\eta(\omega) d\omega \quad (6.9)$$

The wave drift coefficient  $C_{wa}(\omega)$  in the input file is obtained from test, which doesn't change with damping term. Thus the mean wave drift force and also total mean excitation  $\bar{Q}$  keep a constant value. No matter how much variation the damping term may have, the mean offset will not have much difference.

2. The main effect from damping term is on LF response. Based on LF motion derivation from Equation 2.44 to Equation 2.46, it is obvious to obtain that:

$$\sigma_{xLF} \sim \sqrt{\frac{S_{xLF}(\omega)}{D_{eq}}} \quad (6.10)$$

Here  $D_{eq}$  is the equivalent damping term after linearization of linear damping term  $D_l$  and quadratic damping term  $D_q$ . Since there is no quadratic damping term in the input, so  $D_{eq} = D_l$ . Therefore  $D_l$  is inversely proportion to LF response. When the linear damping value increases, the LF response will decrease.

3. The correction formula method is not reliable to use compared to slender element method, since it ignores the viscous effect on other terms in motion equation except excitation. The damping effect makes great difference, and according to the result, it still needs a really large extra damping to make the result reasonable. More improvement should be done to this method in the future.

### 6.6.2 Comparison in tension

Similarly, only line 6 and 7 are picked out and their tension are compared under different damping value. Detailed tension information for all lines can be found in Appendix C.

Table 6.12: Tension of Line 6 and 7 after modification in damping (unit:[kN])

Cases	Line 6			Line 7			
	Max	Mean	Standrad Deviation	Max	Mean	Standard Deviation	
Slender element(Case 2)	4139.1	1813.6	382.97	4149.2	1824.1	384.65	
Correction formula(Case 5)	5115.6	1947.1	493.72	5109.7	1958.4	494.81	
	<i>i</i>	4947.4	1941.5	457.47	4942	1953	458.16
Modify Case 5 with	<i>ii</i>	4800.8	1937.2	430.37	4795.1	1948.9	430.88
extra damping	<i>iii</i>	4552.4	1929.6	390.31	4550.1	1942	390.77
	<i>iv</i>	4340.8	1922.7	360.1	4339.9	1935.5	360.63

*Observation:*

1. For all tension components, line 6 and 7 share quite close value in all cases.
2. With the increase in damping term, the max tension value and standard deviation drop obviously, while mean tension value has the trend to decrease but with slow and little process.
3. When the Case *iv* has the closet offset with the slender element case, there is still certain discrepancy in the tension value. Both the max tension and mean tension are larger than Case 2.

*Analysis:*

1. For observation 1, line 6 and 7 are symmetry about the force propagating direction in the system layout, with same exposure area and angle to the propagating environment forces. Thus they are expected to have similar tension response.
2. The mean tension corresponds to mean offset, since mean tension is obtained at the displacement of mean offset as Figure 2.11. When there is little variation in mean offset as Table 6.11, it is supposed to have stable value in mean tension.

3. The tension value of mooring lines is calculated at specific fairlead displacement. When the motion changes, the tension value will vary. Since the damping term has a suppressive effect on the structural motion, the tension will also be suppressed.

### 6.6.3 Evaluation of damping increase

Increasing the linear damping value is indeed having an impact on the structural response. And the 300% percent increase shows the closest result with Case 2. But it is essential to consider how much percent increase is reasonable in real practise. Therefore, the damping level is considered again.

When the linear damping value is  $1.5 \times 10^6$ , the damping level is around 27% of the critical damping. When the critical damping holds the same value, the increase linear damping value will cause an increase in damping level. The increased damping level is summarized in Table 6.13.

Table 6.13: Damping level comparison

Case	Original damping level [Ns/m]	Increase	New damping level [Ns/m]
Correction formula(Case 5)		0	27%
	<i>i</i>	50%	40.5%
Modify Case 5 with	<i>ii</i> 27%	100%	54%
extra damping	<i>iii</i>	200%	81%
	<i>iv</i>	300%	108%

In real practise, the linear damping value will not beyond 70-80% of the critical damping. Thus the Case *iv* is not practical. And Case *iii* shows acceptable result which close to Case 2. In practise, Case *iii* will be selected.



# Chapter 7

## Relative importance of different environmental load effects

In this chapter, model with slender elements is checked under single environment force, i.e. only wave, only wind, and only current. From the separation, the contribution of each force and interaction between forces are analyzed.

The motion equation is used again in order to analysis the environmental force effect on structure response.

$$(M + A(\omega)) \cdot \ddot{x} + C(\omega) \cdot \dot{x} + D_l \cdot \dot{x} + D_q \cdot \dot{x} |\dot{x}| + K(x) \cdot x = Q(t, x, \dot{x})$$

where  $Q(t, x, \dot{x}) = q_{wi} + q_{cu} + q_{wa}$ .

And for slender elements, the current excitation on a strip is expressed as:

$$q_{cu} = C_{cu} [(\bar{V} + u) - x_{tot}^{\dot{}}] |(\bar{V} + u) - x_{tot}^{\dot{}}|$$

where  $x_{tot}^{\dot{}} = x_{LF}^{\dot{}} + x_{WF}^{\dot{}}$ .

### 7.1 Separation of environmental excitation

The case as the comparison base is selected as Case 2 in Section 6.4. It contains six slender elements with zero quadratic current coefficient in surge. These two conditions also applies to

the following single environmental excitation cases.

- *Case a*: Only wave

When there is only wave affects the model,  $Q(t, x, \dot{x}) = q_{wa} + q_{cu}$ . Here  $q_{cu}$  exists due to the wave-current interaction, since there is also wave velocity component in this term.

When the current velocity  $\bar{V} = 0$ ,  $q_{cu}$  becomes:

$$q_{cu} = C_{cu} (u - \dot{x}_{tot})^2 \quad (7.1)$$

When expanding this equation, the term with structure response velocity  $C_{cu} \cdot \dot{x}_{tot}^2$  can be moved to the left side of motion equation and become a quadratic damping term. The term with wave velocity  $C_{cu} \cdot u^2$  remains the excitation term and stays at the right side of equation.

- *Case b*: Only wind

When there is only wind affects the model,  $Q(t, x, \dot{x}) = q_{wi} + q_{cu}$ . Here  $q_{cu}$  exists due to the structure response, since there is also structure response velocity component in this term.

When the current velocity  $\bar{V} = 0$  and wave velocity  $u = 0$ ,  $q_{cu}$  becomes:

$$q_{cu} = C_{cu} (\dot{x}_{tot})^2 \quad (7.2)$$

Thus this term is total related with the structure response, and should be moved to the left side of equation and become a damping term.

- *Case c*: Only current

When there is only wind affects the model,  $Q(t, x, \dot{x}) = q_{cu}$ .

When the wave velocity  $u = 0$ ,  $q_{cu}$  becomes:

$$q_{cu} = C_{cu} (\bar{V} - \dot{x}_{tot})^2 \quad (7.3)$$

When expanding this equation, the term with structure response velocity  $C_{cu} \cdot \dot{x}_{tot}^2$  can be moved to the left side of motion equation and become a quadratic damping term. The term with current velocity  $C_{cu} \cdot u^2$  remains the excitation term and stays at the right side of equation.

To make it more straight-forward, all the cases and the main characters are summarized as Table 7.1.

Table 7.1: Cases summary for single environment excitation

Case	Slender Elements	Quadratic current coefficient $C_{21} = 0$	Wave	Wind	Current
Base case	×	×	×	×	×
a	×	×	×		
b	×	×		×	
c	×	×			×

## 7.2 Result analysis

Since wave and wind are stochastic process, the wave seed and wind seed are set as variable to control the phase angle of different components. Then 20 simulations are proposed. However, current is always considered as stationary, thus there is no "current seed" concept. Only one simulation is available.

### 7.2.1 Comparison in motion

All motion components in surge is summarized as Table 7.2. The  $LF_{max}$  offset and  $WF_{sig}$  offset are obtained by using frequency filter as the same process in Section 5.4.4.

Table 7.2: Motion for single environments (unit:[m])

Case	Max	Mean	$LF_{max}$	$WF_{sig}$	Simu. no.
Base case	42.38	13.9	34.73	3.26	20
a	31.15	4.31	23.41	3.27	20
b	12.28	6.42	11.93	0.1518	20
c	1.3166	1.3089	/	0.004512	1

*Observation:*

1.  $WF_{sig}$  of the base case is almost the same with that of Case a with only wave effect, while the other two cases almost have no contribution in the WF response.
2. When adding the max offset from Case a,b and c, the result is 44.76, a little bit higher than the value in the base case. On the contrary, when adding the mean offset from Case a,b and c, the result is 12.04, a little bit smaller the base case.
3. Current doesn't have LF response, thus the LF response of the base case only consists of wave effect and wind effect. And its value is almost the same with the summation of Case a and b. The 2<sup>nd</sup> order wave loads provides more LF response than wind gust does.
4. Wind gives the largest mean offset compared to other two forces.

*Analysis:*

1. Based on the separation of wave effect in a frequency domain, it has a 1<sup>st</sup> order forces (wave drift) proportional with wave amplitude in the WF band, which is described by force transfer functions. The wave effect is the only origin of  $WF_{sig}$  in base case, since the other two environmental almost have no response in the WF band, only some noise which can be ignored.
2. The response of three forces can not be added up directly, because they are not working separately. It always has some interaction between each other, especially the wave-current interaction, which is really important in the viscous effect. Thus it is concluded that the wave-current interaction has a smaller impact on motion than just adding these two effect together. Because wave-current interaction will produce extra damping to the system, further has an suppressive effect on the motion.

3. Wind only affects the superstructure over MWL and can not give much effect on the slender elements. Thus when we try to compare Base case with Case a in aspect of viscous effect, the main difference has nothing to do with wind, but strongly connects with wave-current interaction.
4. For Case c, it is observed that current has really close value in max offset and mean offset due to its stationary characteristic. On the contrary, wind and wave are stochastic process, and have great variation under different phase of components.

### 7.2.2 Comparison in tension

Here only line 6 and 7 are picked out as the most-loaded lines, and their tension are compared under different environment condition. Detailed tension information for all lines can be found in Appendix D.

Table 7.3: Tension for single environments (unit:[kN])

Cases	Line 6			Line 7			Simu.no.
	Max	Mean	Standrad Deviation	Max	Mean	Standard Deviation	
Base Case	4139.1	1813.6	382.97	4149.2	1824.1	384.65	20
a	3180	1228.5	261.05	3177	1226.6	260.51	20
b	1665.4	1305.5	88.884	1704.3	1322.6	94.02	20
c	1061.3	1060.9	89.66	1059.3	1058.9	89.777	1

*Observation:*

1. For all tension components, line 6 and 7 share quite close value in all cases.
2. Wave has the largest max tension, it is more dominating than the other two environmental forces. Wind has quite large mean tension. Current has really stable response in the simulation.

*Analysis:*

1. Line 6 and 7 are symmetry about the force propagating direction in the system layout, with same exposure area and angle to the propagating environment forces. Thus they are expected to have similar tension response.

2. The tension components corresponds to the motion components distribution. For example, when wind has the largest mean offset, it has the largest mean tension.

For wave motion, it consists of mean motion, LF motion and WF motion. The mean motion corresponds to static response, while the other two corresponds to dynamic response. When it has a limit value in static response, the dynamic effect is absolutely more dominating. This also apply to tension. When it has a limit mean tension, the dynamic effect is dominating. That's why the mooring line has the largest max tension but with a moderate mean tension under wave condition. The dynamic effect makes this happen.

3. Then mean wind force is expressed as  $q_{wi} = C_{wi} \bar{U}^2$ . The 100-year wind case has a velocity of 36m/s, which is quite large; also wind affects the superstructure directly and has a larger exposure area than other two forces. Therefore the mean wind force is really large, so the mean tension in mooring line under wind condition has the largest value.
4. For Case c, it is observed that current has really close value in max tension and mean tension due to its similar value in offset. On the contrary, since wind and wave are stochastic process, and have more complicated displacement components, they have different max tension and mean tension.

# Chapter 8

## Effect of line dynamics-comparison of results between SIMO and RIFLEX

Since RIFLEX is a finite element program developed as a tool for analyzing slender marine structures, it is used in this chapter to check the response of most-loaded line of Floatel Superior under same environment condition in one simulation. The motion series in 3-hour from SIMO is used as an input for RIFLEX. The most-loaded line is selected as Line 6 based on previous result, and the tension results of it in RIFLEX will be compared with that in SIMO.

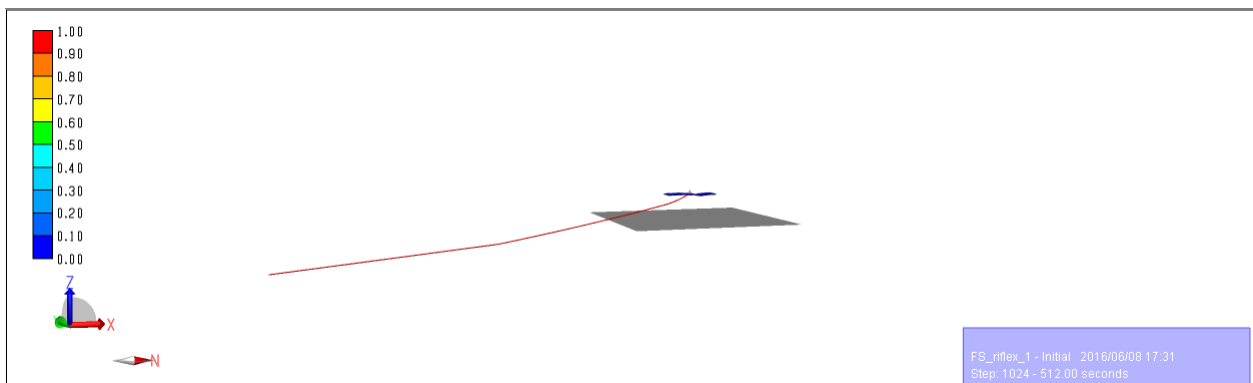


Figure 8.1: 3D view of the most-loaded line in RIFLEX

### 8.1 Difference between SIMO and RIFLEX

1. Segment setting

In SIMO, the segment number is counted from anchor to the topside as Table 5.2. However, different from SIMO, the segment number setting in RIFLEX is counted from fairlead to the anchor as Figure 8.2. Therefore it is the segment 1 matters and the node 1 is the attachment point connected with the supply vessel.

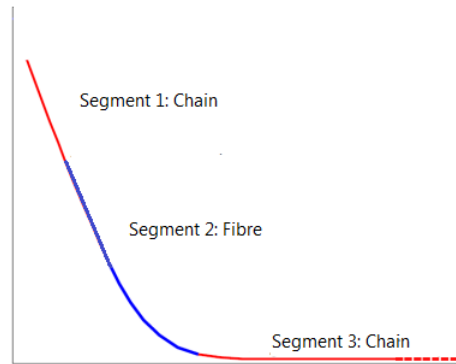


Figure 8.2: Example of a typical line segment composition in RIFLEX

## 2. Calculation method

SIMO uses the quasi-static method to calculate the tension in mooring line. It regards the mooring line as a whole, assumes it to be static and ignores the dynamic effect from velocity and acceleration. Only the position of the fairlead matters.

For RIFLEX, it uses the Finite Element Method and does the calculation in a discrete way. The mooring line is divided into several small elements. It is important to decide the amount of the elements. More elements will bring a accurate result, but too time-consuming. Each element is calculated one by one with small time step. And it is more dynamic, since the mooring line will move with the fluctuation of motion series. Therefore it is supposed to be more accurate than SIMO result.

Due to the difference in calculation methods, it is expected to have some discrepancy in tension result.

## 8.2 Process

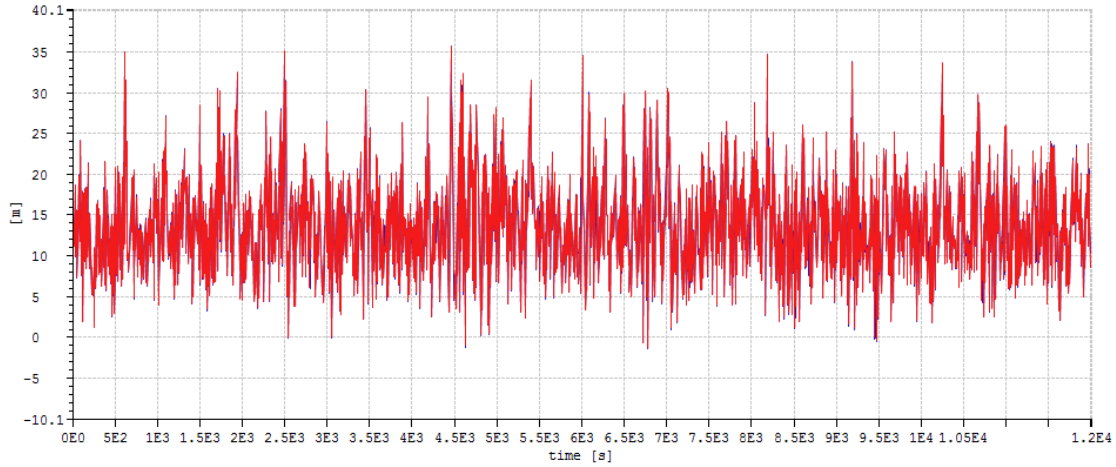
In Chapter 5, the SIMO tension results are obtained from 20 simulations. But here only one simulation is performed just for comparison. Case 2 using slender element method in Section 6.4 is selected as the comparison case. It is the main viscous model, and it is necessary to check, with viscous effect considered, whether the tension value in most-loaded line in SIMO and that in RIFLEX have consistency with each other. The main process are as follows.

- *Step 1: Create the supply vessel*

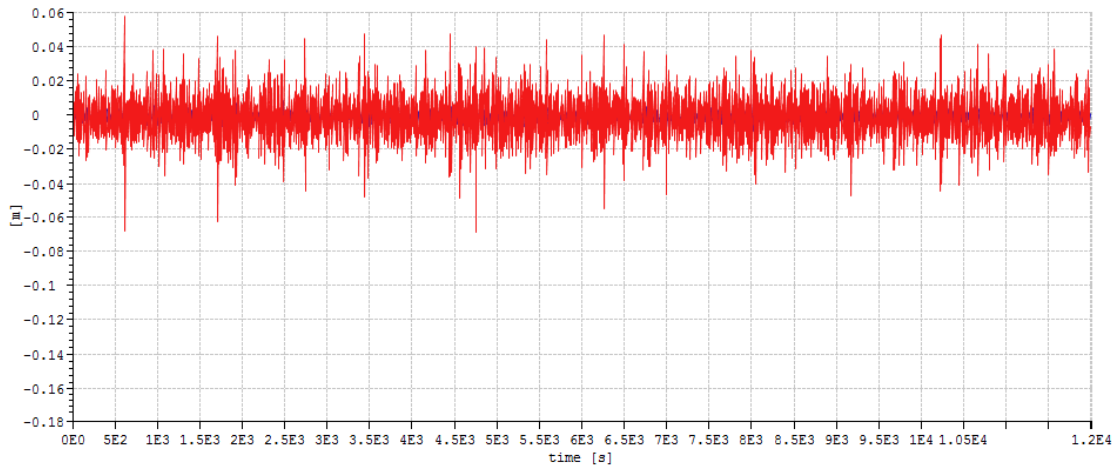
Based on Figure 8.1, only the most-loaded line is modeled in RIFLEX. However, the mooring line should be attached on a structure in order to let the fairlead move with the structure and have corresponding response. Therefore a supply vessel is created. It locates at the original point (0,0,0) and doesn't have mass considered. The first order motion transfer function is copied from SIMO and added to the support vessel. It is used to control the WF response of mooring line. Then the fairlead of line 6 is made connect to the support vessel. The motion series will be imported and added to the supply vessel later, and line 6 will move with the motion series as well.

- *Step 2: Verify the motion series*

The motion series is obtained in SIMO under one simulation as the result file. But for RIFLEX, this motion series is used as an input file. Since it has been exported and imported between two software, it is essential to make sure it still keeps the same characteristic as before. The output motion in SIMO and the input top motion in RIFLEX is plotted as Figure 8.3. Motion both in x and z direction are plotted.



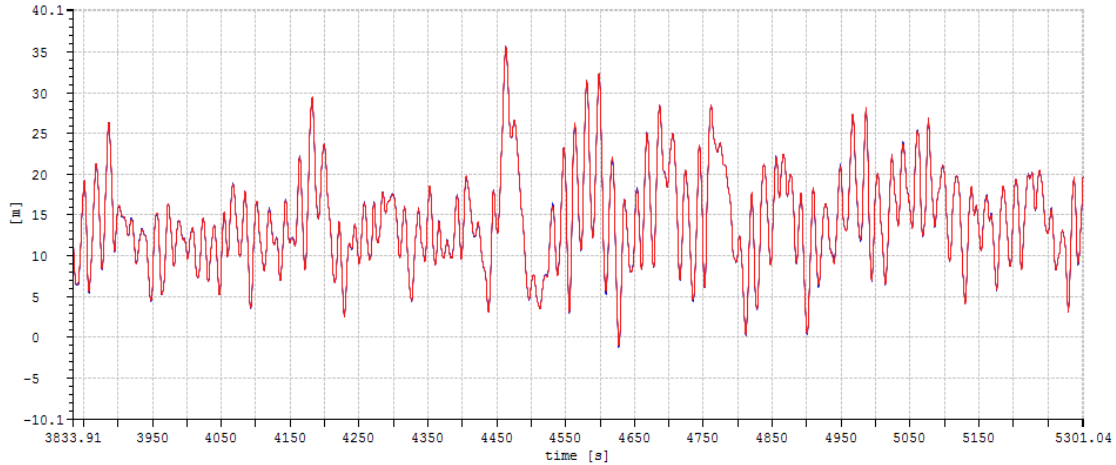
(a)



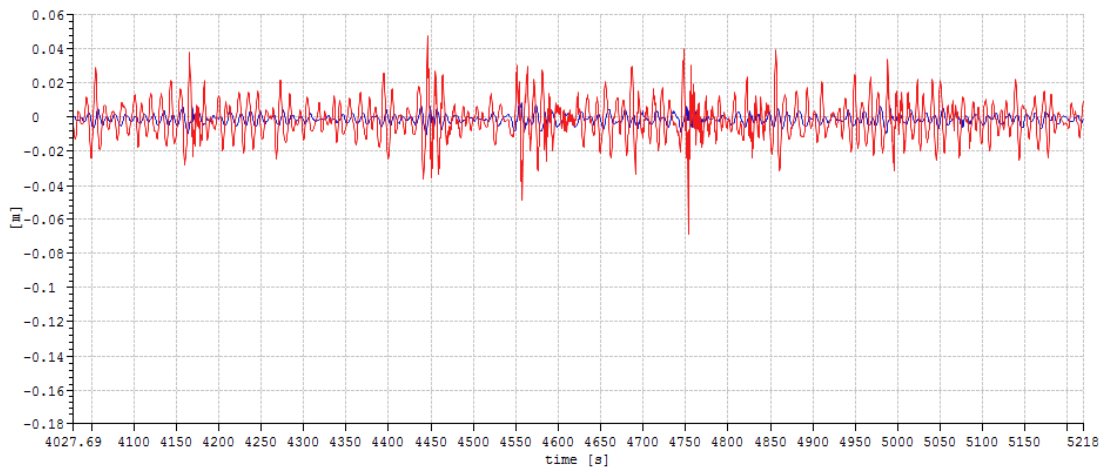
(b)

Figure 8.3: Motion series in (a) x direction (b) z direction

The red signal is obtained from RIFLEX and the blue one is obtained from SIMO. Almost all the signal series is overlapping with each other. To see the detail of the plot, the highest peak in the whole series is selected to zoom in. The period is around 4000-5000s.



(a)



(b)

Figure 8.4: Zoomed motion series in (a) x direction (b) z direction

From the plot, it is observed that the motion series keeps the same characteristic through the import and export, especially in x direction, where the two lines overlap each other all the time. In z direction, RIFLEX shows much larger standard deviation value, which represents the motion series in z direction is not stable as before and have more obvious fluctuation, but it doesn't matter. It still oscillates around the same mean value.

Thus it is concluded that the motion file has consistency with each other and is valid for the further analysis.

- *Step 3:* Set the environment condition and line characteristic

The motion series imported is obtained under the common effect of environmental forces.

So it already includes the environmental force information, and it is not necessary to reset all the force in detail in RIFLEX. Here only the wave spectrum is specified as a JONSWAP double peaked spectrum with  $H_s=16\text{m}$ ,  $T_p=18.2\text{s}$ .

The segments are discrete into many small elements. In order to make the calculation both accurate and efficiency, the length of elements are set as 25m for all segments. Details can be referred to Table 8.1. In this way, the calculation won't be too time-consuming or tedious, but with a pretty good result.

Table 8.1: Segments setting in RIFLEX

Segment	Material	Length	No. of elements	Length of each element
1	Chain	250	10	25
2	Fibre	1200	48	25
3	Chain	1200	48	25

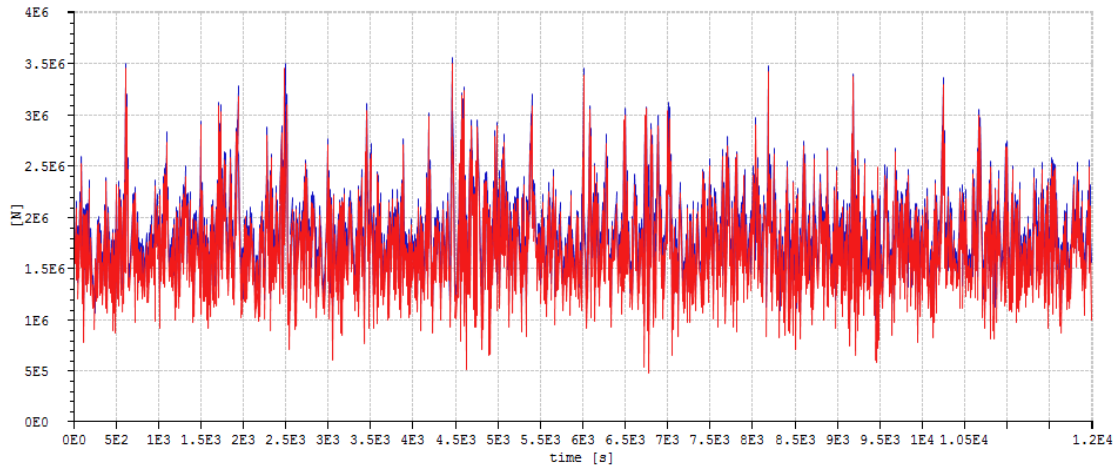
- *Step 4:* Run dynamic analysis

Tension value and envelop curve for the most-loaded line are stored as desired results. The simulation length is set as 12000s as same as that in SIMO, which represents a 3-hour period of time. The time step is set as 0.01s, and each result is stored every 50 steps, equal to half a second time. If the result stored at too small time step, the computer doesn't have enough space and the software will stop running.

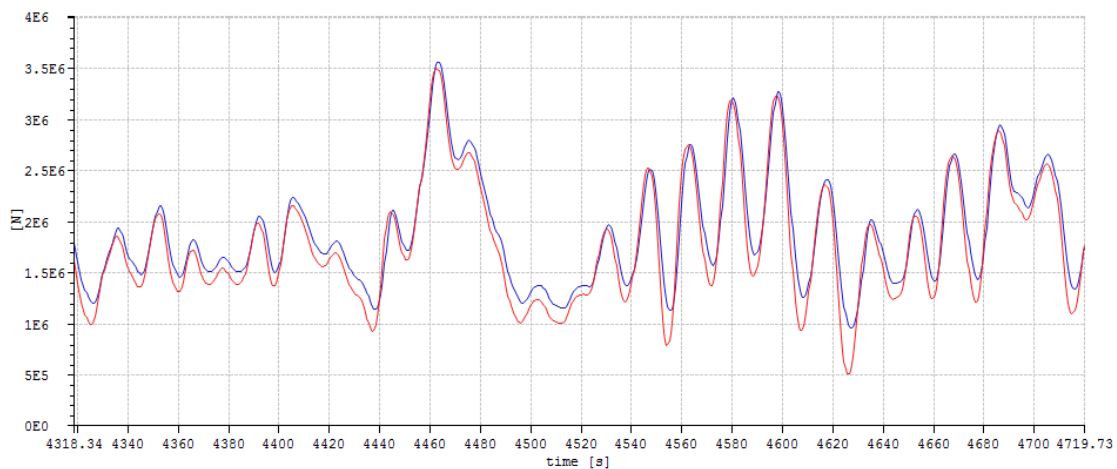
After running the dynamic analysis, tension series in a 3-hour simulation is obtained. It is expected to be plotted with the SIMO tension result and to see if there is any difference.

### 8.3 Results analysis

Figure 8.5 is the plot of total tension series in 3-hour simulation, where the blue signal represents the result from SIMO, and the red signal represents the result from RIFLEX. In order to see the detail, the peak crest is zoomed in, around 4200-4700s.



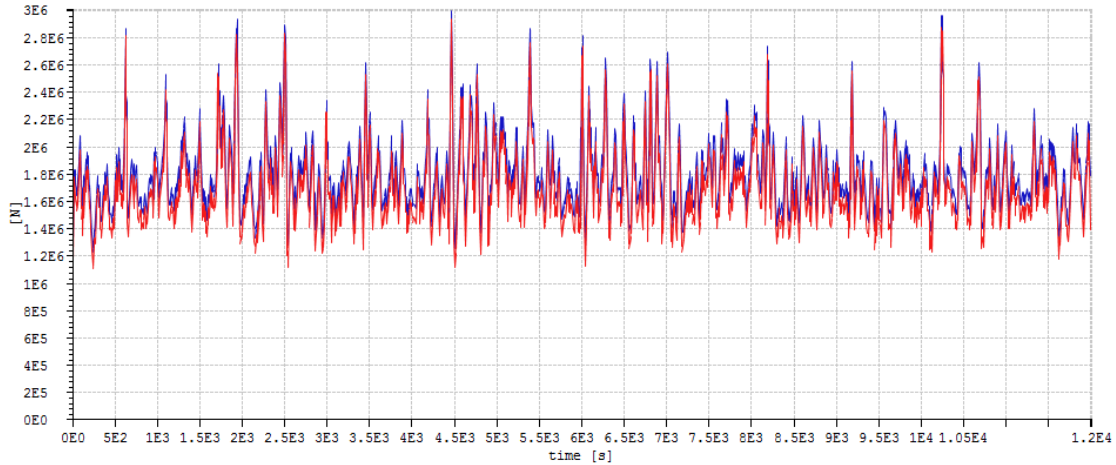
(a)



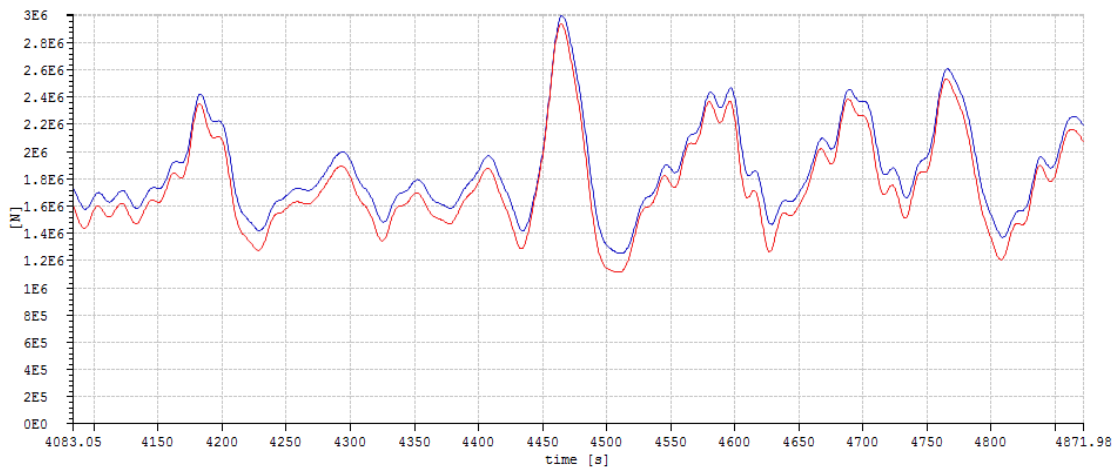
(b)

Figure 8.5: Tension series (a) original (b) zoomed

It is observed that both lines have same trend with same phase, and similar crest and trough at a global extent. However, the red line has much stronger variation. It covers most of the blue signal, but at certain frequency, it has a lower trough or higher crest than the SIMO result. In order to see the effect on different frequency bands, a frequency filter is used, and the cut-off frequency is set as  $0.03333[1/s]$  to divide the LF band and WF band. Several peaks is selected and zoomed to see the detail difference.



(a)

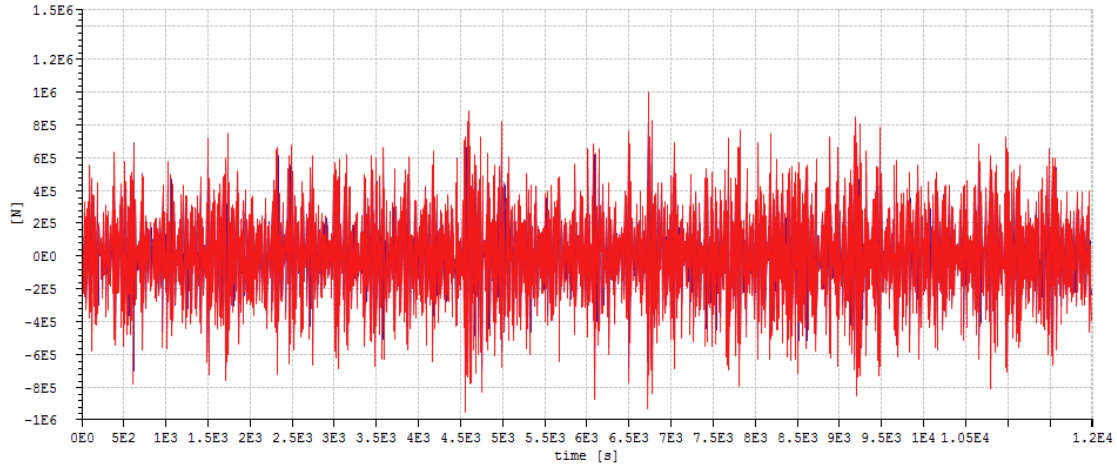


(b)

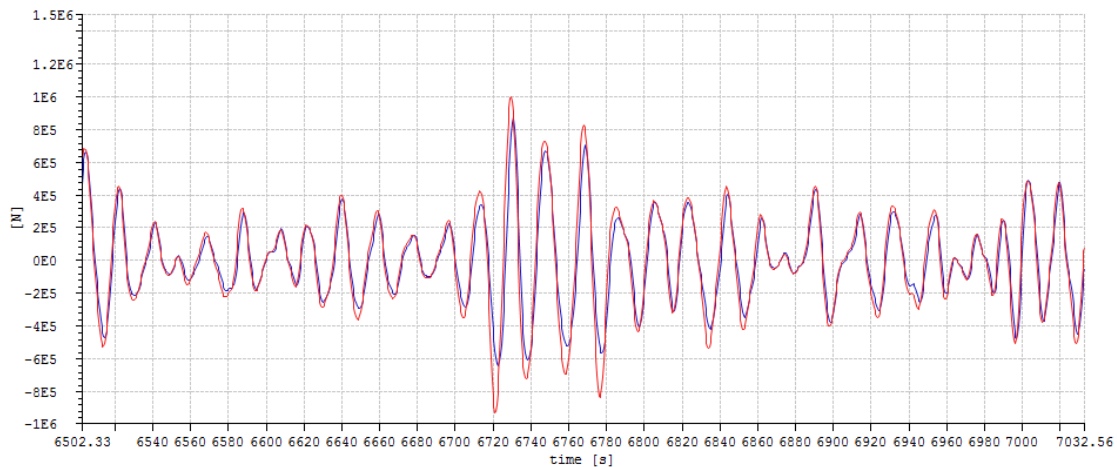
Figure 8.6: Tension series (a) in Low Frequency band (b) in Low Frequency band after zoom

In LF band, the result from RIFLEX shows a little bit lower mean than SIMO result. Because Figure 8.6(a) shows that the red line always has a lower crest than the blue line. After zooming in around 4000-4800s, where locates the highest peak, Figure 8.6(b) shows a more obvious discrepancy between two lines. In most part the RIFLEX line has a lower tension value than SIMO result. But the difference is very small, at most 80kN in line. The difference is an acceptable range.

Therefore it is concluded that in LF band, there is not much difference between two signals. RIFLEX signal matches with SIMO signal with same trend and phase, but a little bit lower tension value overall.



(a)



(b)

Figure 8.7: Tension series (a) in Low Frequency band (b) in Low Frequency band after zoom

In WF band, the RIFLEX signal matches with the SIMO result in a perfect way. They overlap each other at most time. However, RIFLEX has an obvious higher crest and lower trough than SIMO signal at certain time, which represents it has a larger standard deviation value.

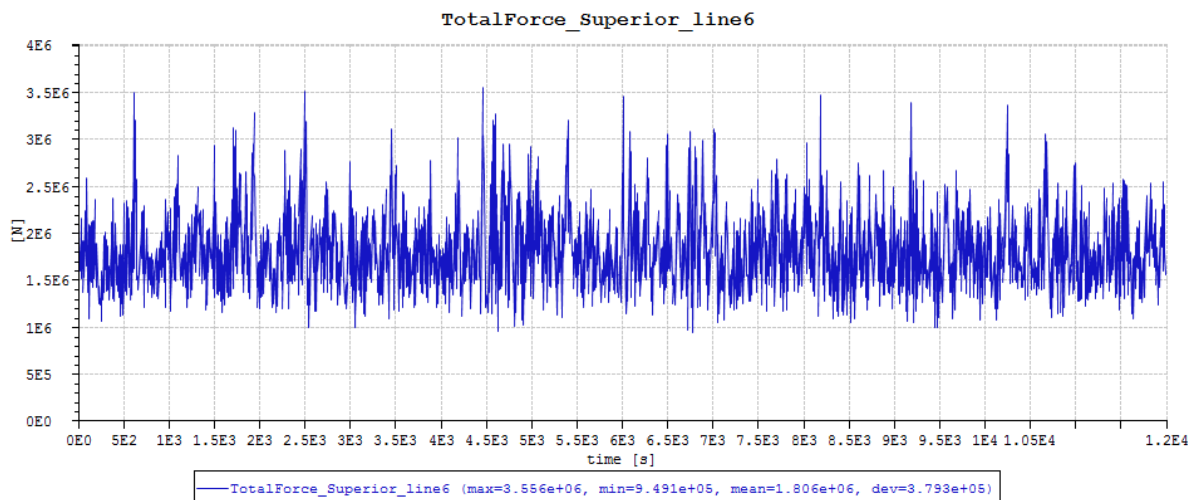
The discrepancy is mainly due to the different calculation method of tension, referred to Section 8.1. RIFLEX takes dynamic effect into account by calculating tension with position, velocity and acceleration at the same time. The total line moves with the motion series. And the discretion makes the tension in RIFLEX more accurate than SIMO.

It is concluded that the dynamic calculation method has more impact on the WF band response. RIFLEX shows more accurate and higher tension result than SIMO result.

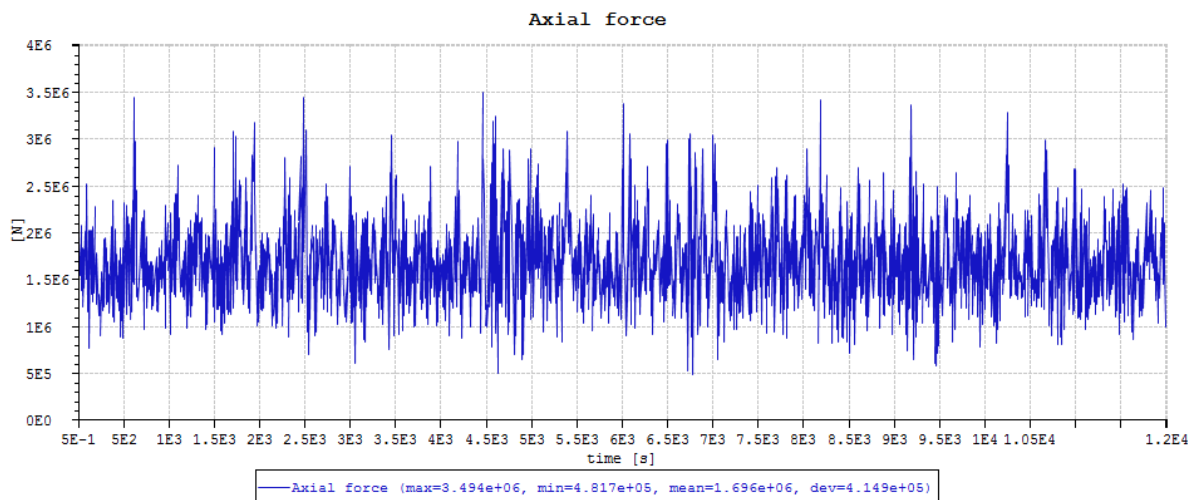
## 8.4 DAF calculation

According to previous section, the tension plot of both SIMO and RIFLEX shows that there is certain discrepancy between each other, mainly due to the different calculation methods. Here the dynamic amplification factor (DAF) is calculated based on the tension result from SIMO and RIFLEX. DAF is used to see how much difference exists between these two software in a more straightforward way.

First the tension series are plotted separately as Figure 8.8, and different tension components are summarized in Table 8.2.



(a)



(b)

Figure 8.8: Tension components in (a) SIMO (b) RIFLEX

Table 8.2: Tension components in both software

Result	Max tension	Mean tension	Standard deviation
SIMO	3556	1806	379.3
RIFLEX	3494	1696	414.9

Then DAF is expressed as Equation 8.1.

$$DAF = \frac{(T_{max} - T_{mean})_{RIFLEX}}{(T_{max} - T_{mean})_{SIMO}} \quad (8.1)$$

Then DAF is obtained as 1.027. Since it is larger than 1, it proves the assumption that RIFLEX brings an 'amplification' effect to the tension result, due to its dynamic and discrete calculation method. Though the amplification effect is not so large, because the DAF is only a little bit larger than 1.



# Chapter 9

## Conclusion

Based on the result and discussion presented above, several important conclusions are made.

### 1. Comparison between FD analysis and TD analysis

FD analysis and TD analysis have the same theoretical basis on the equation of motion. Given a same signal, the fundamental difference between these two methods is how they deal with the signal: FD method separates signal into LF and WF band, and uses the linearisation principle to linearize all the non-linear term; while TD analysis uses numerical integration, solves the signal at one-go. Thus FD method is easy to apply, while TD method is more accurate. They are both widely used and complete each other.

### 2. Viscous effect

Viscous effect is really important in the marine operation, especially for the structure with small cross-section. Ignoring viscous effect may induce an obvious underestimation of LF excitation force and damping force, then further provide a quite conservative estimation in mooring line tension and structure motion.

### 3. Methods for accounting for viscous effect

Based on the result and comparison in this thesis, the slender element method is a reliable method to account for viscous effect. It accounts for viscous effects both on LF excitation and damping term, and obtains the structural response under the balance of excitation and damping.

however, the accuracy of correction formula is doubted since it only accounts the viscous effect on excitation. Adding extra damping to the system will make this method become more accurate and reliable, but the process is slow and requires a large extra damping term. More research should be performed on improving this method.

#### 4. Sensitivity test of drag coefficient

The drag coefficient is modified according to 'tuning' formula. It assumes that all the viscous effect comes only from column or only from pontoon. The tuned drag coefficients are always smaller than the proposed one from regulation. Modifying the drag coefficient will certainly affect the viscous effect. Smaller coefficient brings smaller viscous force.

#### 5. Relative importance of different environmental loads

In aspect of response under single environmental condition, wave force is more dominating than other two forces. Wind ranks the second due to its large velocity under 100-year case and big exposure area of the structure. Instead of working separately, wave and current have interaction between each other.

# Chapter 10

## Recommendation for further work

Following are some recommendation for future work in connection with this thesis.

1. In Section 2.1.1, linear theory is applied to obtain the maximum velocity  $u_0$  and further derive the expression for viscous drag force. However, linear theory is applicable for infinitesimal wave amplitudes and is valid up to MWL, use of the expressions for the water particle kinematics up to the free surface of a finite wave is questionable. Thus some 'stretching' formulas should be applied to cover this shortage.
2. The water depth was remained fixed during the case studies. Previous literature reviews suggest that the importance of mooring line forces on the system response increases with the water depth. Similar investigation as performed in this thesis should be studied for different water depth and check whether the water depth alters the overall trends.
3. This case study is performed without bottom friction, which may has an impact on the mooring line characteristics, and consequently the restoring characteristic and stiffness. This is likely to reduce damping estimate, as the bottom friction will restrict the vessel motion.
4. When applying the slender element method, the drag coefficients are selected from the regulation. However, the drag coefficient selected from DNV-RP-C205 is applicable for steady flow. In our case, the oscillating flow should be considered. For oscillating flow,

the drag coefficient is considered as the coefficient in steady flow multiply with a factor as Equation 6.4. Thus in further work, the drag coefficients need further modification.

5. When applying the slender element method, the total drag force is obtained by calculating the force on each slender element and add them up. However, for the four columns, simply adding is not accurate. According to the layout in Figure 6.1(b), it is observed that the left two columns encounters the environment force with total exposure area in the first group, while the other two columns meet the force later and are somewhat covered with a smaller exposure area. Thus the drag force on the latter two columns are smaller than the previous one. Simply adding them up may give a larger estimation in drag force.
6. The correction formula should be researched and modified in the future work. It shows quite low reliability in this paper. Though adding extra damping makes it show a more acceptable result, it requires too large damping term and maybe not practical in real practise.
7. Through the thesis, the viscous effect is considered under ULS only. If having enough time, more analysis should be done under ALS. It will be worthy to see how the viscous force affect a damaged system, and whether the intact mooring lines show a more intense response.
8. In Chapter 8, only the most-loaded line is verified in RIFLEX. More lines can be selected and verified, in order to prove the validity of SIMO result and also discover the difference between SIMO and RIFLEX.

# Bibliography

- Burns, G. E. (1983). Calculating viscous drift of a tension leg platform. In *ASME Proceedings of the 2nd International Offshore Mechanics and Arctic Engineering Symposium, Houston, Tex*, pages 22–30.
- Chakrabarti, S. K. (1984). Steady drift force on vertical cylinder-viscous vs. potential. *Applied Ocean Research*, 6(2):73–82.
- Faltinsen, O. (1993). *Sea loads on ships and offshore structures*, volume 1. Cambridge university press.
- Ferretti, C. and Berta, M. (1980). Viscous effect contribution to the drift forces on floating structures. In *International Symposium on Ocean Engineering and Shiphandling*.
- Fylling, I., Larsen, C., Sødahl, N., Passano, E., Bech, A., Engseth, A., Lie, E., and Ormberg, H. (1998). Riflex user's manual. *MARINTEK report, Trondheim*.
- Haver, S., Larsen, K., Meling, T. S., et al. (2001). Reliability assessment of a mooring system. In *The Eleventh International Offshore and Polar Engineering Conference*. International Society of Offshore and Polar Engineers.
- Kobayashi, M., Shimada, K., and Fujihira, T. (1987). Study on dynamic responses of a tlp in waves. *Journal of Offshore Mechanics and Arctic Engineering*, 109(1):61–66.
- Kvitrud, A. (2014). Lessons learned from norwegian anchor line failures 2010-2013. paper omae2014-23095. *Proc. OMAE2014, San Francisco, Cal., USA*.
- Lie, H., Mo, K., and Kaasen, K. (2003). Mimoso–user's documentation, program version 5.7. *MARINTEK (Norwegian Marine Technology Research Institute)*.

- Low, Y. and Langley, R. (2006). Time and frequency domain coupled analysis of deepwater floating production systems. *Applied Ocean Research*, 28(6):371–385.
- Lundgren, H., Sand, S. E., and Kirkegaard, J. (1982). Drift forces and damping in natural sea states—a critical review of the hydrodynamics of floating structures. *Cambridge, Massachusetts, August*, pages 592–607.
- Morison, J., Johnson, J., Schaaf, S., et al. (1950). The force exerted by surface waves on piles. *Journal of Petroleum Technology*, 2(05):149–154.
- Newman, J. t. (1967). The drift force and moment on ships in waves. *Journal of ship research*, 11(1):51–60.
- Ormberg, H., Fylling, I. J., Larsen, K., and Sødahl, N. (1997). Coupled analysis of vessel motions and mooring and riser system dynamics. In *PROCEEDINGS OF THE INTERNATIONAL CONFERENCE ON OFFSHORE MECHANICS AND ARCTIC ENGINEERING*, pages 91–100. American Society of Mechanical Engineers.
- Ormberg, H. and Larsen, K. (1998). Coupled analysis of floater motion and mooring dynamics for a turret-moored ship. *Applied Ocean Research*, 20(1):55–67.
- Pijfers, J., Brink, A., et al. (1977). Calculated drift forces of two semisubmersible platform types in regular and irregular waves. In *Offshore technology conference*. Offshore Technology Conference.
- Pinkster, J. (1974). Low-frequency phenomena associated with vessels moored at sea. In *JOURNAL OF PETROLEUM TECHNOLOGY*, volume 26, pages 302–302. SOC PETROLEUM ENG 222 PALISADES CREEK DR, RICHARDSON, TX 75080.
- Reinholdtsen, S. and Falkenberg, E. (2001). Simo—theory/user manual. *MT51 F93-0184, MARINTEK*.
- Snell, R. O., Wisch, D. J., et al. (2008). Iso 19900 series: offshore structures standards. In *Offshore Technology Conference*. Offshore Technology Conference.

Standing, R., Brendling, W., Jackson, G., et al. (1991). Full-scale measured and predicted low-frequency motions of the semi-submersible support vessel “uncle john”. In *The First International Offshore and Polar Engineering Conference*. International Society of Offshore and Polar Engineers.

Stansberg, C. T., Kaasen, K. E., Abrahamsen, B. C., Nestegård, A., Shao, Y., Larsen, K., et al. (2015). Challenges in wave force modelling for mooring design in high seas. In *Offshore Technology Conference*. Offshore Technology Conference.

Veritas, D. N. (2008). Offshore standard dnv-os-e301: Position mooring.

Veritas, D. N. (2010). Dnv-rp-c205. *Environmental Conditions and Environmental Loads*.

# Appendix A

## Comparison between two input files

This is an example of an Appendix. You can write an Appendix in the same way as a chapter, with sections, subsections, and so on.

### A.1 Quadratic wind coefficient

There are 25 directions chosen evenly from 0 deg to 360 deg. Based on the chosen directions, the coefficients of six degrees of freedom are plotted. The quadratic wind coefficient in surge is chosen as the example, the other five d.o.f are similar.

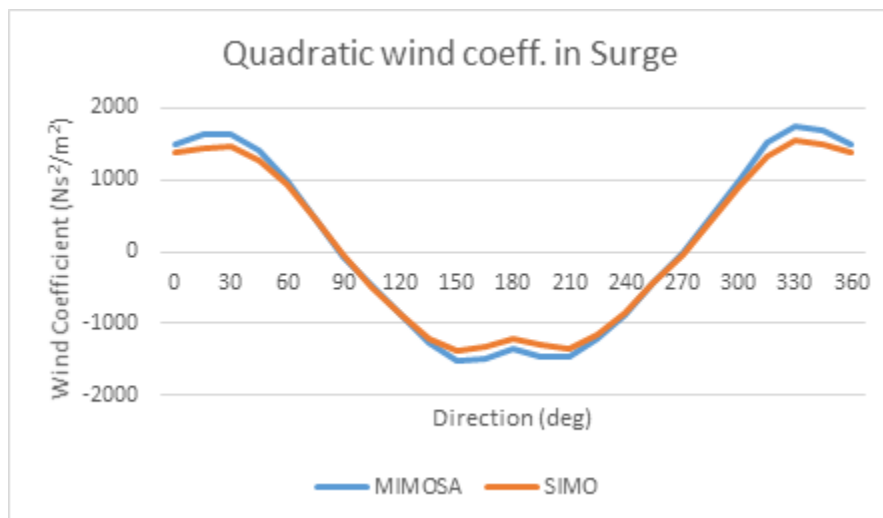


Figure A.1: Quadratic Wind Coefficient in Surge

From the plot, it is easy to tell that the quadratic wind coefficient in surge in both files are

consistent with each other, though with a little discrepancy in values.

## A.2 Quadratic current coefficient

There are 25 directions chosen evenly from 0 deg to 360 deg. Based on the chosen directions, the coefficients of six degrees of freedom are plotted. The quadratic current coefficient in surge is chosen as the example, the other five d.o.f are similar.

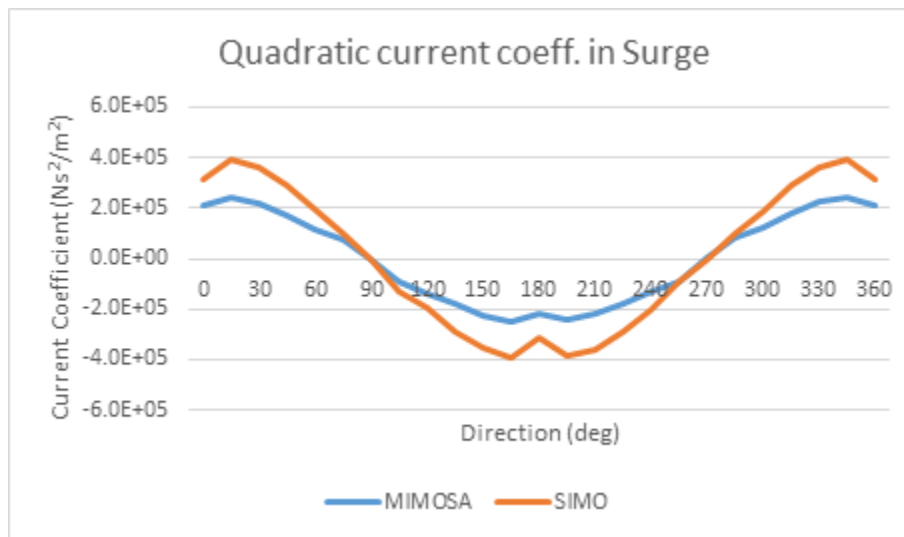


Figure A.2: Quadratic Current Coefficient in Surge

From the plot, it is observed that there is certain discrepancy between two lines, especially in 0, 180 and 360 deg. However, the trend of the lines are similar, thus it can be regarded as consistent.

## A.3 Second order wave drift force

In order to compare the 2<sup>nd</sup> order wave drift force, only the overlapped frequencies are chosen (31 frequencies in total), and its corresponding values are used in the plot. And the chosen directions under comparison are 0, 45 and 90 deg.

Here only the plots of 2<sup>nd</sup> order wave drift force in surge under 0 deg and in sway under 90 deg are plotted and analyzed in the following. Since these two are much more important than other d.o.f or direction.

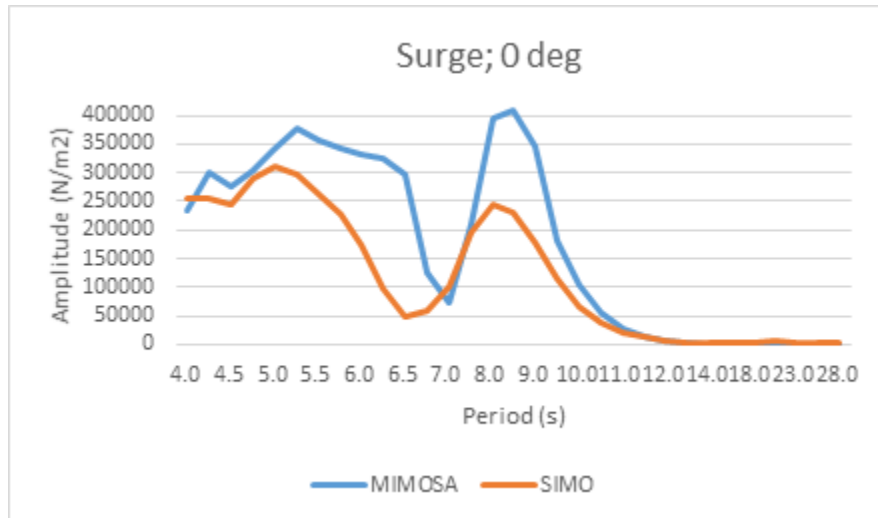


Figure A.3: Wave Drift Force in Surge under 0 deg

From the plot, an obvious difference in phase is observed, but the whole lines are in same trend. Both amplitudes approach 0 around 14s, which is more important.

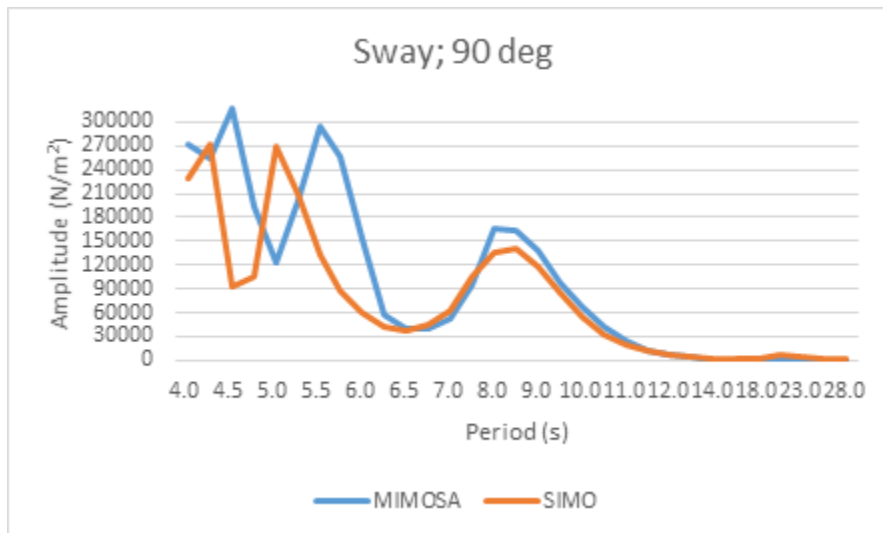
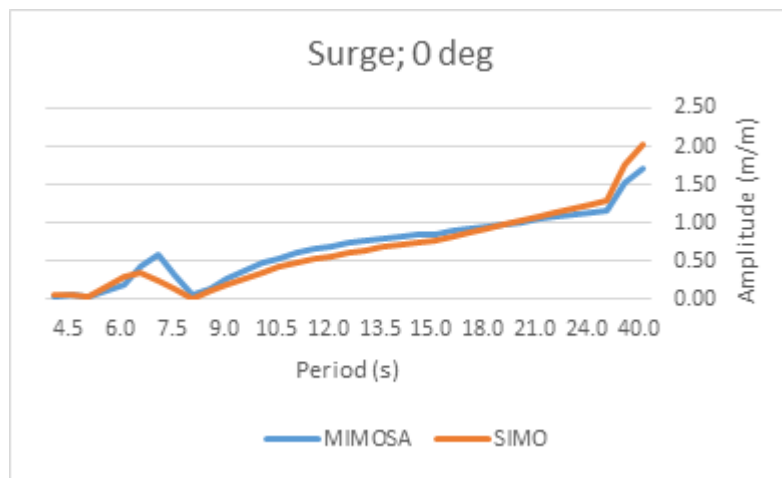


Figure A.4: Wave Drift Force in Sway under 90 deg

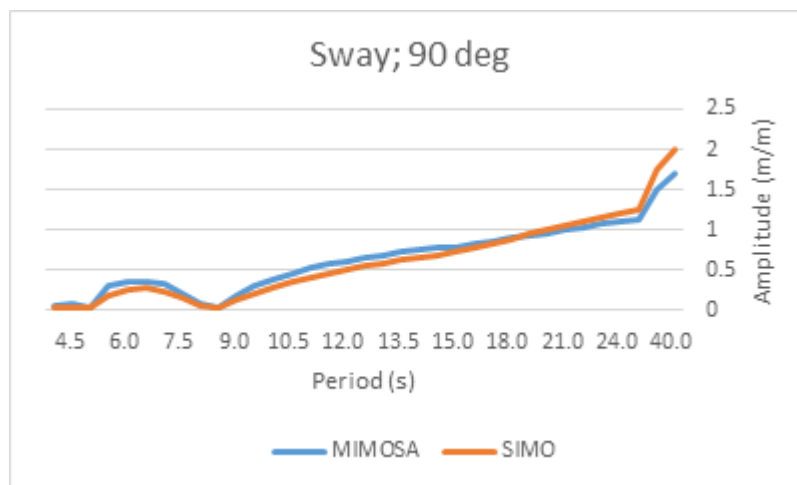
Similar as Figure A.4, there is also an obvious difference in phase when checking the wave drift force in sway under 90 deg, but the whole lines are in same trend. Both amplitudes approach 0 around 14s.

## A.4 First order motion transfer function

The 1<sup>st</sup> order motion transfer function is expressed both in amplitude and phase. Amplitude has a much higher importance than phase does. Then only the plots of amplitude will be showed. Only 35 common frequencies are chosen since they appear in both input files. Similarly, three directions are chosen, including 0, 45 and 90 deg. Only some of the plots will be showed here and analyzed.



(a)



(b)

Figure A.5: 1<sup>st</sup> Order Motion Transfer Function in (a) Surge;0 deg (2) Sway; 90 deg

The 1<sup>st</sup> order motion transfer function in surge under 0 deg and in sway under 90 deg are always the important cases need to check. From the plots, it is observed the two input files are consistent with each other, with similar trend and minor discrepancy in amplitude.

On the contrary, the 1<sup>st</sup> order motion transfer function in surge under 90 deg and in sway under 0 deg are always 0 because of the perpendicular directions of motion and d.o.f respectively.

Little discrepancy in amplitude is observed in the plot, with the main trend are the same; and both input files have the resonance period around 19s.

Based on Figure A.5 and Figure A.6 above, it is concluded that the SIMO input file is consistent with the MIMOSA input file in all three translation degree of freedom. Then the three rotation d.o.f are checked.

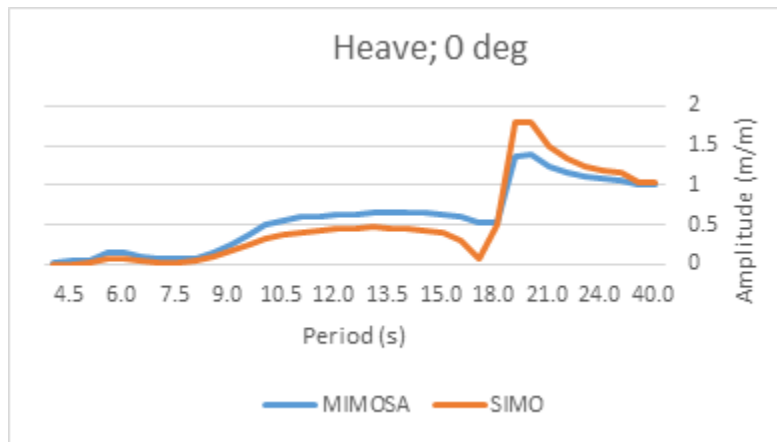
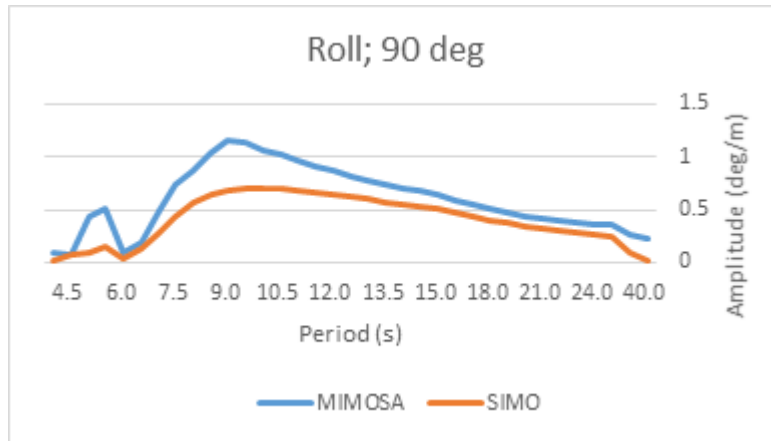


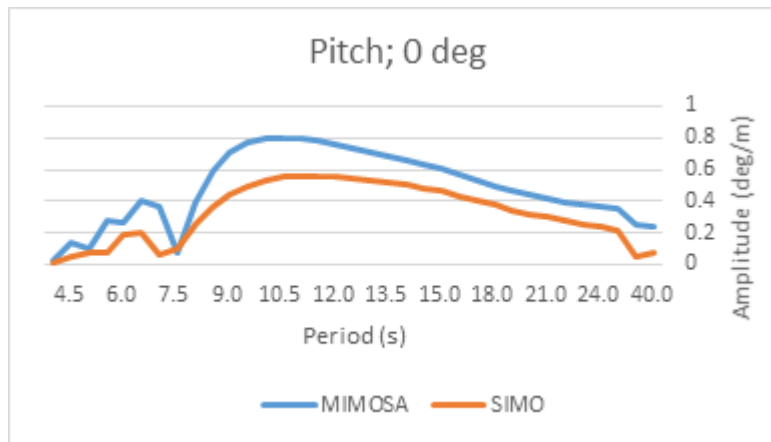
Figure A.6: 1<sup>st</sup> Order Motion Transfer Function in Heave; 0 deg

Based on Figure A.7, an obvious discrepancy is observed between two lines. It is assumed that SIMO input file has a lower damping level, then further leads to the lower amplitude in transfer function. However, both the lines show a similar trend. Thus here comes the conclusions:

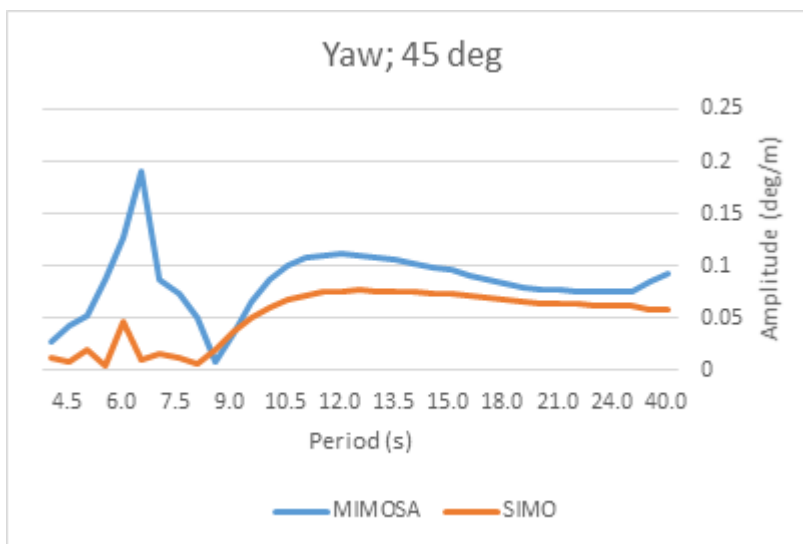
- The SIMO input file is consistent with MIMOSA input file in all parameters checked. Even some of the plots show some discrepancy, but the same trend is guaranteed. Therefore it is reasonable to use SIMO input file in the future analysis;
- In the aspect of 1<sup>st</sup> order motion transfer function, the SIMO input file has consistency in all translation d.o.f, but shows a lower damping level in rotation d.o.f, which may cause some difference in the future comparison about dynamic analysis.



(a)



(b)



(c)

Figure A.7: 1<sup>st</sup> Order Motion Transfer Function in (a) Roll; 90 deg (b) Pitch; 0 deg (c) Yaw; 45 deg

# Appendix B

## All lines tension comparison in viscous cases

Here all the tension results are listed in the following tables under category of max tension, mean tension and standard deviation. The cases description is referred to Section 6.4.

Table B.1: Max tension result of all lines in viscous cases(unit:[kN])

Line no.	Max Tension				
	1	2	3	4	5
1	1162.8	1142.7	1413	1222.3	1106.7
2	1131.9	1115.9	1327.6	1179	1086.6
3	1094.3	1083.7	1219.2	1124.7	1061.6
4	2441.4	2636.3	2491.7	2456.9	3190.1
5	3194.7	3478	3265.4	3213.8	4273.4
6	3791	4139.1	3876.6	3812.4	5115.6
7	3787.6	4149.2	3884	3815.7	5109.7
8	3200.4	3490.4	3275.8	3221.1	4271.7
9	2454.6	2649.7	2503.8	2466.9	3192.5
10	1095.5	1084.9	1225.2	1126.8	1067.3
11	1136.7	1119.9	1339.6	1185.4	1091.7
12	1171.8	1149.9	1433.2	1234.4	1111

Table B.2: Mean tension result of all lines in viscous cases(unit:[kN])

Lino no.	Mean Tension				
	1	2	3	4	5
1	711.16	687.9	738.04	715.15	666.94
2	746.18	724.5	770.55	749.88	704.14
3	800.81	781.86	821.04	803.83	763.66
4	1358.8	1410.3	1317	1353.3	1483.2
5	1544.7	1634.1	1479.6	1535.9	1738.2
6	1698.2	1813.6	1613.8	1686.7	1947.1
7	1708.8	1824.1	1623.4	1696.7	1958.4
8	1551.7	1640.9	1485.5	1542.1	1746.2
9	1362.4	1419.6	1319.6	1356.1	1488.1
10	803.02	783.77	822.99	805.75	765.81
11	746.58	724.81	770.79	750.11	704.65
12	710.13	686.96	736.89	714.03	666.2

Table B.3: Standard deviation result of all lines in viscous cases(unit:[kN])

Line no.	Standard Deviation				
	1	2	3	4	5
1	79.478	77.434	98.446	82.862	84.168
2	73.704	72.591	89.405	76.458	80.017
3	63.847	63.355	74.786	65.72	70.933
4	171.85	191.08	180.11	172.52	249.35
5	267.98	297.36	279.56	268.66	385.5
6	346.31	382.97	360.81	347.03	493.72
7	348.06	384.65	363.36	349.01	494.81
8	269.49	298.74	281.17	270.04	387.13
9	173	192.06	180.8	173.27	251.25
10	64.056	63.595	75.082	65.96	71.143
11	73.807	72.712	89.821	76.653	80.001
12	79.448	77.422	98.886	82.971	83.904

*Observation and analysis:*

- Common for all cases:

1. The variation trend for max tension, meant tension and standard deviation are the same.
2. Since the layout of line 1-6 are symmetry with line 12-7 about the force propagating

direction correspondingly, their tension value are always close to each other.

3. Line 4-9 always have larger tension value than the other 6 lines. Because they are located at the side near force propagating direction, they stay in a more stretched status when the structure have a offset in the same direction with the force direction.
  4. When the tension value of line 4-9 increase, which means they become more stretched, maybe due to a larger motion of structure, the tension of other 6 lines will have decreasing tension, which means they are in more slack status. Vice versa.
- For separate cases:
    1. Compared to Case 1, the original case, both Case 2 with slender elements and Case 5 with correction formula show a increase in tension of line 4-9. It corresponds to the larger offset in surge under the extra effect due to viscous effect. Meanwhile, the tension of other 6 lines decrease.
    2. After modifying the drag coefficient in Case 3 and Case 4, they not only have a similar offset with Case 1, but also similar tension values.

# Appendix C

## All lines tension comparison with different damping value

Here all the tension results are listed in the following tables under category of max tension, mean tension and standard deviation. The cases description is referred to Section 6.6.

Table C.1: Max tension result of all lines with different damping value(unit:[kN])

Line no.	Max Tension					
	S.E(case 2)	C.F(Case 5)	<i>i</i>	<i>ii</i>	<i>iii</i>	<i>iv</i>
1	1142.7	1106.7	1025.7	979.57	938.97	918.47
2	1115.9	1086.6	1021.5	983.04	948.69	931.35
3	1083.7	1061.6	1016.3	988.51	961.93	949.2
4	2636.3	3190.1	3093.7	3009.3	2866.8	2745.5
5	3478	4273.4	4135.7	4015.8	3812.8	3639.6
6	4139.1	5115.6	4947.4	4800.8	4552.4	4340.86
7	4149.2	5109.7	4942	4795.1	4550.1	4339.9
8	3490.4	4271.7	4135.5	4016.5	3818.1	3648.4
9	2649.7	3192.5	3097.8	3015.5	2878.4	2762
10	1084.9	1067.3	1019.2	990.45	963.29	950.3
11	1119.9	1091.7	1023.4	984.06	950.77	932.7
12	1149.9	1111	1026.7	980.06	941.63	920.28

Table C.2: Mean tension result of all lines with different damping value(unit:[kN])

Line no.	Mean Tension					
	S.E(case 2)	C.F(Case 5)	<i>i</i>	<i>ii</i>	<i>iii</i>	<i>iv</i>
1	687.9	666.94	665.14	664.1	663.02	662.61
2	724.5	704.14	702.66	701.81	701.02	700.85
3	781.86	763.66	762.54	761.84	761.12	760.84
4	1410.3	1483.2	1480.1	1477.6	1473.5	1469.7
5	1634.1	1738.2	1733.5	1729.9	1723.7	1718.1
6	1813.6	1947.1	1941.5	1937.2	1929.6	1922.7
7	1824.1	1958.4	1953	1948.9	1942	1935.5
8	1640.9	1746.2	1741.7	1738.3	1732.5	1727.2
9	1419.6	1488.1	1485	1482.7	1478.7	1475.2
10	783.77	765.81	764.72	764.08	763.45	763.25
11	724.81	704.65	703.15	702.32	701.57	701.42
12	686.96	666.2	664.36	663.3	662.2	661.77

Table C.3: Standard deviation result of all lines with different damping value(unit:[kN])

Line no.	Standard Deviation					
	S.E(case 2)	C.F(Case 5)	<i>i</i>	<i>ii</i>	<i>iii</i>	<i>iv</i>
1	77.434	84.168	76.495	71.552	65.034	60.455
2	72.591	80.017	72.946	68.259	61.964	57.492
3	63.355	70.933	64.955	60.816	55.01	50.748
4	191.08	249.35	230.42	216.29	195.45	179.79
5	297.36	385.5	356.9	335.52	303.94	280.15
6	382.97	493.72	457.47	430.37	390.31	360.1
7	384.65	494.81	458.16	430.88	390.77	360.63
8	298.74	387.13	358.28	336.81	305.21	281.46
9	192.06	251.25	232.21	218.05	197.22	181.58
10	63.595	71.143	65.185	61.065	55.28	51.031
11	72.712	80.001	72.881	68.18	61.877	57.404
12	77.422	83.904	76.15	71.184	64.671	60.104

*Observation and analysis:*

- Common for all cases:
  1. Since the layout of line 1-6 are symmetry with line 12-7 about the force propagating direction correspondingly, their tension value are always close to each other.
  2. Line 4-9 always have larger tension value than the other 6 lines. Because they are located at the side near force propagating direction, they stay in a more stretched status when the structure have a offset in the same direction with the force direction.
  
- For separate cases:
  1. Compared Case 2 and 5, they have great difference in tension value, due to the viscous-induced damping effect. After modifying the linear damping value, there is certain effect on the max tension and standard deviation. Table C.1 and Table C.3 show that, with the increase in damping, tension of all lines decrease. It means that the whole structure bears less damping force, so all lines are in less tensioned status.  
However, it doesn't apply to mean tension as Table C.2. The mean response doesn't change much with the increase of damping term.
  2. After modifying the drag coefficient in Case 3 and Case 4, they not only have a similar offset with Case 1, but also similar tension values.

# Appendix D

## All lines tension comparison under different environment condition

Here all the tension results are listed in the following tables under category of max tension, mean tension and standard deviation. The cases description is referred to Section 7.1.

Table D.1: Max tension result of all lines under different environment condition(unit:[kN])

Line no.	Max Tension			
	Base Case	a	b	c
1	1142.7	1662.8	958.33	951.04
2	1115.9	1519.7	964.54	958.22
3	1083.7	1344.4	974.94	971.02
4	2636.3	2117.3	1350.5	1035.9
5	3478	2707.6	1525.1	1050.1
6	4139.1	3180	1665.4	1061.3
7	4149.2	3177	1704.3	1059.3
8	3490.4	2705.6	1544.7	1049.6
9	2649.7	2116	1354.3	1036.7
10	1084.9	1345.5	975.19	971.08
11	1119.9	1527.2	963.11	959.04
12	1149.9	1677.6	956.16	952.67

*Observation and analysis:*

- Common for all cases:

1. The variation trend for max tension, meant tension and standard deviation are the

Table D.2: Mean tension result of all lines under different environment condition(unit:[kN])

Line no.	Mean Tension			
	Base Case	a	b	c
1	687.9	890.49	813.85	950.83
2	724.5	906.17	842.46	958.05
3	781.86	929.73	883.16	970.83
4	1410.3	1120	1166.1	1035.7
5	1634.1	1179.2	1243.4	1049.8
6	1813.6	1228.5	1305.5	1060.9
7	1824.1	1226.6	1322.6	1058.9
8	1640.9	1178.6	1252.7	1049.3
9	1419.6	1120.5	1168.4	1036.5
10	783.77	929.69	886.79	970.89
11	724.81	906.87	841.76	958.87
12	689.96	891.93	809.04	952.46

same.

2. Since the layout of line 1-6 are symmetry with line 12-7 about the force propagating direction correspondingly, their tension value are always close to each other.
  3. Line 4-9 always have larger tension value than the other 6 lines. Because they are located at the side near force propagating direction, they stay in a more stretched status when the structure have a offset in the same direction with the force direction.
  4. When the tension value of line 4-9 decrease, which means they become less stretched, maybe due to a limited motion of structure, the tension of other lines will have increasing tension, which means they are more balanced than previous.
- For separate cases:
    1. The base case is the one with all forces, thus it has the largest tension compared to other three separate cases.
    2. Case a under wave effect is more dominating than other two forces, since it has the largest tension value and also the max offset in surge. The dynamic effect consists of both LF response and WF response.

Table D.3: Standard deviation result of all lines under different environment condition(unit:[kN])

Line no.	SD Tension			
	Base Case	a	b	c
1	77.434	138.24	40.006	58.541
2	72.591	117.64	36.045	47.846
3	63.355	88.208	26.592	51.717
4	191.08	134.74	45.09	51.869
5	297.36	203.87	69.947	73.416
6	382.97	261.05	88.884	89.66
7	384.65	260.51	94.02	89.777
8	298.74	203.63	72.692	73.087
9	192.06	134.68	46.001	51.666
10	63.595	88.283	25.698	52.079
11	72.712	118.09	36.14	48.29
12	77.422	139.19	40.284	58.973

3. Case b under wind effect has largest mean tension compared to other cases, due to the largest static response.
4. Case c under only current effect has the most stable value in all tension parameters. Because current is always assumed as a stationary process.